Electrical Vestibular Stimulation for Parkinson's Disease Treatment

by

Soojin Lee

B.Sc., Korea University, 2008
M.Sc., The University of British Columbia, 2010

A THESIS SUBMITTED IN PARTIAL FULFILLMENT OF
THE REQUIREMENTS FOR THE DEGREE OF

DOCTOR OF PHILOSOPHY

in

The Faculty of Graduate and Postdoctoral Studies

(Biomedical Engineering)

THE UNIVERSITY OF BRITISH COLUMBIA

(Vancouver)

July 2019

The following individuals certify that they have read, and recommend to the Faculty of Graduate and Postdoctoral Studies for acceptance, the thesis entitled:

Electrical Vestibular Stimulation for Parkinson's Disease Treatment

submitted by **Soojin Lee** in partial fulfillment of the requirements for the degree of **Doctor of Philosophy** in **Biomedical Engineering**.

Examining Committee:

Martin J. McKeown, Faculty of Medicine (Neurology)
Supervisor

Z. Jane Wang, Electrical and Computer Engineering
Co-supervisor

Silke Cresswell, Faculty of Medicine (Neurology)
Supervisory Committee Member

Purang Abolmaesumi, Electrical and Computer Engineering
University Examiner

Todd Woodward, Faculty of Medicine (Psychiatry)
University Examiner

Hong Bo, Biomedical Engineering, Tsinghua Univeristy
External Examiner

Additional Supervisory Committee Members:

Cyril Leung, Electrical and Computer Engineering
Supervisory Committee Member

Abstract

Parkinsons disease (PD) is a progressive movement disorder characterized by degeneration of dopaminergic neurons and abnormal brain oscillations. While invasive deep brain stimulation can improve some motor deficits by disrupting pathological brain oscillations, achieving comparable results with non-invasive brain stimulation (NIBS) remains elusive. Previous studies have suggested that electrical vestibular stimulation (EVS) may ameliorate some motor symptoms in PD. However, the investigated effects are limited to a few domains, only a handful of stimulation waveforms have been explored, and neuroimaging studies capable of probing the mechanisms are greatly lacking. The overarching objective of this thesis is to utilize biomedical engineering approaches to fully explore the EVS technique as a potential therapeutic intervention for PD. This involves development of new stimuli, development of new artifact rejection methods, and thorough investigations of brain and behavioural responses, as outlined below.

To achieve the objective, noisy EVS is firstly revisited and tested with PD and healthy subjects to investigate effects on visuomotor tracking behaviours. Next, novel EVS stimuli are developed using multisine signals in distinct frequency bands and tested in the experiment where the stimuli are applied to PD and healthy subjects during rest and task conditions while EEG are being recorded. This simultaneous EVS-EEG study aims to provide insights into modulatory effects of EVS on brain oscillations and motor behaviours altered in PD and whether the effects are a function of different stimulation types. One critical challenge involved with EVS-EEG studies is that EEG recordings are severely corrupted by the stimulation artifacts. To resolve this, a quadrature regression and subsequent independent vector analysis method is developed and its superior denoising performance to conventional methods is demonstrated. Finally, underlying mechanisms of EVS effects in PD are investigated in a resting-state functional MRI study.

The results from this thesis suggest that sub-threshold EVS in PD induces widespread motor changes and brain activities that are stimulus-dependent, suggesting subject-specific stimuli may ultimately be desirable to achieve a clinically meaningful effect.

Lay Summary

People with Parkinsons disease (PD) experience debilitating motor symptoms, which are associated with abnormal brain activities. Current treatments include medication and invasive surgical implantation of electrodes into a deep region of the brain to deliver electrical impulses. There is keen interest in finding ways to *non-invasively* stimulate the brain safely to treated PD. Electrical vestibular stimulation (EVS) is a non-invasive brain stimulation technique that delivers weak electrical currents to the balance organ located in the inner ear, and also induces changes in brain activities. The purpose of this dissertation is to understand how it might go about relieving motor symptoms in PD and provide a deeper understanding of how EVS works. In addition, to further our understanding, this thesis demonstrates that customizing the stimulation to the individual may be necessary.

Preface

This dissertation is primarily based on five journal publications (three are under review), one conference paper and nine conference presentations, resulting from a collaboration between multiple researchers. These publications have been modified to make the dissertation coherent. The author was responsible for design of experiment and data collection. Participants recruitment and scheduling was assisted by Ms. Christina Jones and Ms. Tammy Kang. The author was also responsible for the data analyses, evaluation of the methods and the production of the manuscripts. All co-authors have contributed to the editing of the manuscripts and providing feedback and comments. The dissertation work was conducted in UBCs Pacific Parkinson Research Centre. Approval of this study was obtained by the UBCs Clinical Ethics Board (Certificate number: H09-02016).

The study from Chapter 2 is based on:

- Soojin Lee, Diana J. Kim, Daniel Svenkeson, Gabriel Parras, Meeko Mitsuko K. Oishi and Martin J. McKeown. Multifaceted effects of noisy galvanic vestibular stimulation on manual tracking behavior in Parkinsons disease. Frontiers in Systems Neuroscience, 9(5), 1-9, 2015.

and was presented at:

- Soojin Lee, Daniel Svenkeson, Meeko Oishi and Martin J. McKeown. Multifaceted effects of noisy galvanic vestibular stimulation on manual tracking behavior in Parkinsons disease. IEEE EMBS BRAIN Grand Challenge, November 2014, Washington, USA.

- Soojin Lee, Diana Kim, Daniel Svenkeson, Meeko M.K. Oishi and Martin J. McKeown. Synergistic effects of noisy galvanic vestibular stimulation and oral L-dopa in improving manual tracking performance in Parkinsons disease. 1st International Brain Stimulation Conference, March 2015, Singapore.

The contribution of the author was the data analyses and writing the manuscript. Diana Kim contributed to collecting the data and editing the manuscripts. Dr. Meeko Oishi, Daniel Svenkeson and Gabriel Parras provided valuable feedback on the data analyses.

The study from Chapter 3 is based on:

- Soojin Lee, Z. Jane Wang, Martin J. McKeown, and Xun Chen, Removal of High-Voltage Brain Stimulation Artifacts from Simultaneous EEG Recordings. IEEE Transactions on Biomedical Engineering, 66(1), 50-60, 2019.

and was presented at:

- Soojin Lee, Z. Jane Wang and Martin J. McKeown, Removal of high-voltage brain stimulation artifacts from simultaneous EEG recordings. 2nd International Brain Stimulation Conference, March 2017, Barcelona, Spain.

The contribution of the author was the data collection, the analyses of the data and writing the manuscript. Dr. Jane Wang contributed to provided valuable scientific inputs to improve the proposed method and feedback on the data analyses.

The study from Chapter 4 is based on:

- Soojin Lee, Aiping Liu, Z. Jane Wang, and Martin J. McKeown.,Abnormal phase coupling in Parkinsons disease and normalization effects of subthreshold vestibular stimulation. Frontiers in Human Neuroscience, 13(118), 1-15, 2019.

The contribution of the author was the development of the EVS stimuli, design of the experiment, the data collection and the analyses of the data, and writing the manuscript. Dr. Aiping Liu and Dr. Jane Wang provided valuable feedback on the data analyses.

The study from Chapter 5 is based on:

- Soojin Lee, Z. Jane Wang, and Martin J. McKeown, High-frequency vestibular simulation jointly affects motor performance and beta oscillations in Parkinson's disease. (under review).

and was presented at:

- Soojin Lee, Z. Jane Wang and Martin J. McKeown, Engineering Approaches to Non-Invasive Electrical Stimulation of the Brain: Application to Parkinsons Disease. Emerging Technologies 2018, May 2018, Whistler, Canada.
- Soojin Lee, Z. Jane Wang and Martin J. McKeown, Non-Invasive Galvanic Vestibular Stimulation Augments Event-Related Desynchronization and Improves Motor Performance in Parkinsons Disease. Canadian Student Health Research Forum, June 2018, Winnipeg, Canada
- Soojin Lee, Z. Jane Wang and Martin J. McKeown, Non-Invasive galvanic vestibular stimulation augments beta desynchronization and improves motor performance in Parkinsons Disease. 3nd International Brain Stimulation Conference, February 2019, Vancouver, Canada.

The contribution of the author was the development of the EVS stimuli, design of the experiment, the data collection, the analyses of the data, and writing the manuscript. Dr. Jane Wang provided valuable scientific input for the data analyses.

The study from Chapter 6 is based on:

- Soojin Lee, Aiping Liu, Jowon L. Kim, Saurabh Garg, Z. Jane Wang, and Martin J. McKeown. Effects of electrical vestibular stimulation on thalamic activity and disrupted basal ganglia-thalamic connectivity in Parkinsons disease. Parkinsonism and Related Disorders (under review).

The contribution of the author was the data collection, the analyses of the data, and writing the manuscript. Jowon Kim contributed to the data collection, and Saurabh Garg contributed to preprocessing of the fMRI data and interpretation of the data. Dr. Aiping Liu contributed to preprocessing of the fMRI data, performance of normalized cut spectral clustering analysis, and interpretation of the results. Dr. Jane Wang provided feedback and technical input to the data analyses.

Finally, my supervisor, Dr. Martin McKeown, helped with the development, implementation and evaluation of all of the methods in the above

publications and this dissertation. He also significantly contributed to biological interpretation of the results and improvement of the manuscripts through valuable comments and feedback.

Table of Contents

List of Tables

List of Figures

Glossary

BG Basal Ganglia
CCA Canonical Correlation Analysis
CF Crest Factor
DBS Deep Brain Stimulation
DCA Discriminant Correlation Analysis
EEG Electroencephalography
ERD Event-Related Desynchronization
EVS Electrical Vestibular Stimulation
fMRI Functional Magnetic Resonance Imaging
ICA Independent Component Analysis
IVA Independent Vector Analysis
JBSS Joint Blind Source Separation
L-dopa Levodopa
LDA Linear Discriminant Analysis
LFP Local Field Potential
MCCA Multiset Canonical Correlation Analysis
MEG Magnetoencephalography
NIBS Non-Invasive Brain Stimulation
PCA Principal Component Analysis
PD Parkinson's Disease
PLV Phase Locking Value
SDA Sparse Discriminant Analysis
SNR Signal-to-Noise Ratio
tACS Transcranial Alternating Current Stimulation
tDCS Transcranial Direct Current Stimulation
tES Transcranial Electrical Stimulation
TMS Transcranial Magnetic Stimulation
tRNS Transcranial Random Noise Stimulation
UPDRS Unified Parkinson's Disease Rating Scale

Acknowledgements

First and foremost, I would like to express my sincerest gratitude to Dr. Martin McKeown, my supervisor, for the opportunity he gave me that opened a new chapter of my life. I am especially grateful for his great mentorship, invaluable support and trust that led me to be able to continuously grow and become a better person who, like him, devotes talent and knowledge to contributing to society. Thanks for the advice and generosity you offered me both academically and personally throughout my experience at UBC. This thesis and my career about to start would never be possible without your support.

I am very grateful for my co-supervisor, Dr. Jane Wang, whose insightful advice helped me throughout the course of my PhD journey. Her genuine support and dedication were well beyond the role of co-supervisor, which I not only appreciate but also admire.

I would like to thank thesis examination committee members and chair, Drs. Abolmaesumi, Cresswell, Leung, Woodward and Shaw for their valuable time, constructive comments and encouragement.

Throughout the span of five years, I have been fortunate to work with and getting to know many great individuals. I am thankful to all my lab mates, Saurabh Garg, Christy Jones, Stephanie Tran, Marcus Cheung, Maria Zhu, Robert Baumeister, Sue-Jin Lin, Jowon Laura Kim, Emma Kiss and Sun Nee Tan for creating supportive and fun environment. I also would like to thank Aiping Liu, Jiayue Cai, Azadeh Hosseini, and Xun Chen for their insightful advice and supports, Sangwook Han, Esther Song, Agnes Kwok, Inae Lee, and my office mates, Drs. Pratibha Surathi, Michele Matarazzo, Devavrat nene and Jose Wijnands for bringing me laughter and comfort throughout this journey.

To the research participants, thank you all for your enthusiasm and interests in participating in my research.

I am deeply grateful for my parents' endless love, encouragement and sacrifice from when I was born till I grew up. I am happy you are my mom and dad and you will be always in my heart throughout my life. My sister and brother, Sooyoon and Yongmoon, thank you for always being supportive

and unconditionally helping me out. A special thank you goes to Matthew for his supports, love and humours that have strengthen me in many ways.

Finally, this work was supported by PPRI/UBC chair in Parkinson's Disease awarded to my supervisor and a generous gift from the Mottershead Foundation and PPRI.

Dedication

To people with Parkinson's disease
—for generous support and great inspiration for this research

Chapter 1

Introduction

1.1 Parkinson's Disease (PD)

1.1.1 Brief History, Epidemiology and Clinical Features

Parkinsons disease (PD) is a progressive neurodegenerative disorder characterized by a large number of motor and non-motor features. In his landmark publiation in 1817 of "An essay on the shaking palsy", James Parkinson first described the clinical syndrome that was later to bear his name [279]. About 100 years passed (1919) after the first description of PD before it was recognized that patients with PD prematurely lose cells in the substantia nigra *pars compacta*, and after 140 years had passed (1957) dopamine was discovered as a putative neurotransmitter [36, 160]. Later in 1961, the first trials of levodopa injection to improve akinesia in patients with PD were conducted followed by the development of oral levodopa later in the decade [34, 73], which has remained the gold standard of treatment to date.

PD is the second most common neurodegenerative disorder affecting 1–2% of people over age 65 years [335], with its prevalence escalating to as high as 4% with increasing age [396]. Worldwide incidence estimates of PD range from 5 to > 35 new cases per 100,000 individuals yearly, depending the demographics of the populations studied [297]. The mean age of onset is around 55 years old and the incidence increases 5–10-fold from the sixth to the ninth decade of life [334, 387, 396]. The number of people with PD is expected to double between 2005 and 2030 according to recent meta analyses [152, 305], which is presumably due to growing elderly populations. The prevalence of PD varies according to sex, race, ethnicity and environment. The incidence is greater in men in most populations, and African Americans and Asians may be less likely to be diagnosed with PD [78, 396], but it is difficult to determine the relative contribution of each of the factors. Mortality in PD increases to double compared to non-PD population after the first decade of disease onset [295], and mean PD duration until death ranges from 6.9 to 14.3 years [226].

PD is most recognized for its cardinal motor symptoms including bradyki-

nesia (slowness of movement), tremor, rigidity and postural instability and clinical diagnosis is defined by the presence of bradykinesia and rigidity and/or rest tremor. In addition to the motor features, a multitude of non-motor symptoms such as cognitive impairment (including executive dysfunction, dementia, memory retrieval deficits and hallucination), autonomic dysfunction, disorders of sleep and depression are part of the disease [297]. Progressive disease ultimately results in treatment-resistant motor symptoms such as freezing of gait, falling and dyskinesia. PD evolves with different clinical courses and prognoses in individuals and thus it is increasingly recognized that PD is not a single entity but a heterogeneous disorder with a broad spectrum of motor and non-motor features [378].

1.1.2 Neuropathology

Pathologically, the disease is defined by the degeneration of dopaminergic neurons in the substantia nigra pars compacta (SNc) that project to the basal ganglia (BG), a group of subcortical nuclei located deep within the brain. The BG include the caudate, putamen, globus pallidus, the substantia nigra and the subthalamic nucleus (STN) and are associated with a variety of functions, including control of voluntary motor movements. The degeneration of dopaminergic SNc neurons and their projections to the striatum may take decades to develop and recognizable motor or non-motor features appear only after substantial degeneration ($\sim$60%) of the nigrostriatal neurons [102]. Earlier degeneration of SNc projections to the putamen than those to associative or limbic areas of the striatum may result in earlier development of the motor symptoms than the non-motor symptoms in PD [121]. The motor and non-motor symptoms in PD are multifactorial and also linked to damage of specific brainstem nuclei [130]. The brainstem is divided into mesencephalon, metenchephalon (pons), and medulla oblongata and includes the sensory and motor nuclei of 10 cranial nerves [170]. The dorsal motor vagal nucleus, intermediate reticular zone, pedunculoponine nucleus are known to be particularly affected by PD and associated with gastrointestinal system dysfunction, pain, sleep disturbances, and gait [130].

For decades, a functional and anatomical model of the BG circuitry has been proposed to explain the clinical symptoms of PD (Fig. 1.1). According to the model, the internal segment of the globus pallidus (GPi) receives signals from the putamen through "direct" and "indirect" pathways. As dopamine produced from the SNc modulates antagonistic functions in the direct and indirect pathways, imbalanced activity between these two path-

ways has been proposed to underlie the motor symptoms observed in PD [190]. However, recent data from different experimental approaches indicate that this model alone cannot explain many key features of the disease [37, 212]. For instance, it does not account for tremor and rigidity commonly observed in PD, and fails to explain why lesion treatments such as GPi pallidotomy paradoxically improve dyskinesias without any clear deleterious effects on motor function [47].

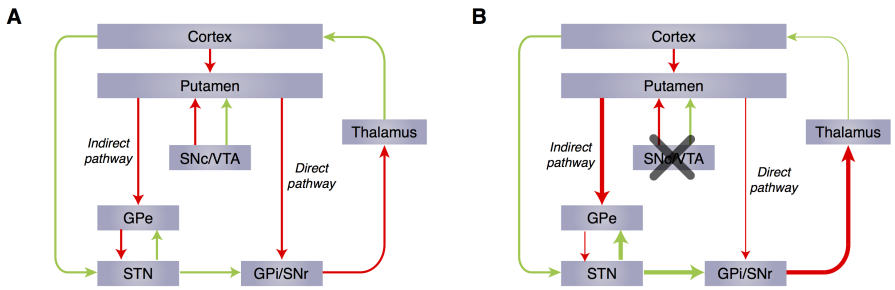

Figure 1.1: Simplified illustration of the main connections of the BG. The direct and indirect pathways from the putamen have net effects of disinhibition and inhibition on the cortex, respectively. Reduced dopaminergic stimulation from SNc to the putamen in PD is marked with a black cross. Dopamine deficit leads to increased activity in the indirect pathway, in which STN hyperactivity is a key characteristic, and hypoactivity in the direct circuit. Together, these alterations result in increased GPi/SNr output inhibition of the thalamus and reduced activation of cortical and brainstem motor regions. Green and red arrows denote excitatory and inhibitory activity, respectively. Figure modified from [317] and [435] (GPe: external globus pallidus; GPi: internal globus pallidus; SNc: substantia nigra; SNr: substantia nigra pars reticulta; STN: subthalamic nucleus; VTA: ventral tegmental area)

Another characteristic feature of PD is abnormal accumulation of intracellular protein (α-synuclein) in widespread brain regions. Lewy bodies, fibrillary aggregates largely made up of α-synuclein, initially can be seen in neurons in the brainstem and olfactory system and are found in limbic and neocortical brain regions as the disease progresses [297]. The abnormal aggregation of α-synuclein are found in 10% of pigmented neurons in the substantia nigra and >50% in the locus ceruleus in PD [411].

1.1.3 Aberrant Neural Oscillations in PD

Research has suggested that, in addition to the dopaminergic biochemical changes, aberrant neural synchrony is closely associated with manifestation of motor symptoms in PD. The functional role of the aberrant patterns

of neural oscillatory activities in PD has been well investigated in studies where local field potentials (LFPs) were recorded from neurons in BG structures through electrodes implanted for direct brain stimulation (DBS) [211, 213, 214]. Since then, many studies have demonstrated that oscillatory activities of the BG are found in frequency bands ranging from low delta (2–4 Hz) to high-gamma (250–330 Hz). In particular, neural oscillations in the beta band (13–30 Hz) appear to reflect motor states of PD patients [308]: PD patients in an off-medication condition have enhanced beta oscillations, and following administration of levodopa medication this beta power is decreased in both the subthalamic nucleus (STN) and GPi [50]. The beta-band LFPs have also been shown to correlate with movement preparation and execution as well as motor performance in PD patients [417]. One hypothesis for the functional association of exacerbated beta oscillation with PD is that normal motor command for initiation of movement cannot override it, resulting in difficulty of generating voluntary movement for PD patients [155]. Apart from the abnormality in the beta-band, neural oscillations in lower frequencies have also been suggested to relate to dopaminergic medication responses of PD patients. Oscillatory activities in the 4–10 Hz range have been shown to increase after dopaminergic medication and correlate with the improvement in clinical condition [307, 350], and abnormal synchronized oscillations around 8 Hz have been shown to correlate with levodopa-induced dyskinesia [9, 112, 351].

Compared to the well-characterized oscillatory characteristics of PD presented in the subcortical structures, how PD influences functional neural networks in cortical regions (which can be relatively easily assessed with the electroencephalography—EEG) are unknown. In early EEG studies, one of the findings presumed to be relevant to PD was slowing of neural rhythms and resultant increased neural activity in low frequency bands (<10 Hz). It was postulated that occipital slowing may have resulted from the subcortical structures affected in PD [260]. However, a limitation of the argument is that slowing of the occipital peak frequency is not specific to PD and it has been commonly observed in people with other neurodegenerative conditions, such as Alzheimers disease (AD) [163, 285].

Multimodal studies that record electrical potentials simultaneously from the cortex and the subcortical structures may provide useful clues in search for neurophysiological biomarkers specific to PD. For example, it was found that recordings of LFPs in GP and EEG in the supplementary motor areas were closely related at <10 Hz and in 20–30 Hz when a PD patient was off-medication [47]. As the pathological neural activities in the subcortical structures were represented in the cortical areas, it is natural to

ask whether it would be possible to distinguish between Parkinsonian and non-Parkinsonian states inferring from cortical activity alone. This could provide neurophysiological non-invasive PD biomarkers and would be especially important in developing non-invasive brain stimulation techniques aiming to provide therapeutic benefits to PD populations.

1.1.4 Current Treatment Options for PD

PD is normally treated pharmacologically with administration of dopaminergic medications, such as the dopamine precursor levodopa (L-dopa), that is converted to dopamine after crossing the blood brain barrier. While early response to the medication is robust and satisfying, the medication likely does not alter progression of the disease. Prolonged use of the medication often induces dyskinesia (involuntary hyperkinetic movement) and end-of-dose deterioration (early wearing off) that can cause motor fluctuations between being "on" and mobile and "off" and stiff. In addition, not all symptoms are L-dopa responsive. L-dopa has little effect on gait and balance dysfunction and non-motor symptoms such as autonomic dysfunction, sleep disorders, mood disturbances and dementia [345].

DBS is a surgical treatment option for people with advanced PD. DBS electrodes are implanted into the target structure in the brain to send electrical signals and a battery pack/implanted pulse generator (like a pacemaker) is inserted into the chest. Since the first use in 1986 of DBS with electrodes implanted in the ventral intermedius nucleus of the thalamus to treat tremor in PD, DBS has been developed into an effective treatment for several medically refractory movement disorders. In PD, DBS of the thalamus, GPi and STN at high-frequency (>100 Hz) has been an effective and safe intervention and attenuate pathological neural oscillations. A five-year follow-up study reported that 130-Hz DBS at the STN effectively treated motor symptoms of people with advanced PD, resulting in general improvement in rest tremor, rigidity, gait, and akinesia as well as persistent improvement in motor symptoms [188]. Dyskinesia was also found to be alleviated by 50–70% in other studies [89, 181].

Present understanding of the therapeutic effects of DBS from functional imaging, neurochemistry and neural recording studies suggests two strongly debated general hypotheses: 1) DBS acts as a functional ablation to suppress the stimulated nucleus, which is analogous to lesion of target structures in the thalamus or BG, or 2) DBS results in activation of the stimulated nucleus that is transmitted throughout the network [244].

Although DBS can provide some benefits in managing motor symptoms

in PD, it has several limitations. DBS is less effective for medication-unresponsive symptoms such as postural imbalance, freezing of gait and non-motor symptoms [125, 318]. Furthermore, several studies reported cognitive decline (in particular executive function), reduction of verbal fluency, transient neuropsychiatric symptoms including hypomania, impulse control disorders or hypersexuality, and suicidal ideation as side effects of DBS [77, 131, 274, 282]. Surgery-related complications such as intracerebral hemorrhage and postoperative infections remain a possibility [131], which can be increased by periodic replacement (mostly every 4 years) of the battery of the controllers and hardware malfunctions including lead breakage or malfunction of the pulse generator [225, 406].

1.2 Non-invasive Brain Stimulation (NIBS)

1.2.1 Background

With a growing consensus on the important role of abnormal dynamics of the neural network involved in PD, non-invasive brain stimulation (NIBS) has been attracting substantial attention as a safe and effective means of disrupting abnormal oscillations. NIBS refers to stimulation techniques that do not require an incision or insertion in the body for electrode placement. The field is growing exponentially as NIBS methods are recognized as an important tool to probe brain-behaviour relationships [300]. While the inferences from brain imaging methods alone are purely correlative, combined with NIBS to causally manipulate neural activity, the methods allow for directly studying how the altered neural activity causally affects behaviour.

The most established NIBS techniques are transcranial magnetic stimulation (TMS) and transcranial electrical stimulation (tES). As they induce electrical fields over relatively large areas of tissue, the spatial focality is much lower than invasive methods (Fig. 1.2) and generally entail neuroimaging methods and computational modeling to visualize and interpret the affected brain areas. Focused ultrasound stimulation (FUS) is a relatively new method and known to change neuronal activity with a resolution of millimeters [386]. Although successful modulation of event-related potentials (ERP) in primary somatosensory cortex in humans was reported in a recent paper [208], safety studies and further research are required in the future to explore capabilities and limitations of the technique [388].

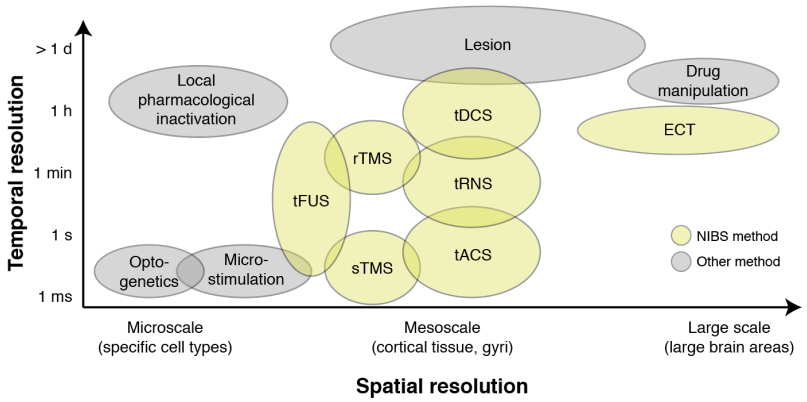

Figure 1.2: The spatial and temporal resolution at which different brain interventions work. NIBS methods work at the mesoscale level with the temporal resolution varies between high and low depending on the specific type of the stimulation. Figure modified from Polana and colleagues [300]. (tFUS: transcranial focused ultrasound stimulation; rTMS: repetitive transcranial magnetic stimulation; sTMS: single-pulse transcranial magnetic stimulation; tDCS: transcranial direct current stimulation; tRNS: transcranial random noise stimulation; tACS: transcranial alternating current stimulation)

1.2.2 Stimulation Parameters and Protocols

The basic principle underlying TMS is that time varying magnetic fields generate electric fields. TMS applies strong but short (∼1 ms) magnetic pulses to the scalp through a coil, inducing an electrical field in the brain and depolarizing cell membranes [21]. The effects of TMS depend upon a number of effects, including the geometry of the stimulating coil with respect to the head, the frequency, intensity and pattern of the magnetic pulses [320], and the duration of the stimulation. The spatial resolution of TMS for cortical stimulation is relatively higher (a few square centimeters in the cortex) than tES [223] and specific coil designs may also allow for stimulation of deep brain structures [87]. Single-pulse TMS delivers a monophasic pulse and evaluates excitability and conductivity of corticospinal motor pathways [186], and paired-pulse TMS consists of two successive pulses delivered with an inter-stimulus interval ranging from a few milliseconds to hundreds of milliseconds and allows the investigation of intracortical mechanisms of inhibition and facilitation [320]. Repetitive TMS is a new generation of TMS introduced in the late 1990 that delivers biphasic pulses repetitively with a low (< 1 Hz) or high (up to 60 Hz in general) frequency [319], and can lead to long-lasting after-effects compare to the single-pulse TMS [186].

tES applies electrical currents to the brain through two or more stimulation electrodes attached to the scalp with conductive gel. tES methods are categorized into transcranial direct current stimulation (tDCS), transcranial alternating current stimulation (tACS), and transcranial random noise stimulation (tRNS) depending on the stimulation waveforms. tDCS induces constant depolarization and hyperpolarization to the cortical neurons close to anodal and cathodal electrodes that are fixed, whereas tACS applies time-varying current (i.e., the anodal and cathodal electrodes are not fixed) with a single or multiple frequencies usually in a range of the oscillatory frequencies of the brain [17]. tRNS uses random values with particular probability distributions as the stimulation current [322], which is currently not as common as tDCS and tACS.

As the primary technique used in this dissertation is electrical stimulation, the following two sections (1.2.3 and 1.2.4) describe proposed mechanisms and clinical effects on PD with respect to transcranial electrical stimulation.

1.2.3 Proposed mechanisms of tES

Priori and colleagues [306] conducted the first modern study demonstrating modulation of cortical excitability with tDCS, whereby anodal and cathodal tDCS on the motor areas affects motor-evoked potential elicited in hand muscles in 15 subjects in an opposite direction. This was confirmed by the study of Nitsche and Paulus [264] that showed anodal tDCS augments motor cortex excitability and cathodal DCS produces the opposite effect. This polarity-specific effects have become the reference for subsequent studies, which have demonstrated that the stimulation current can induce the response in the form of plasticity such as long-term potentiation (LTP) or long-term depression (LTD) [284]. However, it is becoming more evident that the underlying processes involved in tDCS is more complex than simply observing anodal and cathodal tDCS decreases and increases excitability, respectively, as the effects also depend on other stimulation parameters such as stimulation time and intensity [24, 255]. Beyond the most accepted effects of tDCS to change threshold for action potential generation by modulating neuronal membrane polarity [217, 363], a number of cellular and molecular pathways are also affected by tDCS [284] with the mechanisms underlying these changes still being actively explored.

For tACS, an important mechanism is entrainment of oscillatory brain activity at or near the stimulation frequency. Zaehle and colleagues [436] demonstrated that 10-min tACS applied at individual's EEG alpha fre-

quency (IAF) increased the post-stimulation EEG spectral power specifically in the range of the IAF, indicating that tACS can induce frequency-specific effects on brain oscillations measured by EEG. This was replicated in a following study [261] and additionally it was reported that the increased alpha power persisted for at least 30 min after stimulation cessation. Entrainment is a theoretical concept originally conceived to explain synchronization phenomena in nonlinear systems [293] and described by the so-called "Arnolds tongue" that predicts the degree of synchronization of an oscillator with a given natural frequency to a rhythmic driving force as a function of driving force amplitude and frequency [267]. In the context of neural oscillations, the following list of features formulated by Thut and colleagues [382] can guide one to determine if brain oscillations induced by tACS qualify as "neural entrainment":

1. Entrainment requires the involvement of a neural oscillator (i.e., a neural population that exhibits oscillations at the entrainment frequency or is capable of doing so under natural conditions).

2. Entrainment requires periodicity in the input stream of external events. The external events can be in any form (e.g., electric, magnetic, visual) and have any periodic shapes (e.g., sinusoidal, a square-wave, repeated pulses).

3. Entrainment requires synchronization (phase alignment) between the input stream and the neural oscillator.

4. Crucially, the models also assume that the external force influences the oscillating elements by direct interaction (i.e., there should be no secondary stages such as connected brain areas).

Although this framework provides a conceptual framework for investigating the mechanisms of tACS, this model is clearly a coarse approximation to the mechanisms governing the brain and does not explain phenomena such as the fact that entrained brain oscillations are not always found after tACS [408] and it can vary depending on other parameters such as stimulation intensity and duration [409]. Another line of reasoning for tACS effects at large-scale network level has been recently proposed. This network activity-dependent model is based on the fact that our brain is a network consisting of spatially distributed but functionally linked regions [397] and electrical stimulation induces an activity-dependent modification of the system not only in a local area but also in specific networks [33, 224, 250]. In this

approach, tACS effects on neuronal activity and behaviour outcomes are dependent on the on-going state of relevant brain networks [106] that may cooperate or compete with each other. In support of this, several studies have demonstrated that behaviour changes via same type of stimulation can vary depending on the level of network engagement induced by the task [106].

The mechanisms underlying tRNS are largely unknown, but *stochastic resonance* is considered as one potential mechanism. Stochastic resonance (or *stochastic facilitation* in some fields) describes the contribution of added noise to a nonlinear dynamic system, and according to this view, the injection of appropriate level of random noise can paradoxically enhance the response of a nonlinear system (e.g., nervous system) to a weak signal [237] depending on the intensity of the noise and the state of the system. For instance, it was demonstrated that the ability to detect a subthrehold tactile stimulus in healthy subjects was enhanced when receiving the subthreshold stimulus with particular level of noise compared to receiving the stimulus alone [71]. As for tRNS, this framework views the week-current applied via stimulation as the introduced noise and activations of a network of neurons responsible for executing a specific process or function as the state of the signal, and their interaction may in part can explain several cases of facilitatory or inhibitory effects of stimulation [106, 296, 398].

1.2.4 Clinical Research Findings on PD using tES

Despite the field of tES has expanded rapidly over the last decades, most therapeutic studies in PD have applied rTMS, and tES remains a prospective therapeutic tool [28]. A summary of literature reviews on tES studies in PD is provided in Table 1.1. Ten tDCS studies reported therapeutic effects on motor and cognitive functions in PD and three tACS studies reported modulatory effects on cortico-muscular couplings. No tRNS study was found with respect to PD.

1.2.5 Challenges and Open Questions

To understand the neurophysiological mechanisms and ongoing effects of NIBS, it is necessary to monitor the changes in the brain activity using neuroimaging techniques. EEG and magnetoencephalography (MEG) are two most widely used neuroimaging techniques with NIBS, and to date electrophysiological changes in the brain have mostly been investigated by comparing the recordings before and after stimulation due to the strong artifact that

Table 1.1: A summary of tES research on PD

Type	[1]Methods	Current Intensity	Duration	[2]N	Outcome	Year (Ref.)
DC	A: premotor C: mastoids	2 mA	20 min (8 sessions within 2.5 weeks)	25 PD	- Improved gait and bradykinesia - No effect on UPDRS, reaction time, physical and mental wellbeing, self-assessed mobility	2010 [29]
DC	A: motor C: orbitofrontal	2 mA	20 min (5 consecutive days)	10 PD	- Improved total and motor UPDRS scores, FOG-Q and Gait and Falls Questionnaire scores	2014 [395]
DC	A: DLPFC C: supraorbital	2 mA	20 min	18 PD	- Improved accuracy in working memory task	2006 [38]
DC	A: DLPFC C: supraorbital	2 mA	20 min	16 PD	- Enhanced verbal fluency - Improved phonemic fluency task	2013 [287]
DC	A: DLPFC C: supraorbital	2 mA	20 min (10 sessions over 2 weeks)	18 PD	- Improved executive function	2014 [92]
DC	A: DLPFC C: supraorbital	2 mA	7 min	10 PD	- Improved locomotor performance	2014 [230]
DC	A: M1 C: supraorbital	1 mA	20 min	17 PD	- Improved UPDRS, simple reaction time, motor-evoked potential	2006 [114]
DC	A: right M1 C: left M1	2 mA	25 min	10 PD 15 H	- Decreased noise in arm movement - Increased willingness to exert effort	2015 [329]
DC	A: Cerebellar or M1 C: deltoid muscle	2 mA	20 min (5 consecutive days)	9 PD	- Decreased UPDRS IV (dyskinesias section) score	2016 [105]
AC	20 Hz at M1	1 mA	15 min	10 PD 10 H	- Decreased cortico-muscular coupling in 13–30 Hz	2014 [189]
AC	77.5 Hz at frontal area	15 mA	45 min (10 sessions over 2 weeks)	23 PD	- Insignificant changes in UPDRS compared with sham - Significant changes in UPDRS from baseline	2011 [348]
AC	Individual tremor frequency at cerebellum	2 mA	up to 10 min	24 PD 21 ET	- Intrained tremor phase to stimulation	2015 [45]
AC	Individual tremor frequency at M1	2 mA	10 min	14 PD	- Average 50% reduction in tremor amplitude	2013 [151]

[1]A and C denote anode and cathode, respectively
[2]PD: Parkinson's disease, H: healthy, ET: essential tremor

NIBS produces in both EEG and MEG recordings during the stimulation [151, 249, 381]. In fact, these stimulation artifacts can be up to 3 orders of magnitude larger than normal brain signal, completely obscuring EEG and MEG signals. In addition, the delivered current can undergo possibly non-stationary transformation, causing the morphology of stimulation artifacts in EEG and MEG recordings do not exactly match the delivered currents at the stimulation electrodes, making it even more technically challenging to remove the artifacts. For example, tACS stimulation with a single sinusoidal wave generates EEG and MEG artifacts with the same frequency but time-varying amplitudes and shifted phases [268, 269]. A thorough characterization of the stimulation artifacts and development of effective denoising methods are required to address these issues.

One crucial unresolved issue is the question as to whether tES protocols elicit their strongest effects under the electrodes. Due to the high conductivity of the skin compared to the skull, most of the stimulation current runs through the skin and only a small fraction of the applied current actually reaches the brain. This leads to not only a decrease in the effectiveness of the stimulation (as one can only endure so much high intensity of the current) but also focality of the stimulation. This poor spatial resolution can be improved at the expense of intensity by optimizing the arrangement of stimulating electrodes using details of a subjects anatomy and computer stimulations [91, 323], which is currently an active area of research.

The effects of stimulation are rather heterogeneous and there is a lack of replicability across studies, raising concerns with regard to the validity and reproducibility of the results [151]. This is partially attributed to large options for stimulation parameter selection including stimulation frequency, intensity and electrode montage, leading to a lack of consistency in stimulation protocols adopted in each study. Moreover, a range of cognitive and behaviour tasks used and study populations add to the variation of stimulation outcomes. Other part of this heterogeneity may be explained by poor focality of the NIBS and intersubject variability at baseline that are not accounted in the study. Therefore, continuous efforts such as providing rationales for selected stimulation protocols, conducting replication studies, and identifying factors for heterogeneous results are recommended for future NIBS studies.

Although remarkable progress in the understanding of NIBS has been made, mechanisms that could explain the stimulation effects still remain largely unknown and each model proposed to date provides conceptualization and explanation of the observed phenomenon from a slightly different point of view [106]. Underlying mechanisms are likely explained when inte-

grating the different concepts rather than a single explanation. New theoretical models are currently being actively developed based on experimental evidence and computational simulations.

1.3 Electrical Vestibular Stimulation (EVS)

1.3.1 Background

Electrical Vestibular Stimulation (EVS) is a NIBS technique where electrical current is applied to the mastoid process behind the ear to alter the firing rates of the vestibular afferents. Stimulation of vestibular nerves by EVS ultimately influences the activity in various cortical and subcortical areas related to the vestibular network and multisensory processing including the prefrontal cortex, premotor region, somatosensory cortex, posterior parietal cortex, intraparietal sulcus, inferior parietal lobule, temporo-parietal junction, insula, hippocampus, and putamen. While the mechanisms are not fully established, it has been proposed that EVS activates these regions based on the broadly distributed thalamocortical fibres distributed throughout numerous brain regions [221].

EVS has many advantages as an investigative and potential therapeutic approach. Different from tDCS/tACS where it is currently difficult to know which brain regions the externally applied electrical current is delivered [325], EVS bypasses the vestibular end organ and acts directly at the spike trigger zone of the afferent nerve [111, 128]. Because EVS allows for the delivery of precise levels of applied electrical current, it is well-suited for subliminal stimulation so that the subject is unaware that they are receiving *verum* or *sham* stimulation, often precluding the additional requirements of trials to control for the placebo effect in clinical studies. Furthermore, the low currents typically involved suggest the feasibility of battery-powered, portable stimulation. In comparison to other means of vestibular stimulation, such as caloric, EVS does not commonly induce adverse side effects such as seizures, vertigo or nausea; however, symptoms of tingling and slight itching underneath the electrodes have been reported [393].

The results of EVS are varied and complex, reflecting the complex role of the vestibular system. While the primary induced physiological responses from EVS are gaze stabilization, posture and balance maintenance and self-motion perception, this requires integration of visual, proprioceptive and somatosensory information from the earliest thalamic stage to cortical network interactions [75]. As a result, the vestibular system has a broad range of functions from reflexes (e.g., vestibulo-ocular and vestibulospinal) to higher

levels of voluntary motor and even cognitive behaviour such as visual memory recall [422, 424] and mental object transformation strategies [209]. Thus, augmenting vestibular input has been investigated for number of conditions, including neuropathic pain [240, 241], tactile extinction [339], and figure copying deficits [423].

1.3.2 The Vestibular System

The vestibular system, consisting of three semicircular canals, saccule, and utricles in the inner ear, is a sensory system that provides the sense of motion, equilibrium, and spatial orientation to the brain. It is different from other senses in that central vestibular processing is highly convergent and multimodal as signals from muscles, joints, skin, and eyes are continuously integrated with vestibular inflow [16]. Because of the features, the vestibular stimulation does not induce a separate and distinct conscious sensation and contributes to a range of functions from simple reflexes to the highest levels of perception and consciousness [16].

Anatomically, the vestibular nerve combines with the cochlear nerve and becomes the vestibulocochlear nerve. Traveling by the cerebellopontine angle, this nerve enters the brainstem at the pontomedullary junction in which the vestibular and cochlear nerves are separated out [173]. Some of the nerve fibers project to the flocculonodular lobe and nearby vermis of the cerebellum while the majority of the fibers projects to the ipsilateral vestibular complex in the pons [173]. The vestibular complex is where vestibular inputs are primarily processed and consists of four major nuclei including medial, superior lateral and inferior [421] and several adjacent cell groups. The vestibular pathways from the vestibular nuclei can be functionally categorized. Projections to the spinal cords are essential for postural reflexes to adjust the head and body movement [167], and projections to the ocular motor nuclei are critical for compensatory eye movements during head motion (i.e., vestibular-ocular reflex). Projections to the cerebellum are important for balance, postural control, and movement coordination [173], and the pathways to the thalamus, hippocampus and ultimately to the cortical areas are responsible for multisensory integration [368, 421] contributing to movement planning and execution, spatial navigation and memory, attention, and emotions [43, 134, 312, 314, 368].

1.3.3 EVS Effects on PD

Several studies have investigated effects of EVS on postural responses in PD. Compared to a group of age-matched control subjects, PD patients showed no difference in the speed or direction of the body sway response induced by EVS (2 s), but when the patients were subdivided into two groups, the patients with greater postural deficit responded with significantly greater body speed than those with milder postural deficit [283]. In another study, EVS was applied for a longer duration of 20 minutes to PD patients with postural instability and it was found that the instability was reduced after the EVS [171]. Similarly, EVS improved body sway in the anteroposterior and mediolateral directions [277], balance corrections and postural response time after a backward perturbation [330], and anterior bending posture in PD patients [272], suggesting that EVS may be beneficial to balance and posture control in PD. In support of this, a recent rodent study demonstrated that EVS improved balance and motor planning of a 6-hydroxydopamine hemilesioned rat model in the accelerating rod test [331].

EVS has also shown beneficial effects on motor symptoms in PD. Yamamoto and colleagues [432] demonstrated that EVS ameliorated autonomic and motoric disturbances and decreased reaction time in Go/NoGo tasks without affecting omission and commission errors. Akinetic symptoms of PD patients were improved after 24-hour EVS [278], and EVS improved motor symptoms of upper and lower extremities as measured in finger tapping task and the Instrumented Timed Up and Go test [174]. Recent evidence that showed EVS induces significant neurochemical changes in the striatum may partially explain mechanisms underlying the motoric effects of EVS [369]. In summary, EVS may possibly carry an effective therapeutic benefit to improve autonomic and voluntary motor responses for PD patients, although rigorous assessments with quantitative motor metrics and demonstrated efficacy beyond that provided by medication are needed.

1.3.4 Stimulation Parameters

Various stimulation parameters including signal types (i.e., DC, AC, or noisy (stochastic)), frequencies, and current intensities have been utilized in EVS studies to elicit neurological or physiological responses of interest (Table 1.2). A large number of EVS studies on PD have been based on noisy stimulation (i.e., randomly varying stimulation currents) [278, 331, 424, 432]. In particular, rather than broadband white noise, pink noise with a $1/f$ type power spectrum (i.e., the power density of the stimulus is inversely

proportional to the frequency) is used, as this reflects the power distribution found in cortical and subcortical functional networks [56]. Similar to tRNS, one of the justifications to explain how the randomly-varying stimuli may provide beneficial effects is a stochastic resonance phenomenon where a sub-threshold random stimulus enhances sensory information processing and perception [257]. For example, 40 Hz responses of the human auditory cortex to auditory stimuli was enhanced when weak noise was added to the stimulus [413]. However, it was recently shown that induced EEG changes from noisy EVS tend to be linearly related to the intensity of the noise level in healthy subjects [177], which may appear inconsistent with stochastic facilitation seen in non-linear systems. A reasonable explanation for this apparent discrepancy is that while stochastic facilitation may be apparent at the level of the individual neuron, collectively at the overall network level, linear responses may prevail although this needs to be further verified.

Taken together, it is clear that comprehensive investigation needs to be done to understand the underlying mechanisms of EVS effects and ultimately maximize clinical effects it can bring. Especially, one crucial component to study would be to design stimuli with properly selected parameters to extract sufficient information of neural responses rather than blindly choosing stimulation parameters as has been done in previous work. As there are literally an infinite number of ways to select stimulation parameters, more rigorous and systematic approaches are warranted.

1.3.5 Multisine Signal

The majority of EVS studies have used general-purpose stimulus such as square-wave pulses and random (white or pink) noise to investigate stimulation effects on vestibular function and corresponding physiological responses. A significant limitation of the stimulation method is relatively small responses induced by these stimuli [81, 110], possibly due to poor excitation of the neurological system. Although greater responses might be induced by higher stimulus amplitudes, the stimulus level is often restricted by the range where subjects feel comfort or nature of the study where subjects need to be blinded from stimulation to avoid the placebo effect. Another limitation of general-purpose signals is that they do not provide enough information of the systems under study and are difficult to set signal parameters to achieve an optimal result.

Multisine signals are optimized test signals utilized most commonly in the field of system identification, which are designed to concentrate power at a precise number of frequencies within the bandwidth of interest. They are

Table 1.2: Effects of varying EVS parameters on physiological responses

Type	Current Intensity	Duration	[1]N	Outcome	Year (Ref.)
DC	0.3, 0.5 mA	8 s	10 H	Increased postural sway with higher current	2003 [414]
DC	0.1-0.9 mA	2 s	10 H	Tilted head and torso toward anodal electrode	1997 [80]
DC	0.7 mA	3-6 s	12 H	Tilt of the body dependent on the timing of stimulation with respect to movement phases	1998 [62]
DC	1.5-3 mA	5 s	12 H	Ocular torsion and rotation of the fovea and peripheral visual field	1997 [438]
DC	0.1-0.9 mA	4 s	6 H	Ocular torsion and horizontal eye movements at higher currents	2003 [346]
DC	2 mA	20 s	6 H	Torsional eye movements	2002 [340]
DC	1.25, 2.5 mA	20 s	14 H	Tilt of the subjective vertical	2001 [232]
DC	0.8-1.2 mA	15 s	8 H	Increased response time for body rotation and illusory sensation of motion of self or visual field	2001 [209]
DC	0.2, 0.5, 0.7 mA	20 min	7 PD	Improved anterior bending posture	2015 [272]
DC	0.7 mA	20 min	5 (5) PD	Reduced postural instability for 3 out of 5 patients with PD with postural instability and/or abnormal axial posture	2001 [171]
DC	Twice of the individual threshold	During task	11 PD	Improved variation of the step duration in gait and improved motor performance in finger tapping task	2018 [174]
AC (0.2, 0.5, ..., 2 Hz)	2 mA	200 cycles (1 min 40 s - 16 min 30 s)	14 H	Postural illusions of 'rocking' or 'swinging' and vestibular modulation of muscle sympathetic nerve activity	2018 [174]
AC (0.2, 0.5, ..., 2 Hz)	2 mA	200 cycles (1 min 40 s - 16 min 30 s)	11 H	Postural illusions of 'rocking' or 'swinging' and increased burst incidence of skin sympathetic nerve activity	2010 [159]
AC (1 Hz) $1/f$ noise (0.1-10 Hz)	90% of individual threshold	5 min	23 PD / 12 H	Increased overall connectivity of Pedunculopontine Nucleus with 10 regions of interest	2018 [57]
Noise (0-1000 Hz)	90% of individual threshold	During task	24 H	Shorter reaction time with the stimulation when answering questions about faces	2008 [424]

Type	Current Intensity	Duration	[1]N	Outcome	Year (Ref.)
Noise (frequency is not reported)	0.5-1.5 mA	25 min (1-5 sessions)	49 H	Improved hemispatial neglect	2004 [425]
$1/f$ Noise (0.1-10 Hz)	90% of individual threshold	72 s	10 H	A mild suppression of gamma power in lateral regions / Increased beta and gamma power in frontal regions	2013 [177]
$1/f$ Noise (0.01-2 Hz)	60% of individual threshold	24 h	12 H / 7 MSA	Improved autonomic system regulation / Decreased reaction time to visual cue	2005 [432]
$1/f$ Noise (0.01-2 Hz)	0.09-0.49 mA	24 h	8 (8) MSA / 3 PD / 2 CCA / 1 PA	Improved motor function in patients with PD	2008 [278]
$1/f$ (frequency is not reported)	0.1, 0.3, 0.5 mA	26 s	5 PD / 20 H	Decreased body sway with eyes closed	2009 [277]
White noise (0-30 Hz)	Below individual threshold	< 3 h	10 PD	Improved balance corrections after a backward perturbation, shorted the postural response time	2015 [330]
White noise (frequency is not reported)	70 % of individual threshold	60 s	13 PD / 12 H	Changes in posture and increased sway amplitude and mildly decreased sway frequency	2018 [384]

[1]PD: Parkinson's disease, H: Healthy, MSA: multi system atrophy, CCA: cortical cerebellar atrophy, PA: pure akinesia

advantageous to target specific components of the responses, enable considerable reduction of the measurement time without unwanted loss of accuracy, and can be used to detect and quantify the presence of nonlinear distortions in the system. With the properties, the multisine signals are considered to be advanced test signals than general-purpose excitation signals such as the swept sine (also called periodic chirp) or random noise that are applied to the system without any optimization aside from selecting the bandwidth of the excitation signal [294]. Multisine signals are composed of sinusoids with period equal to (or integer ratios of) the observation time, which keeps excitation power as low as possible outside frequencies of interest avoiding unnecessary nonlinear effects [353]. Further optimization is done by choosing the frequency phases such that the crest factor (CF), defined below, of

the signal to be minimized [294, 341, 342]:

$$CF = \frac{max\,|I_{stim}(t)|}{RMS_{I_{stim}}} \tag{1.1}$$

where RMS_I is the RMS of the applied current $I_{stim}(t)$.

It is advantageous to excite the system with the optimized multisines as the signals with a large CF inject much less power into the system than those having the same peak value and a small CF [294].

Multisine Signals for EVS

Multisine signals for EVS were designed through two steps, the first being the selection of a period (i.e., frequency resolution) as well as a frequency band of interest followed by a crest factor minimization of the signals in the second step. The 4–200 Hz frequency band was chosen as it includes the range human EEG responses [150]. The CF of all multisine EVS was minimized using a clipping algorithm, an iterative method developed in [400, 401] to optimize the phases. The basic idea behind this method is illustrated in Fig. 1.3. With the specified amplitude spectrum, the iteration procedure starts with arbitrary phases and a discrete time-domain signal is calculated by the inverse Fourier transform. All the values larger than a given maximum is clipped off to generate a new time signal whose spectrum and phases are calculated using the FFT. These new phases are retained as a first approximation to the solution [294], but the amplitude spectrum is rejected in favor of the original one.

In this dissertation, all multisine signals were designed to have a period of 5 s [113], providing a frequency resolution of 0.2 Hz. Seven kinds of multisine stimuli were designed over the frequency range from 4 to 200 Hz (Table 1.3). The division of the frequency bands between 4–50 Hz refers to canonical EEG frequency bands.

Table 1.3: Seven multisine stimuli and corresponding frequency bandwidths

Multisine Stimulus	1	2	3	4	5	6	7
Frequency (Hz)	4–8	8–13	13–30	30–50	50–100	100–150	150–200

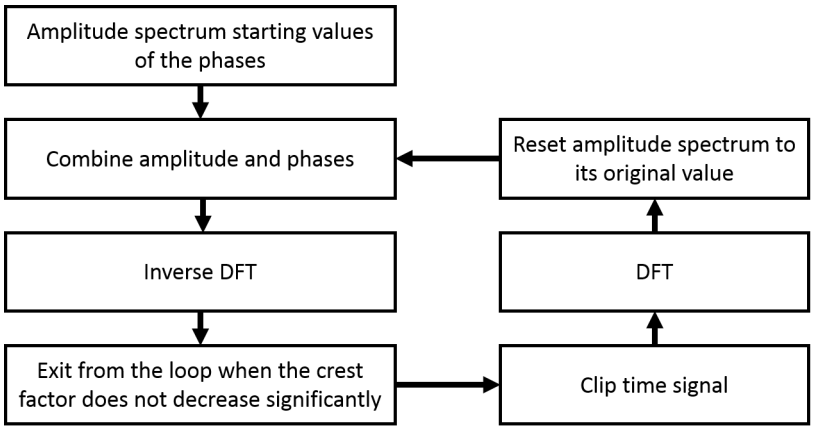

Figure 1.3: Clipping algorithm for minimizing crest factor of multisine signals [294]

1.4 Research Objectives and Thesis Outline

1.4.1 Research objectives

The therapeutic potential of EVS has been demonstrated in previous studies – even with applying relatively simple stimuli such as DC or random noise – by showing voluntary motor and postural responses in people with PD. However, despite many years of the research, there is a huge lack of 1) understanding of the relations between stimulation parameters and resultant behaviour responses in PD and 2) brain imaging studies that can provide insight into underlying neurological mechanism of EVS effects.

The goal of this dissertation is to advance application of EVS as a potential therapeutic intervention for PD through development of novel stimuli and thorough investigation of neuronal and behaviour effects by utilizing behaviour tasks and brain imaging modalities including EEG and functional MRI (fMRI). This research will particularly investigate subthreshold EVS effects so that it could provide the foundation for a safe, non-invasive, and ultimately portable ancillary therapy for PD patients, focusing on the following objectives:

- **Objective 1. Development of new EVS stimuli and design of experiment**: The first objective is to design new stimulus candidates that can systematically provide information on the effects of stimulation parameters on brain activities. As mentioned above, multisine signals have advantages as exogenous input signals to perturb a system (i.e., the brain) over random noise and single-frequency sinusoids.

Multisine signals in distinct frequency bands are proposed as stimulus candidates (see 1.3.5 for details). As a non-invasive brain imaging modality, EEG has merits that it can measure the brains electrical activity with high temporal resolution (a millisecond) and is relatively inexpensive compared with other technologies and is simple to operate. Thus, EEG is proposed as a primary modality to monitor brain activities before, during and after EVS. Experiments are designed to investigate brain responses to EVS 1) when subjects are resting and 2) when subjects are performing a motor task. Motor task performance of the subjects is used as behavioural outcomes from the EVS. Finally, fMRI is utilized as a primary brain imaging modality to investigate mechanism of EVS as it can measure brain activities (hemodynamic responses) with excellent spatial resolution.

- **Objective 2. Detection of PD-related features in the EEG and fMRI data**: A two-step approach is proposed to evaluate EVS effects in PD patients. The first step is to identify PD-related features in the EEG and fMRI data collected in the pre-EVS condition (i.e., before applying EVS). To do this, it is proposed to collect the data from PD and healthy subjects and extract features to discriminate brain activity of the two groups (e.g., functional connectivity). For the PD group, the data are collected in off- and on-medication conditions in order to compare effects of each of the EVS and medication interventions and their interactions in PD. Following successful identification of the PD-related features, the second step is to assess modulatory effects of EVS on the features (Objective 3).

- **Objective 3. Establishment of the extent that EVS modulates the PD features and improves motor performance**: The effects of EVS on the identified PD features are investigated focusing on addressing the following questions:

  - Is the stimulation able to normalize PD features?
  - How do the stimulation effects vary according to stimulation parameters?
  - Are there any differences between online- and after- effects of the simulation?
  - Are there group-specific effects (i.e., PD vs. healthy controls)?
  - Is the stimulation able to induce significant improvement in motor behaviour of the PD patients? How do the downstream behaviour

outcomes relate to stimulation-induced changes in the brain?

- **Objective 4. Development of a new method to remove stimulation artifacts in EEG**: High-voltage electrical artifacts in EEG generated by brain stimulation have been a major challenge to date for analyzing online effects of stimulation (during stimulation) on brain activities, which is critical to probe fundamental mechanisms underlying stimulation effects. Most studies have resorted to avoiding the artifact problem by simply comparing the EEG in pre- and post-stimulation condition. A solution is proposed to resolve the artifact issue by developing a novel denoising method utilizing joint blind source separation methods.

- **Objective 5. Probing fundamental mechanisms of action through which EVS improves motor performance**: Noisy EVS has shown its efficacy to improve motor symptoms and postural responses in PD in prior studies, but the mechanisms of these effects are largely unknown. To probe these fundamental mechanisms, it is proposed to analyze resting-state fMRI data acquired during noisy EVS from PD patients and healthy controls, focusing on the thalamus, a hub of integrating multisensory information and mediating functional networks [156]. The thalamus is of interest in particular based on the direct afferent projections from the vestibular nuclei and it's close relationships with the BG.

1.4.2 Thesis Outline

The rest of this dissertation is subdivided into six chapters as outlined below:

Chapter 2: Discriminant Feature Detection in Manual Tracking Behaviours in PD and Effects of Noisy EVS

In this chapter, effects of noisy EVS (0.1–10 Hz) on the manual tracking behaviours of PD and healthy subjects who performed a visuomotor joystick tracking task. Exploratory (linear discriminant analysis with bootstrapping) and confirmatory (robust multivariate linear regression) methods are used to determine if the presence of EVS significantly affected prediction of cursor position based on target variables, and signal-to-noise ratio of cursor trajectories is computed to quantify smoothness of tracking movement. The results show that noisy EVS resulted in robust changes in tracking, mostly related to increased sensitivity to perceived error.

Chapter 3: Quadrature Regression and IVA Approach to Removal of High-voltage EVS Artifacts from Simultaneous EEG Recordings

This chapter describes the technical difficulties associated with removing artifacts in EEG that are induced by electrical brain stimulation and limitations of conventional denoising methods. Quadrature regression and subsequent independent vector analysis (q-IVA) method is proposed for removing the stimulation artifacts and applied to simulated and real EEG datasets recorded from ten subjects who received 4–8 Hz multisine EVS. It is demonstrated that q-IVA significantly improves the denoising and robustly recovers the EEG compared to conventional methods (principal component analysis, independent component analysis) and other joint blind source separation approach (multiset canonical correlation analysis and independent vector analysis). The results provide a promising way to effectively isolate simulation artifacts in EEG, paving the way for future studies attempting to uncover ongoing modulation of brain activity *during* electrical brain stimulation.

Chapter 4: Sparse Discriminant Analysis for Detection of Pathological Dynamic Features of Cortical Phase Synchronizations in PD

In this chapter, altered cortical functional coupling in PD is identified using resting-state EEG data and effects of multisine EVS at 4–8 Hz, 50–100 Hz, and 100–150 Hz are examined. Phase locking value (PLV), a nonlinear measure of pairwise functional connectivity between electrodes, is computed over sliding windows and the mean, variability and sample entropy are extracted as dynamical features of the functional connectivity. To extract most discriminant features from the high-dimensional data sets, sparse discriminant analysis is utilized. It is demonstrated that lower PLV variability and entropy in PD compared to healthy controls is normalized by EVS in a stimulus-dependent manner, suggesting that EVS with optimized parameters may provide a new non-invasive means for neuromodulation of functional brain networks.

Chapter 5: Discriminant Correlation Approach to Joint Estimation of Maximal EVS Effects on Motor Behaviour and Cortical Beta Oscillations in PD

Using EVS and simultaneously recorded EEG, this chapter demonstrates the modulatory effects of high-frequency (50–100 Hz and 100–150 Hz, respectively) multisine EVS on movement-related beta desynchronizations (beta

ERD) and resultant changes in the motor behaviour of PD and healthy subjects who performed a motor squeeze task. In order to investigate maximal EVS effects across the subjects with regard to the task performance and the beta ERD, discriminant correlation analysis, a feature fusion method, is used. It is demonstrated that EVS modulates the magnitude and timing of beta ERD in left motor, broad frontal and medial parietal regions during performance of the motor task. The beta power in the rest period, when the subjects were not engaged in the motor task, was not significantly affected by EVS. This joint EEG/behavioural analysis suggests a potential neurophysiological mechanism of EVS in motor improvement, whereby vestibular input is integrated in the motor thalamus, increasing fluidity to a motor system stuck in a state of exaggerated beta rhythms. The results complement previous studies suggesting pathological beta-band oscillations in PD can be disrupted via different stimulation sites, including ones available non-invasively, and emphasize the importance of stimulation parameters for influencing motor behaviour.

Chapter 6: Spectral Clustering and Discriminant Correlation Approach to Estimation of EVS Effects on Functional Thalamic Subregions and BG–thalamic Connectivity in PD—fMRI Study

Pathologic changes within the thalamus itself and its functional interactions with the BG leads to altered cortical-BG-thalamo activity responsible for motor and cognitive dysfunction in PD. As the thalamus receives direct projections from the vestibular nuclei, it may possible to modulate thalamic activity and connectivity with the BG by activating vestibular system afferents with EVS. This chapter probes EVS effects on the thalamus using resting-state fMRI data acquired from PD and healthy subjects to elucidate a potential mechanism of EVS associated with motor improvements in PD. To determine the region-specific EVS effects on the thalamus, normalized cut spectral clustering is used to parcellate the thalamus into subregions and discriminant correlation analysis is applied to investigate functional connectivity between the thalamus subregions and BG structures. The results show that EVS normalizes altered sizes of the functional thalamic subregions, reduces excessive connectivity between the right thalamic subregions, and improves aberrant asymmetry of the connectivity between left BG and bilateral thalami in the PD subjects.

Chapter 7: Conclusion and Future Work

This chapter includes a short of summary of the dissertation followed by a discussion on the limitations of the proposed methods and suggestions for future work.

Chapter 2

Discriminant Feature Detection in Manual Tracking Behaviours in PD and Effects of Noisy EVS

In this chapter, we investigated effects of noisy EVS (0.1–10 Hz) on the manual tracking behaviour of PD and healthy subjects. Noisy EVS has been recently used in prior PD studies to assess effects on motor symptoms and has positive influences on balance and simple motor task performance. Here, we implemented a visuomotor joystick tracking task to assess effects of noisy EVS on more complicated motor behaviours that require sensorimotor processing and fine motor coordination.

2.1 Introduction

Motor symptoms in PD characteristically manifest themselves as tremor, rigidity, akinesia/bradykinesia and postural instability. While levodopa is the gold standard treatment for PD, chronic use eventually leads to the long-term development of side effects, such as motor fluctuations, dyskinesias and psychiatric disorders [302, 418]. Surgical treatments, including DBS targeted to subcortical nuclei, have provided effective therapeutic benefits, but are complex and invasive [273]. With recent technological advances, numerous novel stimulatory techniques for PD treatment are presently being explored [101, 118, 331, 379]. Non-invasive brain stimulation techniques are currently a growing avenue of interest for PD and other neurological disorders due to their safety, tolerability and minimally invasive nature [115]. Additionally, these methods, such as transcranial current brain stimulation (tCS), arguably influence solely the targeted site of stimulation, but also exert effects on associated brain connectivity patterns [224]. Since PD is characterized by abnormally exaggerated beta synchronization throughout

a BG-cortical network [100], non-invasive stimulatory approaches could potentially be used to modulate aberrant network dynamics [115].

A few studies have suggested that non-invasive stimulation of vestibular nerves via noisy EVS may improve motor deficits in PD [277, 278, 331, 432]. Noisy EVS delivers currents with randomly varying amplitudes in time to vestibular afferents and subsequently influences resting state cortical EEG activity, suggesting that cortical-subcortical connections are also modulated by EVS [177]. Akin to how tCS strengthens connectivity patterns in premotor, motor and sensorimotor areas while subjects are engaged in a finger tapping task [299], noisy EVS hypothetically is also able to influence functional BG-cortical motor networks depending on the brain state during stimulation. It is not fully established, however, whether noisy EVS improves motor performance. Yamamoto et al. [432] measured trunk dynamics as well as reaction time in a Go/NoGo paradigm whereas Pan et al. [278] measured wrist activity in akinetic PD patients. Effects of noisy EVS on postural and balance responses have also been measured in both humans and rat models [277, 331], although none of these studies have directly investigated the effects of EVS on bradykinesia with respect to motor coordination and sensorimotor processing.

One potential way to rigorously assess the motoric effect of EVS is to utilize a visuomotor task, which is useful for understanding mechanisms that contribute to motor coordination with accuracy and stability [324]. Corrective movements and behavior are required in response to varying visual error feedback, which are important for maintaining effective perception-action or sensorimotor processing [324]. With respect to clinical significance, the ability to continually adapt ones behavior to changing environmental or sensory stimuli is particularly relevant in PD as these patients demonstrate impaired switching between motor paradigms [97].

In the present study, we implemented a visuomotor tracking task and investigated the effect of noisy EVS on motor performance. Our visuomotor task required subjects to respond to visual error feedback that was, unbeknownst to the subjects, either minimized to 30% of the actual error, or amplified by 200% to create the appearance of Better or Worse motor performance, respectively. We used linear discriminant analysis (LDA) [96] to identify parameters significantly influenced by EVS and to investigate if the effects of EVS are dependent on the task conditions. We then analyzed our data using a robust multivariate linear regression method [108] to test if tracking movement was affected by EVS. We show that subthreshold EVS resulted in robust changes in tracking, mostly related to increased sensitivity to perceived error.

2.2 Materials and Methods

2.2.1 Subjects

12 PD subjects (10 males, 2 females; mean age 61.4 ± 6.5 years; 11 right-handed, 1 left-handed) participated in the study. None of the participants had any reported vestibular or auditory disorders. All PD subjects were recruited from the Pacific Parkinsons Research Centre (Vancouver, Canada). PD subjects had mild to moderate disease severity (Hoehn & Yahr stages 1.5–2.5) with UPDRS (Unified Parkinsons Disease Rating Scale) Part III motor scores at a mean of 22.3 ± 7.8 (Table 2.1). All PD subjects were tested in the off-medicated state after a 12-hour overnight withdrawal from L-dopa medication. Other medications that some subjects were on included: amantadine, ramapril and atorvastatin.

Table 2.1: Demographical data of the PD subjects

Patient number	**Age (Year)**	**Sex**	**Duration (year)**	**UPDRS III**	**Hoehn & Yahr**	**Handedness**
1	58	M	4	18	2	R
2	64	F	4	12	1.5	R
3	67	M	4	16	2	R
4	56	M	2.5	21	2	L
5	53	M	3	32	2.5	R
6	49	M	7.5	35	2	R
7	65	F	5	32	2	R
8	68	M	1.5	22	2	R
9	66	M	1	24	2	R
10	70	M	1	21	2	R
11	59	M	1.5	10	2	R
12	62	M	3.5	24	2	R

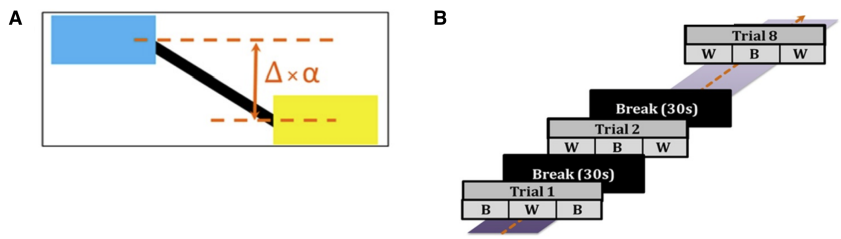

Figure 2.1: Behaviour Task. (A) Subjects faced a screen with a target (blue) that moved vertically up and down, and controlled a cursor (yellow) using a joystick. The error difference (Δ) between the actual positions of the target and cursor was amplified by a scaling factor (α): $\Delta \times \alpha$ = displayed visual error feedback (B) Trials (90 s) alternated between 'Better (B)' and 'Worse (W)' conditions.

2.2.2 Ethics Statement

The study was approved by the University of British Columbia Clinical Research Ethics Board. All subjects gave written, informed consent prior to participation. Research was conducted according to the principles expressed in the Declaration of Helsinki.

2.2.3 Visuomotor Tracking Task

Subjects were comfortably seated 80 cm in front of a screen and performed a manual tracking task. On the screen, a target (blue) and cursor (yellow) connected by a black horizontal rod were displayed (Fig. 2.1). The target box oscillated vertically up and down with the summation of two frequencies (0.06 and 0.1 Hz). Subjects controlled the cursor using a joystick with the objective of matching the horizontal position of the cursor to the target – i.e., to keep the horizontal black rod straight. The tracking error (Δ, difference between the actual positions of the target and cursor) was scaled by a factor (α) to determine the displayed position of the cursor: $\Delta \times \alpha$ = displayed visual error feedback. In the 'Better (B)' task condition, α was set to 0.3, and in the 'Worse (W)' task condition, α was set to 2, such that it artificially appeared to subjects that they performed better or worse, respectively, based on their scaled error feedback.

During the experiment, subjects performed a total of 8 trials. Each trial (90 s) was comprised of three alternating blocks (30 s each) of B and W conditions – with Trial 1 ordered as B-W-B and Trial 2 ordered as W-B-W (Fig. 2.1). During each trial, either a subthreshold *verum* current (90%

of cutaneous sensory threshold) or *sham* current stimulation was delivered. Four trials contained *verum* EVS delivery whereas the other four trials contained *sham* stimulation. Subjects were unaware of either *verum* or *sham* stimulation since the order in which stimuli were delivered was pseudorandom, and the *verum* stimulation was imperceptible to the subject. Each trial was followed by a break (30 s) to preclude a hysteretic effect carrying over to the next trial. Before starting the experiment, subjects were allowed to practice tracking the target and using the joystick as needed in at least one practice trial. Due to technical details of the data capture system, the cursor position was irregularly sampled at ∼55 Hz. We then resampled the data at exactly 50 Hz using linear interpolation before further analyses.

2.2.4 Stimulus

EVS was delivered to subjects through carbon rubber electrodes (17 cm^2) in a bilateral, bipolar fashion. For bilateral stimulation, an electrode was placed over the mastoid process behind each ear, and coated with Tac gel (Pharmaceutical Innovations, NJ, USA) to optimize conductivity and adhesiveness. The average impedance of the subjects was measured around 1 $k\Omega$. Digital signals were generated on a computer using MATLAB and converted to analog signals via a NI USB-6221 BNC digital acquisition module (National Instruments, TX, USA). The analog command voltage signals were subsequently passed to a constant current stimulator (Model DS5, Digitimer, Hertfordshire, UK), which was connected to the stimulating electrodes.

Bipolar stimulation signals were zero-mean, linearly detrended, noisy currents with a $1/f$-type power spectrum (pink noise) as previously applied to PD and healthy subjects [278, 357, 432]. The stimulation signal was generated between 0.1–10 Hz with a Gaussian probability density, with the command signal delivered to the constant-current amplifier at 60 Hz (Fig. 2.2). The stimulus was applied at an imperceptible level to avoid effects by general arousal and/or voluntary selective attention, with the current level individually determined according to each subjects cutaneous sensory threshold.

Since perception of EVS is inherently subjective, we utilized systematic procedures that have been previously used in determining subliminal current levels for both EVS and transcranial stimuli [154, 393, 422]. Starting from a basal current level of 0.02 mA, noisy test stimuli were delivered for 20 s periods with gradual stepwise increases (0.02 mA) in current intensity until subjects perceived a mild, local tingling in the area of the stimulating electrodes. As performed previously, a threshold value was defined once

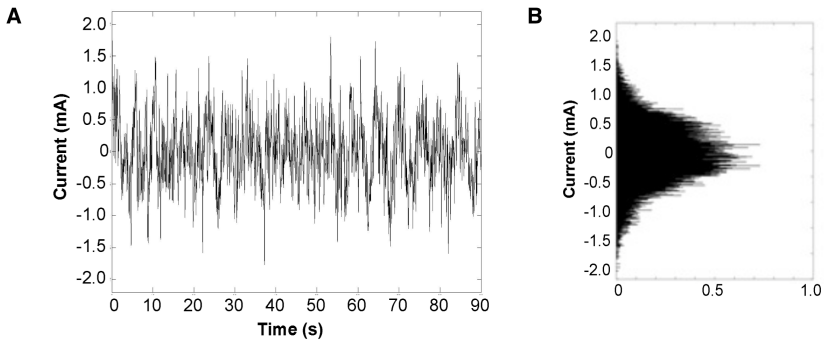

Figure 2.2: Characteristics of the stimulus. (A) Typical recording from a subject receiving a noisy stimulus applied for 90 s duration. The stimulus presented is at the highest current intensity (current level 6), which is set to 90% of the subjects individual sensory threshold (RMS current value of 0.266 mA). (B) Probability density function of the stimulus current follows a Gaussian distribution.

subjects reported a tingling sensation [393, 422], which lasted for the duration of the test stimulus. The current level was then decreased each time by one level until sensation was no longer reported during delivery of test stimulus pulses, and increased by one step in current intensity to confirm threshold. Each delivery of a test stimulus was followed by a period of no stimulation for at least 30 s to preclude a hysteretic effect carrying over to the next test stimulus. Subjects were blind to the onset and duration of test stimuli, as well as the threshold-testing scheme. After completing the threshold test and throughout the experiment, stimuli were delivered at subthreshold intensity (0.19–0.90 mA), which is achieved at 90% of the determined cutaneous sensory threshold value.

2.2.5 Behavioural Data Analysis

We employed both exploratory and hypothesis-driven analysis methods to analyze the behavioral data. We initially analyzed the data on a subject-by-subject basis as we were unclear whether or not there would be substantial intersubject variability to EVS response. LDA was first used to see if tracking behavior could be reliably discriminated depending upon whether EVS was applied or not. We derived a EVS linear discrimination function, $g(X)$, to create maximum separation between means of the projected classes with

minimum variance within each projected class:

$$g(X) = w_1X_1 + w_2X_2 + ... + w_{21}X_{21} + \omega_0 = w^tX^t + \omega_0 \tag{2.1}$$

where $X = [X_1\ X_2\ ...\ X_{21}] \in \mathbb{R}^{n\times d}$ is a data matrix of n d-dimensional samples in which each column represents an independent variable, w= $[w_1,\ w_2,\ ...,\ w_{21}] \in \mathbb{R}^{d\times 1}$ the weight vector containing linear coefficients of the variables in the data matrix X, and ω_0 the bias-weight. LDA was applied to the "Better" and "Worse" conditions separately.

For this exploratory part of the analysis, we included linear (first-order) and non-linear (second- and third-order) combinations of variables in the EVS discriminant function (Table 2.2). During the experiment, we varied the phase of the initial target trajectory not only between subjects but also between the trials to prevent the subjects from easily predicting upcoming target movement. Therefore, variables from X_1 to X_9 were included as nuisance variables in the LDA to account for the target differences.

Table 2.2: Variables in LDA model

Notation	**Variables**[1]
X_1, X_2, X_3	$T(t)$, $T(t)^2$, $T(t)^3$
X_4, X_5, X_6	$V_T(t)$, $V_T(t)^2$, $V_T(t)^3$
X_7, X_8, X_9	$A_T(t)$, $A_T(t)^2$, $A_T(t)^3$
X_{10}, X_{11}, X_{12}	$D(t) - T(t)$, $\{D(t) - T(t)\}^2$, $\{D(t) - T(t)\}^3$
X_{13}, X_{14}, X_{15}	$V_D(t) - V_T(t)$, $\{V_D(t) - V_T(t)\}^2$, $\{V_D(t) - V_T(t)\}^3$
X_{16}, X_{17}, X_{18}	$D(t+\Delta t) - D(t)$, $\{D(t+\Delta t) - D(t)\}^2$, $\{D(t+\Delta t) - D(t)\}^3$
X_{19}, X_{20}, X_{21}	$V_D(t+\Delta t) - V_D(t)$, $\{V_D(t+\Delta t) - V_D(t)\}^2$, $\{V_D(t+\Delta t) - V_D(t)\}^3$

[1] T=target position, V_T=target velocity, A_T=target acceleration, D=displayed cursor position, V_D=displayed cursor velocity, t=time index, and Δt=reaction delay of 0.5 s [168]

To test for significance of the LDA results, we employed bootstrapping techniques. We permuted the EVS labels (on/off) and then re-computed the LDA function with the permuted data. This was repeated 1000 times. Any weight value from the original LDA function $g(X)$ whose absolute value

was greater than all the weights computed from the permuted data was considered to be significantly influenced by EVS.

In addition, a multivariate linear regression model was used to test the hypothesis that EVS had a significant effect on cursor position during tracking. As the traditional least squares regression may be sensitive to noisy and gross errors [5], we chose a robust regression method to analyze our data ("robustfit" function in MATLAB). This method is known to be robust to outliers utilizing an iteratively reweighted scheme to deweight the influences of outliers. With cursor position as a response variable (Y_i), the following regression model was proposed:

$$Y_i = A_i\beta + \epsilon_i \tag{2.2}$$

where for each data point i we have the vector of independent variables $A_i = [A_{i1}, ..., A_{i5}]$, the vector of regression coefficients β solved by a bisquare weighting function, and the residual ϵ_i (assumed to be independent and identically distributed Gaussian). The selected independent variables are summarized in Table 2.3 (note that A_1, A_2 and A_3 are same as the variables X_1, X_4 and X_{10} in Eq. 2.1, respectively). The categorical variable of EVS was denoted with either 0 (EVSoff) or 1 (EVSon). We tested for significance of the coefficients under the null hypothesis that the coefficient estimates were equal to zero.

For a signal-to-noise ratio (SNR) analysis, we utilized "snr" function in MATLAB to calculate SNR of cursor trajectories. This examines the fundamental frequencies of the tracking trajectory plus the next 6 harmonics, and assumes that any power in the spectrum than these peaks are "noise".

Table 2.3: Estimated coefficients in the robust regression model (Eq. 2.2) and the P value

Variables (A)	**Coefficient estimates** ($\boldsymbol{\beta}$)	P **value**
target position (A_1)	1.00	0.0000
target velociy (A_2)	-0.0779	0.0000
displayed cursor position − target position (A_3)	0.501	0.0000
cursor velocity − target velocity (A_4)	-0.0160	0.0002
EVS (A_5)	3.99e-05	0.0410

R^2=0.8811

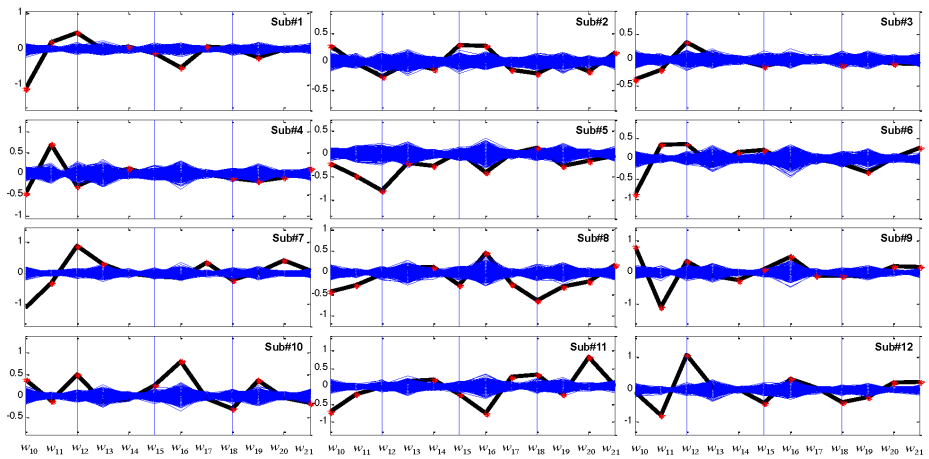

Figure 2.3: Coefficients of the variables of the linear discriminant function in the Worse condition. The x-axis represents variables from X_{10} to X_{21} in Table 2.2 while the y-axis represents weight (w) value. The computed coefficients are depicted as black for the EVS discriminant function and blue for bootstrapping. Red asterisks denote coefficients that are outside the 95% confidence interval of bootstrapping.

2.3 Results

2.3.1 Results of LDA in Worse Condition

Coefficients of EVS discriminant function (Eq. 2.1) were calculated for each subject and are plotted as black lines in Fig. 2.3. For clarity, nuisance variables related to absolute target position (i.e., $X_1 - X_9$) are not shown. The 1000 sets of linear coefficients generated from the bootstrapping are depicted as blue lines. In most subjects, the coefficients w_{10}, w_{11} and w_{12} of $g(X)$ (representing linear and higher powers of the perceived error between the target and the displayed cursor position) were robustly modulated by EVS. In addition, displayed cursor velocity (w_{16} or w_{17}) and acceleration (w_{19}, w_{20} or w_{21}) were also found to be significantly affected by EVS across subjects.

2.3.2 Results of LDA in Better Condition

Fig. 2.4 shows the LDA results in the Better condition. As before, coefficients w_{10}, w_{11} and w_{12} were significant among all the subjects. In addition, 10 out of 12 subjects showed significant w_{18} weightings. Other coefficients were not robustly seen in all subjects. For example, unlike the LDA results

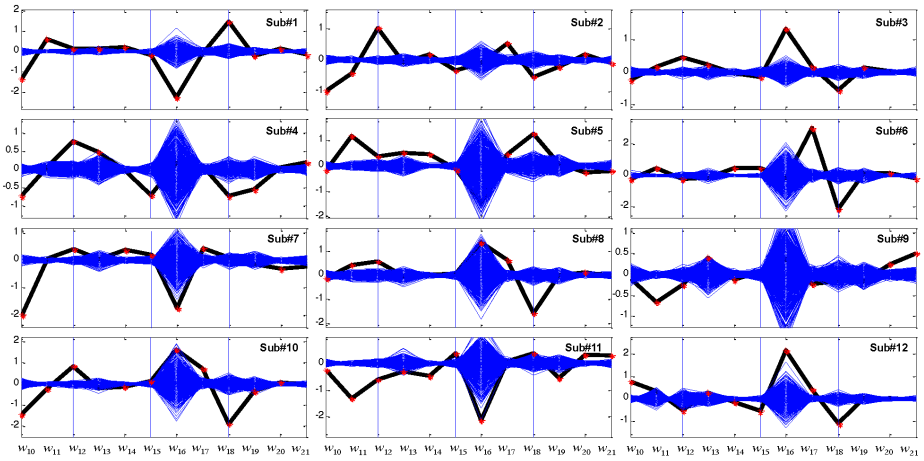

Figure 2.4: Coefficients of the variables of the linear discriminant function in the Better condition. The x-axis represents variables from X_{10} to X_{21} in Table 2.2 while the y-axis represents weight (w) value. The computed coefficients are depicted as black for the EVS discriminant function and blue for bootstrapping. Red asterisks denote coefficients that are outside the 95% confidence interval of bootstrapping.

of the Worse condition, displayed cursor acceleration (w_{19}, w_{20} or w_{21}) was no longer significantly influenced by EVS in the Better condition.

2.3.3 Results of Robust Regression Model

Table 2.3 is the coefficient estimates of the variables of the multivariate regression model (Eq. 2.2) and their P values. The computed R^2 of the regression model was 0.8811. EVS was significantly associated with cursor position across all subjects ($P < 0.05$).

2.3.4 Effect of EVS on Cursor Overshooting

In order to get an intuitive interpretation of EVS effects, we calculated the EVS discriminant function values (Eq. 2.1) for each subject. We used data from trials 1 and 7 for the calculation as these two trials had identical phases of the trajectories, with a difference in whether or not EVS was delivered (EVSon for trial 1). Then, Δg was computed by subtracting the function values of trial 7 from trial 1. By plotting Δg, we could not only locate EVS effects on the cursor trajectory but also directly make visual comparison of the cursor movement in the identified location. Fig. 2.5 shows target

trajectory, cursor trajectory and Δg for each subject.

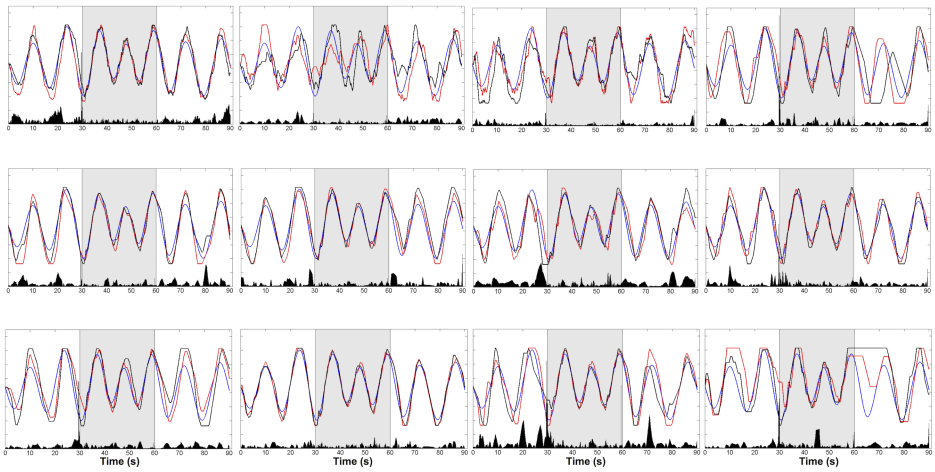

Figure 2.5: Trajectories of target (blue) and cursor (EVSon: red, EVSoff: black) and Δg (black bar in the bottom). Δg was computed by subtracting the linear discriminant function values of trial 7 (EVSoff) from trial 1 (EVSon).The trials alternated between W-B-W conditions (each condition 30 s).

The effect of EVS was greatest near sinusoidal peaks. This trend was found in most of the subjects regardless of how well the subjects tracked the target. For instance, subject 5 tracked the target relatively better compared to the other subjects, and Δg was significant around at 5, 20, 65, and 80 s. Subjects 11 and 12 performed the tracking task poorly, but the EVS effects still appeared near sinusoidal peaks.

One of the noticeable features on the peaks is a degree of overshooting of cursor trajectories. To assess a possible relationship to EVS stimulation, we compared the difference between the cursor position and the target on the peaks. Fig. 2.6 shows a representative example of cursor overshooting near sinusoidal peaks in target. The peaks in cursor appeared with some lagged time (Δt). The amplitude of the target peaks was subtracted from the cursor peaks, and the difference (Δd) was defined as cursor overshooting. Cursor peak was defined when the cursor position was at its max/min point. Cursor overshooting was calculated for all trials and subjects, then averaged depending on the task conditions and presence of EVS stimulation as shown in Table 2.4. The P value was calculated from ANOVA of the means between EVSon and EVSoff (i.e., a single, two-level factor).

In Worse condition, the subjects tended to overshoot significantly less

on the lower peaks while stimulated by EVS. On the upper peaks, the mean overshooting of EVSon was also smaller than EVSoff, but the difference was not significant. In Better condition, however, there was an increasing tendency for cursor overshooting with stimulation.

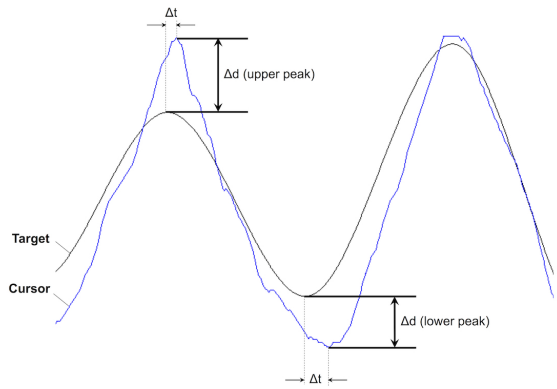

Figure 2.6: Representative example of cursor overshooting on upper and lower peaks from Subject 1. Cursor overshooting (Δd) was calculated as cursor position − target position. Δt represents time difference between peaks in cursor and target trajectories.

Table 2.4: Means of cursor overshooting on sinusoidal peaks and ANOVA results

	Lower peak			**Upper peak**		
	EVSon	**EVSoff**	P **value**	**EVSon**	**EVSoff**	P **value**
Worse	-0.0517	-0.0714	0.0036	0.0695	0.0784	0.22
Better	-0.0946	-0.0451	0.0038	0.0890	0.0690	0.14

2.3.5 Effect of EVS on SNR of Cursor Trajectory

Movement variability is another important feature to characterize the tracking performance. Particularly, in goal-directed behavior, the variability originates from collateral movement to the main goal of a task. In this sense, the cursor trajectories in our tracking test can be seen to a combination of two components. One is the primary movement whose form is similar to the

target trajectory, and the other is submovement that may appear as noise superimposed on the primary movement. In order to investigate if EVS had affected movement variability of the subjects, we calculated SNR of cursor trajectories and compared differences in between EVSon and EVSoff conditions. As shown in Fig. 2.7, the mean SNR of 12 PD subjects was 27.6 when EVS was applied, which was significantly greater than 21.3 in EVSoff condition ($P < 0.05$).

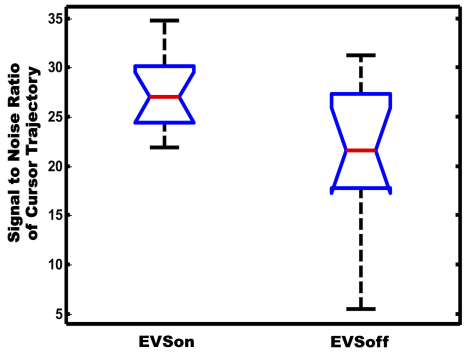

Figure 2.7: Comparison of SNR of cursor trajectories between EVSon and EVSoff conditions.

2.4 Discussion

Our results demonstrate that noisy EVS robustly influences motor tracking performance in PD patients off dopaminergic medication. Motor improvements are consistent with results previously reported in hemiparkinsonian rats [331] whereby EVS with a $1/f$ power density improved rod performance. Previously, we demonstrated that noisy EVS has the ability to modulate synchronization of broadband EEG oscillations in healthy subjects [177]. Our recordings of EEG rhythms were observed at resting-state, suggesting that noisy EVS was able to modulate cortical activity and presumably connected subcortical-cortical projections. In this study, we observed a functional effect of EVS on sensorimotor processing and motor performance in a visuomotor task, suggesting that noisy vestibular stimulation modulates motor networks in PD subjects.

Our results seem to indicate that noisy EVS affects the sensitivity of motor responses (in this case, joystick-controlled cursor position) to visualized error (displayed cursor position – target position). We do not believe

that our observed results are the consequence of an attentional or general arousal effect, such as through activation of the reticular activating system. The imperceptible nature of our stimulus, which subjects were not aware of throughout the experiment trials, precludes this issue which is present with other forms of minimally invasive stimulation methods [118].

Depending on the stimulus parameters (i.e., current intensity, frequency, signal shape), EVS is known to induce a broad range of effects, including eye movements, postural control and movements [111]. Therefore, one interpretation of our results may include the confounding effects of nystagmus and/or ocular torsion through activation of the vestibulo-ocular reflex (VOR) [437]. Since subjects rely on visual error feedback, ocular torsion would potentially hamper the perceived error feedback through a subjective tilt in the visual perceptual field [437]. However, we note that our stimulus levels were weak, whereas the preferred EVS current intensities for inducing ocular torsion and subsequent perceptual tilts through EVS are much higher — at around 1–3 mA [437]. Therefore, we presume that our subthreshold stimulus was not strong enough to notably induce confounding visual effects and corollary perceptual changes in our experiment.

Noisy EVS is known to modulate EEG spectral power. Wilkinson et al. have demonstrated that noisy EVS is able to modulate the EEG spectral power during a face processing task [422]. Our previous study has demonstrated that noisy EVS is able to modulate the EEG synchrony patterns in healthy subjects [177]. Altogether, these findings combined with our present results suggest that noisy EVS is able to modulate oscillatory activity in resting and task-related networks, which involve sensorimotor processing in our particular study. The motoric effects of EVS may be related to modulation of oscillations related to integration of information and error-processing. Since perceived error (i.e., the error between the target and the displayed cursor position) was robustly detected by the LDA analysis, fronto-midline (FM) theta may be a candidate oscillation to be modulated by EVS in PD subjects. FM-theta shows an increased amplitude during tasks requiring concentration [252], which is related to error-related negativity (ERN), an event-related potential seen after errors are made. FM-theta may represent a universal mechanism for action monitoring with the midcingulate cortex acting as hub for the integration of information [63]. Thus, our results suggest that EVS may regulate FM-theta activity in PD subjects.

The increased SNR shown in Fig. 2.7 suggests that application of noisy EVS may have increased synchronization in neuromotor system via stochastic facilitation. Stochastic facilitation is a term to describe phenomena where stochastic biological noise elicits functional benefits in a non-linear system

such as the nervous system [238]. Several studies have reported that a presence of additive noise allows a weak input signal to be better detected, resulting in an increase in SNR in EEG [119, 180, 231, 361, 375, 402, 413] and sensorimotor performance [246]. These findings suggest that noisy EVS input may also be able to modulate detection and transmission of the sensorimotor system via stochastic facilitation, resulting in an increase in synchronization of the neuromotor system. However, a further investigation is required to elucidate whether the synchronization is limited to cortical areas or if it could give rise to corticomuscular synchronization [246].

We further speculate that our results may be at least partly explained by modulation of cortico-BG rhythms involved in sensorimotor processing. Growing observations suggest a concept that the BG regulates action motivation or response 'vigour' [265, 327] as well as the speed and size of movement [360, 380]. Deficient scaling of the initial burst of earliest agonist muscle activity (EMG) to meet the demands of a motor task is frequently observed in clinical disorders of the BG, such as PD. The link between motivation and movement gain may be universally weakened in Parkinsonian subjects [20, 380]. We thus speculate that EVS may also correct deficient vigour caused by BG dysfunction through modulation of pathological brain rhythms.

We note that we used a single noisy stimulus for all subjects. However, the results shown in Fig. 2.3 also emphasize the importance of looking at patient-specific stimuli. For instance, the coefficients regarding the difference between cursor and target velocities (w_{13}, w_{14}, and w_{15}) were found to be significant in some subjects, but were indistinguishable from bootstrapping for the rest of the subjects.

Finally, we note that EVS had fewer effects in the Better condition compared to the Worse condition. Presumably, subjects would have made fewer corrective movements in the former condition. This raises the possibility that EVS may also depend upon the number and form of corrective submovements. As submovements were not captured by the global LDA and multivariate regression methods used here, this warrants further investigation.

Chapter 3

Quadrature regression and IVA approach to removal of high-voltage EVS artifacts from simultaneous EEG recordings

Chapter 2 demonstrated the robust effects of noisy EVS on the motor tracking performance in PD. The positive effects on movement suggest intriguing questions how EVS modulates upstream neural activities in the brain that control downstream movement. One way to investigate this is to record cortical activities via EEG while delivering EVS. However, simultaneous EEG and EVS studies have been hindered by the high-voltage stimulation artifacts that completely distort the EEG signals. In this chapter, we tackled this problem by introducing a novel denoising method.

3.1 Introduction

Over the last decade, noninvasive electrical brain stimulation (NEBS) has been extensively explored as a means of studying fundamental mechanisms underlying cognitive and motor functions, as well as a potential therapy for neurological diseases. NEBS techniques such as tACS and EVS can modulate ongoing neural oscillations, which play a fundamental role in brain functioning [390]. While NEBS studies are often conducted with brain imaging modalities such as fMRI and positron emission tomography (PET), it is the EEG that is particularly valuable for NEBS studies as it is relatively inexpensive, potentially portable, and able to record the electrical brain activity noninvasively with high temporal resolution.

Identifying ways to properly analyze the EEG acquired during stimulation has been a major challenge to date in fully understanding mechanisms

of NEBS. In general, the electrical artifacts induced by NEBS are so disruptive that groups have resorted to avoiding the artifact removal problem entirely by simply comparing EEG in pre- and post-stimulation conditions (for review, see [18] and [392]).

Several factors contribute to the technical difficulties of removing NEBS artifact from EEG. First, the stimulation artifact amplitude is several orders of magnitude larger compared to actual brain signals, often obscuring the EEG completely. Second, the frequency ranges of stimulation and cortical oscillations of interest can potentially overlap, precluding the application of simple signal processing techniques such as digital filtering. Third, stimulation artifacts recorded downstream in the EEG do not exactly match the delivered currents at the stimulation electrodes, differing in phase-shifts, amplitude variations and other morphologic alterations in the waveforms. It is likely that the applied stimulation currents go through a non-linear transformation before being recorded at EEG electrodes due to resistive and capacitive effects present at the interfaces between EEG electrodes, gel, and skin layers and possibly a non-stationary transformation due to electrode impedances changing over time. Fourth, the ground truth of ongoing brain responses to stimulation is unknown, making it difficult to determine the success of methods proposed to disentangle stimulation artifacts from ongoing brain activity. Therefore, to be able to adequately tackle the stimulation artifact rejection problems, a thorough investigation of the characteristics of stimulation artifacts, exploration of more advanced analytical methods, and adequate assessment of the performance of different methods are required.

A few methods have been proposed to remove large-amplitude artifacts in EEG signals. Most of the methods mainly stem from EEG-fMRI studies where EEG signals are severely corrupted by artifacts caused by switching of the magnetic field gradient during MR acquisition [8]. Similar to NEBS, the artifact can have an amplitude a few hundred times greater than the EEG signals. A moving average algorithm is the most commonly-used method to remove this artifact, whereby an artifact template is created from an average of several adjacent time windows (or trials) and then subsequently subtracting this mean template from the raw EEG signal. A similar variant of this approach has been applied in recent EEG-NEBS studies [25, 147, 187, 321, 407] (Table 3.1). Since this approach frequently leaves small remnants of artifact, an additional step is usually taken to separate any remaining artifacts from brain activity using methods such as principal component analysis (PCA) or independent component analysis (ICA). However, the moving average algorithm can fail in removing artifacts when significant phase-shifts and/or amplitude changes are present between time

Table 3.1: Artifact Rejection methods used in EEG-NIBS Studies

Stimulus	**Methods**	**Data used**	**Performance evaluation**
tDCS	High-pass filtering (>2 Hz) followed by ICA	• Real EEG data during transcranial direct current stimulation (tDCS)	• Manual inspection of IC
5,10 and 40 Hz tACS	Artifact template subtraction for each channel	• Real EEG data during tACS	• Comparison of power spectral density in the alpha band during tACS at 5, 10, and 40 Hz • Comparison of individual alpha frequency changes due to eye closure during stimulation to those in the sham condition
10 Hz tACS	Two-step procedure 1) Artifact template subtraction 2) PCA for remaining artifacts	• Simulated EEG • Real EEG data during tACS	• Comparison of mean spectral power before/after artifact rejection • Physiological phase-dependent response to the visual stimulus
2, 6, 12, 25, 40, 70 and 100 Hz tACS	Two step procedure 1) Subtraction from each EEG channel a properly scaled and phase-shifted fraction of the sum of the TP9 and TP10 that are near the tACS electrodes 2) Digital notch filter at the respective stimulation frequency and the first two harmonics	• Real EEG data during tACS	• Demonstration of online effects in lower gamma band

windows. Additionally, if a fraction of neural responses is phase-locked to the stimulation, they will tend to be removed when the average template is subtracted from the EEG signals.

A recently-proposed joint blind source separation (JBSS) technique has been successfully applied to EEG signal denoising applications. For example, gradient artifacts from EEG-fMRI can be more robustly removed by independent vector analysis (IVA) compared to the artifact subtraction method described above [2]. IVA has also shown to be effective in removing muscle artifacts in real ictal EEG data and outperforms ICA in isolating both ocular and muscle artifacts [64, 66].

In this chapter, we propose utilizing JBSS approaches to separate NEBS

artifacts from brain signals by using multiset canonical correlation analysis (MCCA) and IVA. To the best of our knowledge, this is the first attempt to investigate JBSS approaches in NEBS artifact removal. In contrast to PCA and ICA, which decomposes a single dataset into individual components, these relatively new methods simultaneously accommodate multiple datasets and can extract underlying common sources from the signals (for a technical review of the methods, see [67]). By jointly analyzing multiset data, MCCA and IVA identify source components that are maximally correlated across datasets yet constrained to be uncorrelated (or in the case of IVA, maximally independent) within a dataset. Artifact-corrupted EEG can be segmented and restructured into multiple sets (i.e., epochs) based on the period of stimulation signal or repeated trials. As the stimulation artifacts in EEG possess relatively similar (but not identical) amplitudes and phases from epoch-to-epoch and are minimally correlated or statistically independent from brain activities, our hypothesis is that JBSS approaches would result in superior performance in isolating stimulation artifacts as source components compared to conventional artifact rejection methods. Reconstruction of the EEG without artifact component(s) would then results in a "cleaned" EEG.

This chapter is organized as follows: Section 3.2 describes the experiment setup and protocol, EEG data acquisition and preprocessing, and technical details of five different methods tested to remove stimulation artifacts: PCA, second-order blind identification (SOBI), MCCA, IVA, and quadrature regression-IVA (q-IVA) proposed here. The methods were tested through both simulation and real EEG data, and Section 3.3 compares the performance of the artifact removal methods, followed by discussions and suggestions for future work in Section 3.4.

3.2 Materials and Methods

3.2.1 Subjects

Thirteen healthy people (6 females, age=64.9 ± 15.7) participated in the study (Table 3.2). No subjects had any reported vestibular or auditory disorders.

The experimental protocol was approved by the Clinical Research Ethics Board at the University of British Columbia. All subjects gave a written informed consent before the beginning of the experiment.

Table 3.2: Subjects information

Subject ID	Data usage
1	Simulation study (simulated stimulation artifacts)
2	Simulation study (resting EEG)
3-12	Real data study (performance validation using P_{diff})
13	Real data study (performance validation using changes in alpha power by eye closure)

3.2.2 EVS

EVS was delivered in bilateral, bipolar fashion through pre-gelled Ag/AgCl electrodes (BIOPAC Systems Inc., CA, USA) placed over the mastoid process behind each ear. The EVS signal was generated on a computer using MATLAB (MathWorks, MA, USA) software and converted to analog signals through a NI USB-6221 BNC digital acquisition module (National Instruments, TX, USA). The analog command voltage signals were subsequently passed to a constant current stimulator DS5 (Digitimer, UK). A multisine signal in the theta (4–8 Hz) frequency band was used as the EVS stimulus (Fig. 3.1). The frequencies of sinusoids were uniformly distributed every 0.2 Hz and the phases were chosen to minimize the crest factor by a clipping algorithm [401]:

$$x(t, \phi) = a \cdot \sum_{i=1}^{n} cos(2\pi f_i t + \phi_i) \tag{3.1}$$

where $x(t, \phi)$ is the multisine stimulus, a is the amplitude of the multisine, f_i and ϕ_i are the frequency and phase, and i is the index of each sinusoidal component ($f_1, f_2, f_3, ..., f_n = 4.0, 4.2, ..., 8.0$ Hz).
The stimulus was applied at an imperceptible level to avoid effects by general arousal and/or voluntary selective attention, with the current level individually determined at 90% of each subjects sensory threshold (see 3.2.3 Study Protocol).

3.2.3 Study Protocol

Since individuals have inherently subjective perception of EVS, we utilized systematic procedures that have been previously used in determining subliminal current levels [177, 205]. For each subject, the multisine stimulus

was delivered at a basal current level of 0.05 mA for a period of 10 seconds and the level was increased stepwise (0.02 mA) until the subject perceived a mild, local tingling sensation in the area of the electrodes. The current level was then decreased by one level each time until sensation was no longer reported during delivery of the stimulus, and increased by one level to confirm threshold. The measured individual threshold level was in the range of 0.31-0.77 mA.

After the threshold had been determined, the subjects were comfortably seated 80 cm from a screen and were instructed to focus their gaze on a continuously-displayed fixed target to minimize distractions while EEG was recorded. EEG was first recorded without stimulation for 10 s (pre-EVS), blinding subjects to the actual stimulus onset. The multisine stimulus was then delivered for 60 s consisting of 6 consecutive trials. In each trial, EVS was on for 5 s (during-EVS) and off for 5 s (post-EVS) (Fig. 1). For Subject

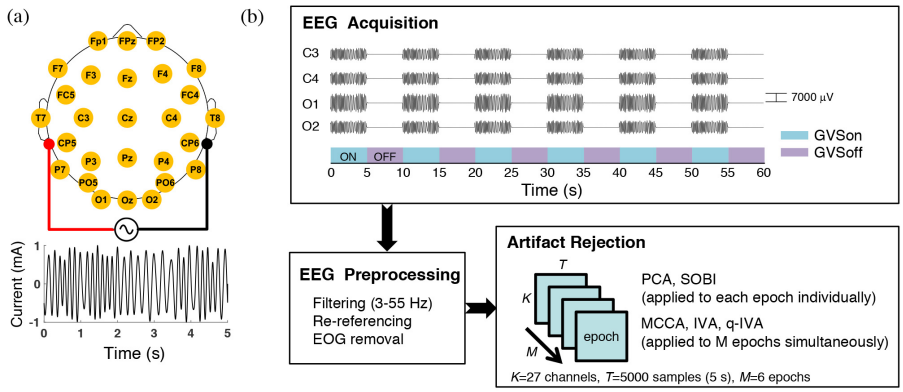

Figure 3.1: Experimental setup and an overall flow diagram for the study. (a) Placement of EEG (yellow) and EVS (red and black) electrodes, and 5-s EVS stimulus. (b) The stimulus was delivered for 60 s with 6 trials of 10-s epochs consisting of 5-s EVSon and 5-s EVSoff. To illustrate relative scales of the stimulation artifacts to EEG, sample traces (channels C3, C4, O1 and O2) from one subject are shown. The EEG data were preprocessed and EVSon segments were formed into M sets of $K \times T$ matrices in order to apply JBSS methods (i.e., MCCA, IVA and q-IVA).

13, we also measured resting EEG with the eyes open (60 s) and closed (60 s) in the beginning of the study. Then, the subject performed the study protocol with the eyes open followed by a 1-min break, repeating it with the eyes closed.

3.2.4 EEG Data Acquisition and Preprocessing

EEG was recorded from 27 scalp electrodes using a Neuroscan SynAmps2 EEG acquisition system (Neuroscan,VA, USA) and a standard electrode cap (64-channels Quik-Cap, Neuroscan, VA, USA). EEG electrodes were positioned according to the international 10-20 placement standard with one ground and one reference electrode, and two earlobe electrodes were placed on each side for re-referencing purposes. The electrodes were attached using Electro-Gel (Electrode-Cap International, OH, USA) and impedances were kept below 10 $k\Omega$. All signals were sampled at 1 kHz, and no clipping was observed during stimulation. The EEG data were bandpass filtered between 3 and 55 Hz using a two-way finite impulse response (FIR) filter (the eegfilt function in EEGLAB [84]), and re-referenced to the average reference (linked earlobe) offline. Ocular artifacts (EOG) in the EEG recorded while stimulation was off were corrected based on cross-correlation with the reference EOG channels using the AAR toolbox included in EEGLAB.

3.2.5 Simulation Data

Simulations were performed in order to quantitatively assess and compare performance of different artifact rejection methods. Simulation data were created by combining the resting (i.e., artifact-free) EEG data from Subject 2 with simulated EVS artifacts that were obtained by fitting an electrical circuit model to the EEG recorded from Subject 1. We note that in previous studies [147], stimulation artifacts were created simply by adding time-jitter to the stimulation model with amplitude weighted differently for each channel depending on the distance from stimulation electrodes (i.e., the artifact amplitude was largest for adjacent channels and gradually decreased with distance further away from the tACS electrodes). While this accounts for some of the characteristics of stimulation artifact such as time lags caused by mismatch of internal clocks of EEG recording and stimulation system, it does not capture the characteristics caused by changes in body impedance. For example, even respiration and heart beats result in head and body movement that slightly change the distance between stimulation current and EEG sensors, modulating the electrode-tissue impedance [268]. Therefore, instead of the conventional method, a resistive-capacitive circuit model for the physical electrode-skin interface [3] was adopted to generate simulated EVS artifacts (Fig. 3.2):

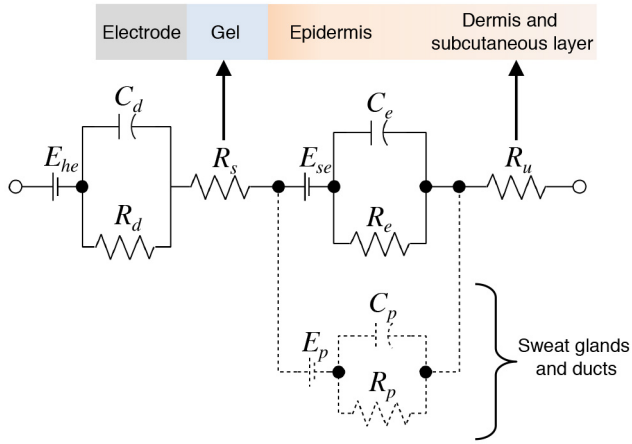

Figure 3.2: The electrical circuit model for the physical electrode-skin interface adapted from [3] (E_{he}: the half cell potential of the electrode/gel interface; R_d and C_d: the resistive and capacitive components of the impedance associated with the electrode/gel interface; R_s: the series impedance associated with the resistance of the electrode gel; E_{se}: the potential difference across the epidermis; R_e and C_e: the resistance and capacitance of the epidermis; Ru: the resistance of the dermis and subcutaneous layer.

$$Z(s) \approx \left(\frac{R_d}{sR_dC_d+1} + \frac{R_e}{sR_eC_e+1} \parallel \frac{R_p}{sR_pC_p+1}\right) \approx \frac{b_1 s + b_0}{s^2 + a_1 s + a_0} \tag{3.2}$$

where R_d and C_d are the the resistance and capacitance associated with the electrode-gel interface, R_e, C_e, R_p and C_p are the resistance and capacitance associated with a skin structure consisting of epidermis, dermis, and a subcutaneous layer, s is the complex frequency variable, and a_0, a_1, b_0 and b_1 are coefficients in the transfer function [3].

We thus modelled the electrode-skin impedance structure as a second-order, continuous-time transfer function with one zero and two poles. The process of generating simulated EEG data using (Eq. 3.2) is described in Fig. 3. For illustrative purposes, an example of one channel is shown instead of 27 channels. Using the system identification toolbox in MATLAB with the multisine signal as the input and the EEG signal recorded from Subject 1 as the output, the coefficients in (Eq. 3.2) were obtained (Fig. 3.3(a)). To ensure robustness of results, a small amount of random variation was added to the obtained coefficients to generate 600 simulated artifacts (= 6 epochs $\times$ 100 realizations) so that each artifact had a small phase and

amplitude variation from the input signal (Fig. 3.3(b)). Specifically, for each realization in (Eq. 3.2), we modelled $a_0 \sim \mathcal{N}(0.6, 0.1)$, $a_1 \sim \mathcal{N}(10.8, 1)$, $b_0 \sim \mathcal{N}(249.6, 10)$, and $b_1 \sim \mathcal{N}(7155.5, 100)$, where $\mathcal{N}(\mu, \sigma)$ refers to a Gaussian distribution with mean and standard deviation. The amplitude was then scaled to obtain $Y_{s,EVS}$ so that its maximum peak matched with the one of the real artifact in Fig. 3.3(a). $Y_{s,EVS}$ was then superimposed on the resting EEG data from Subject 2, $Y_{s,EEG}$, to create the simulation data, Y_s:

$$Y_s = Y_{s,EEG} + Y_{s,EVS} \tag{3.3}$$

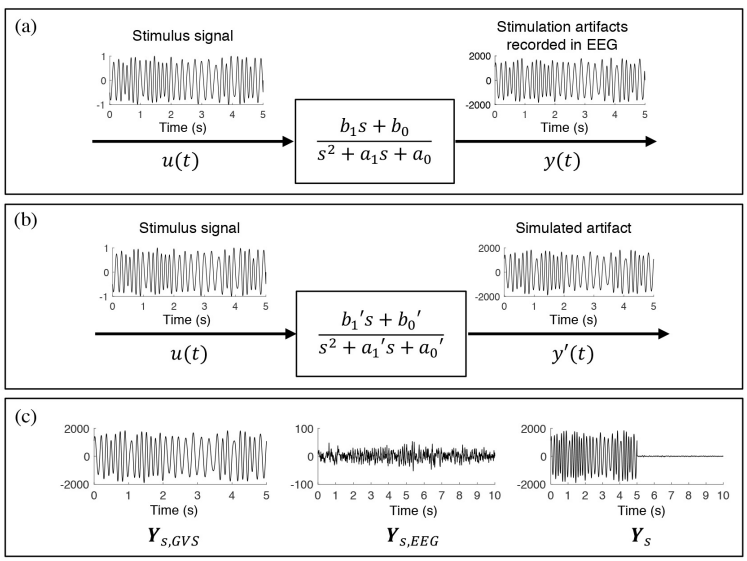

Figure 3.3: Example of generating simulated EEG data, Y_s. (a) The parameters (a_0, a_1, b_0 and b_1) of the second order transfer function in (Eq. 3.2) were estimated using the multisine signal, $u(t)$, as the input, and stimulation artifacts recorded in EEG as the output. (b) New parameters (a_0', a_1', b_0' and b_1') were obtained by adding a small amount of random variation to the original parameters. The new parameters were then used to generate simulated artifact, $y'(t)$. (c) $Y_{s,EVS}$ was created by scaling $y'(t)$ to match the maximum peak value in the raw EEG data. The final simulated EEG data, Y_s, was created by adding $Y_{s,EVS}$ to the resting EEG from another subject, $Y_{s,EEG}$.

3.2.6 Artifact Rejection Methods

PCA and ICA

ICA is a method to find statistically independent sources from mixed signals by using higher-order statistics. Given minimal prior information about the underlying sources as well as the mixing process, ICA decomposes observed signals and finds underlying sources such that every source is independent of the others. ICA has been widely utilized in EEG studies to identify meaningful neurophysiological signals and separate them from a wide variety of artifactual sources [86]. The basic premise for using PCA is that the large amplitude of stimulation artifacts would account for such a large variation of the recorded EEG that the artifacts would not co-vary with (i.e., be orthogonal to) brain activity. For ICA, the assumption is that EEG data recorded from scalp electrodes are considered linear summations of brain activity and stimulation artifacts that are statistically independent from each other. We used a commonly-used ICA algorithm, SOBI [26, 200]. To account for possible non-stationary relations between electrodes across epochs, PCA and SOBI were applied to each epoch separately rather than to a single matrix created by concatenating all 5-s EEG epochs.

MCCA and IVA

CCA identifies canonical variates from two multidimensional variates by maximizing correlation between them. Given two random vectors x_1 and x_2, CCA finds two transformation vectors, a and b, such that the canonical variates, $y_1 = a^T x_1$ and $y_2 = a^T x_2$ have maximum correlation. After the first pair of canonical variates is found, the second pair of transformation vectors is obtained by deflation, so that the next corresponding canonical variates have maximum correlation with each other while still being uncorrelated with the first pair of canonical variates [434].

MCCA is an extension of CCA that allows for the joint analysis of more than two data sets. The goal is to optimize an objective function to achieve the maximum overall correlation across the canonical variates. Since multiple correlations need to be considered, the MCCA algorithm takes multiple stages where one group of canonical variates is obtained in each stage by optimizing the objective function to maximize the overall correlation [72]. In the second stage of the algorithm, a constraint is applied such that the estimated canonical variates are uncorrelated with the previously obtained canonical variates. Among several cost functions proposed in [172], we used the MCCA procedure based on maximizing the sum of squared correlations

(SSQCOR) across the canonical variates.

Similar to MCCA being an extension of CCA with capability of jointly analyzing more than two data sets, IVA is a generalization of ICA from one to multiple data sets [67]. Applying ICA individually to each data set suffers from the permutation problem whereby the recovered source components from each data set may be inconsistently ordered across sets, resulting in ambiguities of which source component in one data set is associated with other components across data sets. IVA addresses the permutation problem by assuming each source component within a dataset is related to a source component in each of the other datasets as well as independent of all the other source components within the dataset [11, 179]. Several algorithms have been proposed for IVA [352] so as to minimize the mutual information between source components. Here, non-orthogonal IVA was used as it allows source components following either multivariate Gaussian or non-Gaussian distributions and does not restrict the demixing matrices to be orthogonal as in MCCA [11].

q-IVA

The q-IVA method proposed here consists of two steps. Firstly, for each epoch and channel separately, we remove high-amplitude stimulation artifact using a regression model that includes the stimulation signal, $x(t)$, and its quadrature component, $\hat{x}(t)$, to compensate for possible phase-shifts. For a narrowband signal like the theta-multisine stimulus used in this study, its analytical signal, $z(t)$, can be expressed as

$$z(t) = x(t) + j\hat{x}(t) \tag{3.4}$$

$$\hat{x}(t) = H[x(t)] = \frac{1}{\pi t} \cdot x(t) \tag{3.5}$$

where t is sampling time, $x(t)$ is the multisine simulus, $\hat{x}(t)$ is the quadrature component (i.e., phase shift by $-\pi/2$), and H is the Hilbert transform.

For the EEG signal in channel k and epoch m, the regression model can be written as

$$y_k(t)^{[m]} = Xb_k^{[m]} + r_k(t)^{[m]} \tag{3.6}$$

$$X = [x(t), \hat{x}(t)] \tag{3.7}$$

where k the channel index ($k = 1, 2, ..., K; K = 27$), m is the epoch index ($m = 1, 2, ..., M; M = 6$), $y_k(t)$ is the $T \times 1$ EEG signal, X is the $T \times 2$ matrix of the stimulation signal and its quadrature component, b_k is the 2×1 vector of regression coefficients, r_k is the $T \times 1$ vector of residuals, and T is the number of time points ($T = 5000$) in the epoch m. Taking the residual of channel k in epoch m, $r_k(t)^{[m]}$, in each row, six sets of residual matrix were obtained:

$$R^{[m]} = [r_1(t)^{[m]}, r_2(t)^{[m]}, ..., r_k(t)^{[m]}]^T \tag{3.8}$$

In the second step, we applied IVA to the residual matrices in order to further reduce the remaining artifact. IVA analyzes the residual matrices jointly and finds the estimated source components by minimizing the mutual information for all components and maximizing the mutual information within each source component across the epochs [11]:

$$R^{[m]} = A^{[m]} \cdot S^{[m]} \tag{3.9}$$

where $A^{[m]}$ is the $K \times K$ mixing matrix, and $S^{[m]}$ is the $K \times T$ estimated source components matrix in the epoch . The cleaned EEG data were obtained by removing artifactual source components and projecting the rest of the components back to the time domain. The number of the removed source components was 2 (Fig. 3.4).

3.2.7 Performance Evaluation

Simulation Study

The cleaned EEG data, $\tilde{Y}_{s,EEG}$, were obtained by applying the aforementioned five artifact rejection methods to the 100 realizations ($N = 100$) of the simulation data. With complete removal of the artifacts, $\tilde{Y}_{s,EEG}$ is expected to be identical to $Y_{s,EEG}$. Three measures were employed to evaluate performance of the artifact rejection methods. As the first evaluation measure, relative root-mean-squared error ($RRMSE$) [65] of channel k was computed as the following:

$$RRMSE_k = \frac{1}{M} \sum_{m=1}^{M} \frac{RMS(y_{s,EEG}^{[m]} - \tilde{y}_{s,EEG}^{[m]})}{RMS(y_{s,EEG}^{[m]})} \tag{3.10}$$

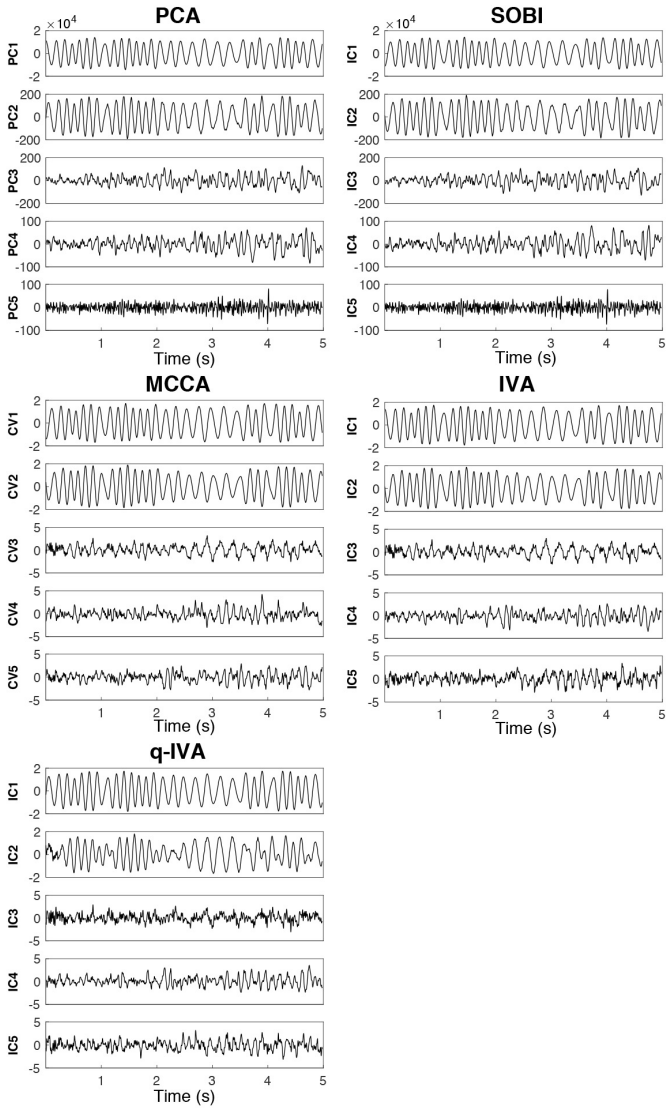

Figure 3.4: The principal components (PC) from PCA, underlying source components (IC) from SOBI, IVA and q-IVA, and canonical variates (CV) from MCCA.

where $y_{s,EEG}^{[m]}$ and $\tilde{y}_{s,EEG}^{[m]}$ are $T \times 1$ time series of channel k in $Y_{s,EEG}^{[m]}$ and $\tilde{Y}_{s,EEG}^{[m]}$ matrices, and $RRMSE_k$ is the averaged value across all epochs for channel k. The root mean square (RMS) for a time series vector y was

defined as,

$$RMS(y) = \sqrt{\frac{1}{T}\sum_{t=1}^{T} y(t)^2} \tag{3.11}$$

In order to measure the capability of preserving the original EEG signals, the correlation coefficient (CC) between and was calculated as the second measure [65]. CC_k was obtained by averaging the coefficient for channel k over all epochs:

$$CC_k = \frac{1}{M}\sum_{m=1}^{M} c_k^{[m]} \tag{3.12}$$

where $c_k^{[m]}$ is the coefficient value in epoch m.

As the third evaluation measure, power deviation (P_{dev}) was calculated to investigate similarity of power spectral density between the cleaned and original EEG data. For each channel and epoch, the spectral power was calculated using Welch's averaged, modified periodogram method (the "pwelch" function in MATLAB) and the average power in theta (4–8 Hz), alpha (8–13 Hz), beta (13–30 Hz) and gamma (30–55 Hz) bands was computed. For each frequency band, P_dev of channel k averaged over all epochs was computed as the following:

$$P_{dev,k} = \sqrt{\frac{1}{M}\sum_{m=1}^{M} (\tilde{P}_k^{[m]} - P_k^{[m]})^2} \tag{3.13}$$

where $\tilde{P}_k^{[m]}$ and $P_k^{[m]}$ are the band power of $\tilde{Y}_{s,EEG}$ and $Y_{s,EEG}$, respectively.

Real Data Study

MCCA, IVA, and q-IVA were applied to the EEG data simultaneously recorded during EVS from 10 subjects. Unlike the simulation approach, the ground truth about "true" brain activities and remaining artifacts in the cleaned EEG data are unknown. We compared the power spectra between the cleaned and immediate post-EVS EEG data to evaluate the performance of the artifact rejection under the assumption that the difference in brain activity during and immediately after the stimulation would be minimal. Six epochs were concatenated together to calculate power spectrum in the cleaned and post-EVS EEG data. Then, power differences (P_{diff}) in the

theta, alpha, beta and gamma bands were calculated for each subject as follows:

$$P_{diff} = \frac{1}{K}\sum_{k=1}^{K} \mid \tilde{P}_k - \bar{P}_k \mid \tag{3.14}$$

where $\tilde{P}_k$ and $\bar{P}_k$ are the power in each frequency band for channel k of the cleaned and post-EVS EEG data, respectively.

The performance of the proposed q-IVA method was further investigated by examining occipital alpha rhythms, as has been previously-used in performance evaluation of artifact removal algorithms [187]. Occipital alpha rhythms are one of the standard physiological responses that have been investigated in many EEG studies, and are dominant during an eyes-closed resting condition and suppressed when individuals open their eyes [23]. For this, we compared the alpha power at the occipital region (channel O1) in the cleaned EEG between when the subjects eyes were open and closed.

Statistical Analysis

We analyzed whether the group means of the performance evaluation measures were significantly different depending on the artifact rejection methods using an analysis of variance (ANOVA). For the simulation results, the ANOVA was performed for each measure with a group factor (MCCA vs. IVA vs. q-IVA) and a within-group factor (EEG channels). For the real data study, the ANOVA was performed for the P_{diff} in each frequency band with a group factor (MCCA vs. IVA vs. q-IVA) and a within-group factor (10 subjects). For each ANOVA test, a Tukey-Kramers test (using the "multcompare" function in MATLAB) was used for multiple pairwise comparion of the mean values between the three groups.

3.3 Results

3.3.1 Simulation Results

Fig. 3.4 shows the principal components (PC) from PCA, underlying source components (IC) from SOBI, IVA and q-IVA, and canonical variates (CV) from MCCA. The correlation coefficient between the stimulation signal and the first component from each method was similar 0.976 ± 0.001 (mean ± standard deviation) for both PCA and SOBI, 0.969 ± 0.04 for MCCA, 0.974 ± 0.03 for IVA, and 0.877 ± 0.04 for q-IVA, indicating a significant

portion of the artifact was identified in the first components. The correlation coefficient between the stimulation signal and the second component was 0.212 ± 0.005 for PCA, 0.213 ± 0.005 for SOBI, 0.214 ± 0.120 for MCCA, 0.292 ± 0.231 for IVA, and 0.263 ± 0.213 for q-IVA, indicating the second components still had a significant correlation with the stimulation signal. For the third component, the correlation coefficient dropped significantly below 0.01 for all methods. Therefore, we removed the first two components and reconstructed EEG from the rest components for all the five methods.

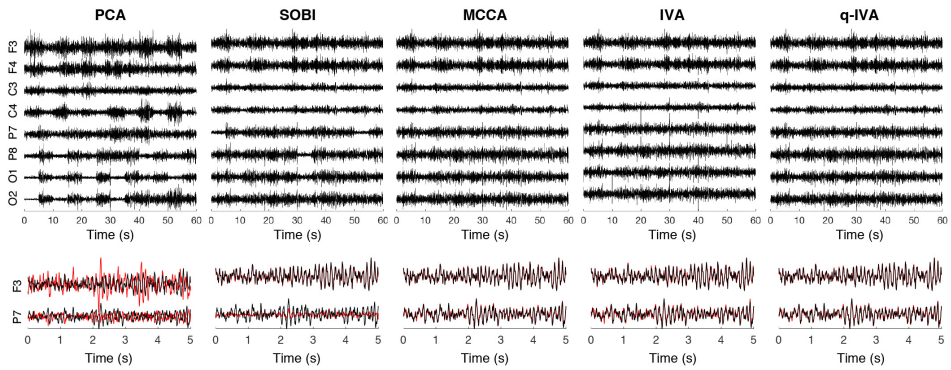

Figure 3.5: Sample traces (8 channels) of the cleaned EEG data after using different artifact rejection methods. Note that for PCA and SOBI, artifacts are inconsistently removed across channels, whereas MCCA, IVA and q-IVA removed artifacts robustly across all channels and epochs. For the illustration purposes, the first 5-s of the channels F3 and P7 are shown at the bottom (red: the cleaned EEG; black: the original EEG).

Fig. 3.5 shows an example of the cleaned EEG data after using different artifact rejection methods in one of the iterations. PCA poorly removed the stimulation artifacts, showing inconsistent performance across channels. It removed artifacts well in a few channels whereas in other channels the artifacts were either insufficiently removed (e.g., F3) or removed with significant amount of non-artifactual signal (e.g., O2). Likewise, SOBI left small artifactual remnants in some channels (e.g., O1) or removed a substantial amount of non-artifactual signals (e.g., P7). In contrast, MCCA, IVA and q-IVA removed the artifacts robustly across all channels.

Fig. 3.6(a) compares the $RRMSE$ values across 27 channels between the different methods. The $RRMSE$ for PCA was highest in all channels followed by SOBI. The JBSS methods, in general, demonstrated much improved results in the $RRMSE$ for all channels with the channel-averaged value being approximately 5.8 and 1.6 times smaller than PCA and SOBI. Statistical results showed significant differences in $RRMSE$ between the

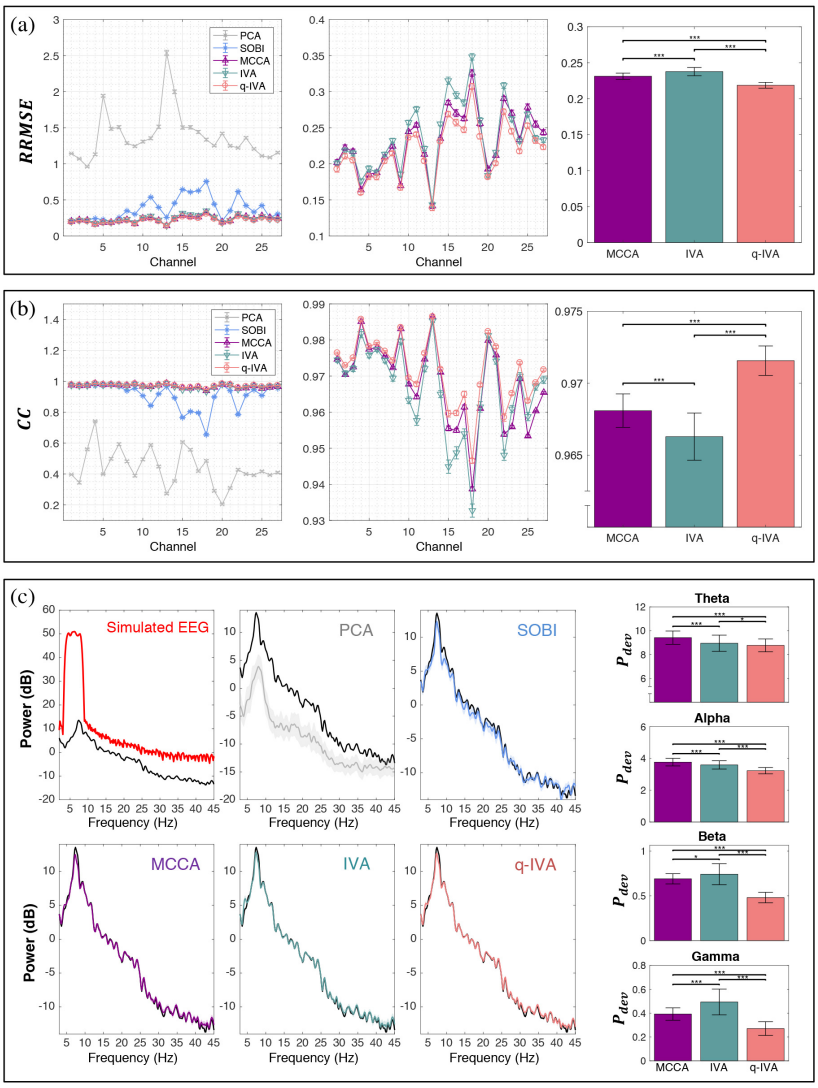

Figure 3.6: Comparison of the performance of different artifact rejection methods in the simulation study (for illustrative purposes, in (a) and (b), the results of MCCA, IVA, and q-IVA in the first panel were taken and magnified in the second panel; the third panel shows the results of ANOVA to test group mean differences; *: $P < 0.05$, **: $P < 0.01$, ***: $P < 0.001$). (a) $RRMSE$. (b) CC. (c) Power spectrum of the channel O1 of the original data ($Y_{s,EEG}$), simulation data (Y_s), and cleaned data ($\tilde{Y}_{s,EEG}$) after using different artifact rejection methods. The bar graphs on the right show the results of ANOVA to test group mean differences in P_{dev} in the theta, alpha, beta, and gamma bands.

JBSS methods; it was smallest for q-IVA (0.219 ± 0.041) followed by MCCA (0.231 ± 0.043) and IVA (0.238±0.057). An interesting finding was that the $RRMSE$ changed across the channels in a similar way for MCCA, IVA and q-IVA. This suggests that the condition in the objective function associated with maximizing overall correlation among multiple data sets has stronger potential for extracting source components than solely restricting sources to being uncorrelated or statistically independent.

Fig. 3.6(b) shows the correlation coefficients between the original and the cleaned EEG data. It can be seen that MCCA, IVA and q-IVA resulted in CC being close to 1 in almost all channels, indicating superior performance to PCA and SOBI. Statistical results showed that the CC was significantly higher for q-IVA (0.972 ± 0.010), followed by MCCA (0.968 ± 0.012) and IVA (0.966 ± 0.016).

The performance of the artifact rejection methods in the frequency domain is demonstrated in Fig. 3.6(c). The first panel shows an example of the power spectrum of the channel O1 of the resting EEG data (black) and after it was corrupted by the simulated artifacts (red). The power of the artifact was around 50 dB obscuring the alpha peak around at 9 Hz in the original data. For all of the artifact rejection methods, the dominant peak at 9 Hz was again detectable in the cleaned EEG data. However, PCA resulted in significantly diminished power in all frequencies suggesting that a significant amount of EEG signals was removed along with the rejected PCs. SOBI also removed some of the EEG signals as can be seen in the decreased power in the frequency range of 6–23 Hz. Although MCCA, IVA and q-IVA also slightly decreased the power around 9 Hz, the overall power spectra were much closer to the original EEG compared to PCA and SOBI. In the right side of Fig. 3.6(c), the results of ANOVA comparing group means of P_{dev} in each frequency band are shown. Q-IVA showed the smallest P_{dev} in all the frequency bands. In the theta and alpha bands, the P_{dev} was significantly lower for IVA than MCCA, while it was significantly greater for IVA than MCCA in the beta and gamma bands. Overall, the results indicate that the power spectrum of the EEG data cleaned by q-IVA was closest to the true value.

3.3.2 Real Data Results

The simulation results in the previous section demonstrated that the JBSS methods outperformed PCA and SOBI. In the real data study, the performance of MCCA, IVA and q-IVA was further investigated.

The first panel of Fig. 3.7(a) shows an example of the channel O1 power

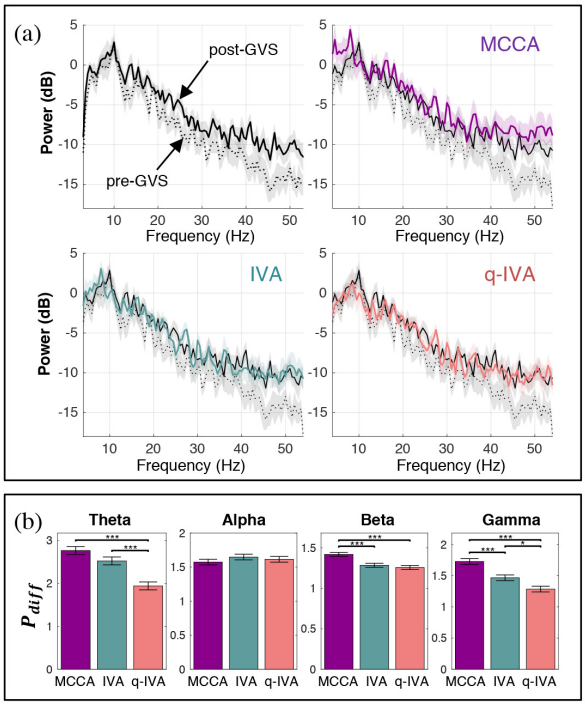

Figure 3.7: Power spectrum of the channel O1 averaged over 10 subjects. (a) Comparison of the pre-EVS, post-EVS and cleaned EEG data after using MCCA, IVA, and q-IVA. (b) The results of ANOVA to test group mean differences in P_{diff} in the theta, alpha, beta and gamma bands (*: $P < 0.05$, **: $P < 0.01$, ***: $P < 0.001$).

spectrum of the pre- and post-EVS EEG data averaged over 10 subjects. It can be seen that the power in the beta and gamma bands increased after stimulation, suggesting nonlinear EVS effects on brain activity, as the stimulation was in the theta band. The power spectrum during EVS was obtained after removing the stimulation artifacts using MCCA, IVA and q-IVA, which is illustrated with the pre- and post-EVS power spectra from the second panel. Before artifact rejection, the stimulation artifact was the dominant feature in the spectral power, with the mean power at the stimulation frequency (4–8 Hz) of around 55 dB across subjects. The power spectrum of the cleaned EEG data was comparable to the one in the post-EVS period for all subjects; the increased power in the beta and gamma bands resulted from the stimulation effects on brain activity was also detectable in the cleaned EEG data. Fig. 3.7(b) shows the P_{diff} in the theta and gamma bands was significantly lower for q-IVA compared to MCCA

and IVA. The P_{diff} of MCCA was significantly higher than q-IVA in the theta, beta and gamma bands, and higher than IVA in the beta and gamma bands. There was no significant difference in the P_{diff} in the alpha band between the three methods. Overall, the results suggest that q-IVA follows the power spectrum of the post-EVS EEG data most similarly.

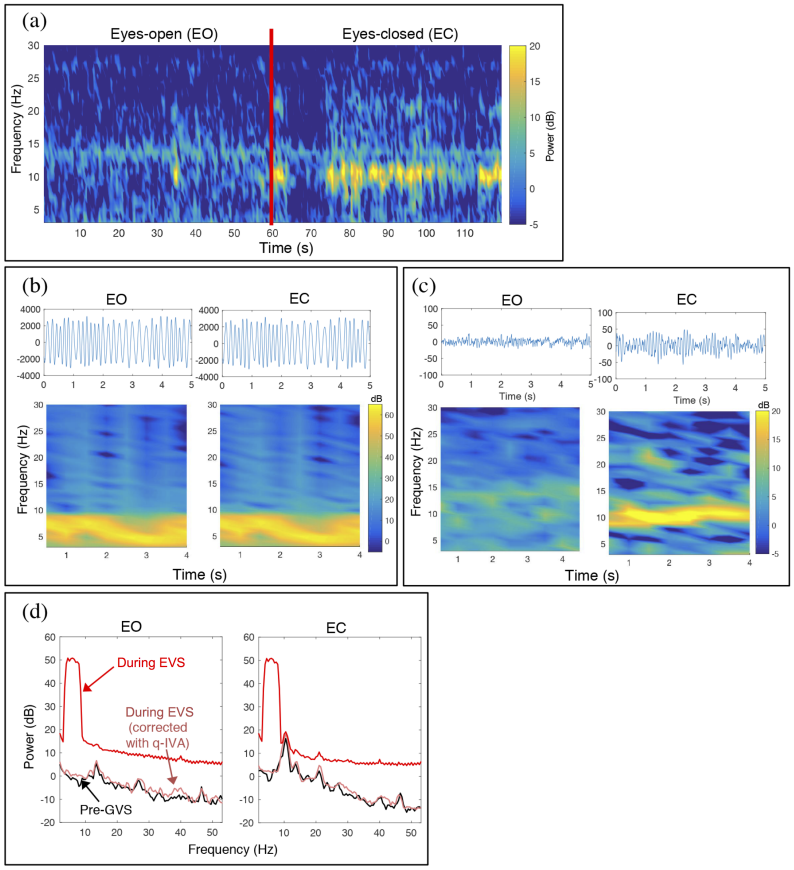

Figure 3.8: The alpha activity at the channel O1 in the eyes-open (EO) and eyes-closed (EC) conditions. (a) Pre-EVS. (b) During EVS. (c) During EVS after applying q-IVA to (b). (d) Comparison of the power spectrum of the pre- and during EVS (before/after the artifact removal using q-IVA).

Fig. 3.8(a) shows a spectrogram of the channel O1 when the subjects eyes were open (EO; 0–60 s) and closed (EC; 60–120 s) in the resting state (i.e., pre-EVS). The enhanced alpha activity can be seen in the EC condition. Fig. 3.8(b) shows the raw EEG signal and its spectrogram in the EO (left) and EC (right) conditions while the EVS was being delivered to the subject. Due

to the prominent power of the stimulation artifact, the alpha power change between the two conditions is not detectable. In contrast, in Fig. 3.8(c), after the artifact was removed using q-IVA, the enhanced alpha activity due to eye closure can be observed in the EC condition. This result is presented as power spectra in Fig. 3.8(d). After removing the artifacts with q-IVA, the power in the 4–8 Hz was attenuated close to pre-EVS levels in both EO and EC conditions. The amount of increased power at the alpha peak due to the eye closure is detectable after applying q-IVA, which is otherwise unable to be detected.

3.4 Discussion

3.4.1 Advantages of JBSS Approaches

In this paper, we demonstrated the feasibility of using JBSS methods, and q-IVA in particular, for removing high-amplitude stimulation artifact from corrupted EEG data. Several previous studies have suggested using an averaged artifact template to remove any stimulation artifacts by subtracting it from the raw EEG signals. The underlying strong assumption of such an approach is that the stimulation artifacts within each time window is perfectly aligned, since any time lag of the artifact between each window would result in significant errors when the averaged template is subtracted from the EEG recordings. This assumption is hard to meet in practice, as it is often found that the stimulation artifact appears in the recorded EEG with variable time lags (up to tens of milliseconds). Moreover, the perfect alignment of the stimulation artifacts across windows becomes more difficult when the frequency of stimulus is relatively low and the length of each averaged window becomes wider accordingly. Another potential problem with the artifact template approach is deciding how many windows to average. Averaging many windows may increase the chance of having not only the artifact, but also true underlying brain responses such as entrained oscillations phase-locked to the stimulation frequency included in the averaged template. In order to address this issue, we carried out a regression on a single-channel and single-trial basis where the stimulus signal and its quadrature component were used to remove the high-amplitude artifact. Our hypothesis was that the quadrature component would account for any phase lag between the stimulus and the artifact recorded in EEG, and the regression would preserve information related to brain activity in the error terms, as the regression matrix only contains stimulus-related information. In the simulation, we demonstrated that IVA was comparable to MCCA

in the performance of rejecting stimulation artifacts, while q-IVA achieved significantly better results in $RRMSE$, CC and P_{dev} than both IVA and MCCA. This suggests that removing the high-amplitude artifact first using the quadrature regression might result in IVA being more selective in disentangling artifactual components from EEG records because the statistical properties of the remnant artifacts and neural oscillations become more distinctive.

The rationale of using IVA in the removal of the remnant artifacts came from the superior performance of JBSS methods in stimulation artifact removal compared to PCA and SOBI, which, to the best of our knowledge, we demonstrate here for the first time. Since the objective of PCA is to reduce the dimension of the dataset and explain most of the variability in the original data, the first principal component accounts for as much of the variability as possible. For the simultaneous EEG-EVS data, the first principal component was largely composed of the stimulation artifact (Fig. 3.4). However, it was found that eliminating the first PC alone was insufficient to remove the artifact and accordingly the second PC had to be removed, but this still did not substantially improve the results. The main problem was that the results varied significantly across channels, as demonstrated in Fig. 3.5, which may possibly result from the misalignment of the first PC (i.e., the artifact) in the time domain across the channels due to time lags.

ICA has become more widely used than PCA in denoising EEG data as it is not restricted to the constraint of the spatial orthogonality between sources and non-brain artifacts are believed to have distinct statistical characteristics compared to brain activity. SOBI is an ICA-based algorithm that finds the unmixing matrix, W, by minimizing the correlation between one recovered source at time t and another at time $t + \tau$ by taking into account the time delay covariance matrices [26] (technical details can be found in [85]). Considering the algorithm, the poor performance of SOBI shown in this study implies that the stimulation artifacts and neural activity share similar second-order statistical properties, making separating the two difficult.

In contrast to PCA and SOBI, the JBSS methods analyze EEG data in multiple epochs jointly and take into account the correlation and covariance of sources in the multiple epochs. This property dramatically improved the results for this specific stimulation artifact removal problem since the artifacts appear highly consistent, but not identical, between time windows. Similarly, as in [2], the JBSS methods can be applied to artifact correction in the simultaneous EEG-fMRI data as the MR artifacts are also considered quasi-periodic.

3.4.2 Recommendations and Limitations

The proposed q-IVA method allows for the investigation of brain stimulation effects on neural dynamics during stimulation. Although the stimulation technique used here is EVS, the developed method could readily be applied to remove artifacts generated by other NEBS techniques such as tACS. It is also noteworthy that the tested stimulus signal in this study was a multisine, with a complex wave form compared to a simple pure sine wave that has been used in the majority of tACS studies. Since the period of the theta multisine was 5 s, we used a 5-s window length for each epoch. In the case of a single-frequency tACS, the period of the stimulus is much shorter than 5 s, which would allow for a greater flexibility in selecting an appropriate window size for the same length of EEG.

There are several limitations to this study. The results are reported based on a case where the theta-multisine was used as the stimulus. We have not investigated effects of the number of epochs, epoch length, frequency of stimulus, and the number of EEG channels on performance results, which need to be thoroughly investigated in a future study to obtain further improvement. In addition, we note that the q-IVA method may not be appropriate for removal of MR gradient artifacts in simultaneous EEG-fMRI recordings, as the artifacts are a sequence of pulses rather than a continuous sinusoidal signal and accordingly the regression based on a quadrature component may not be applicable. Although we demonstrated superior performance of q-IVA compared to the conventional methods, we note that careful interpretation of the results should be made. After removing the artifacts, any changes observed during stimulation compared to pre-stimulation period could be true online effects of stimulation or errors introduced by the data processing. The interpretation is still not definitive as the ground truth is unknown. Here we proposed that comparison of the cleaned EEG data with the immediate post-stimulation data can be one way to minimize erroneous interpretation of online stimulation effects in future NEBS studies.

In summary, we have investigated the performance of various methods to attenuate stimulation artifacts using quantitative measurements in simulations. In contrast to the conventional methods such as PCA and SOBI, the JBSS methods (MCCA, IVA and q-IVA) substantially improved the performance and the proposed method, q-IVA, outperformed all other methods. It was not investigated here whether applying the quadrature regression before PCA and SOBI would improve their denoising performance since our primary interest was the JBSS-based methods, MCCA and IVA, and they

demonstrated significantly superior performance to PCA and SOBI regardless of the quadrature regression. When examining the real data, we demonstrated that the q-IVA successfully attenuated the stimulation artifact, enabling the detection of the stimulation effects that resembled those seen in the post-stimulation data as well as physiological change by eye closure in the cleaned EEG data, which would be otherwise completely obscured by the high-amplitude artifacts. The results of this study suggest that q-IVA is an effective approach for the investigation of neurophysiological online effects of NEBS.

Chapter 4

Sparse Discriminant Analysis for Detection of Pathological Dynamic Features of Cortical Phase Synchronizations in PD

In this chapter, we demonstrate that pathological cortical activities in PD are normalized while EVS is being delivered. First, we introduce novel multisine stimuli that have several advantages over the noisy stimulus used in Chapter 2 to investigate online effects of EVS. Next, using the q-IVA denoising method introduced in Chapter 3, we remove the stimulation artifacts and investigate the changes in EEG during the stimulation. Finally, we provide a means towards optimizing EVS by demonstrating that the normalizing effects of EVS are dependent on the stimulation frequencies.

4.1 Introduction

PD, the second most common neurodegenerative disease [335], is characterized by motor symptoms such as bradykinesia, tremor, rigidity and impaired balance and gait as well as non-motor complications, resulting primarily from degeneration of dopaminergic neurons in the substantia nigra pars compacta (SNc) [79]. Several electrophysiology studies using local field potential (LFP) recordings demonstrated that, in the dopamine-deficient state, the neuronal synchronization in the basal ganglia is exaggerated at frequencies in the beta range (13–30 Hz) [51, 100, 219, 275]. These beta oscillations are also highly synchronized with sensorimotor areas [50, 60, 233, 427] as well as muscle activity of upper limbs during movement [233]. This excessive beta synchronization is considered to be, in part, responsible for the Parkinsonian symptoms and thus reducing the abnormal synchronization

with deep brain stimulation (DBS) has shown to be an effective therapy.

Recent fMRI findings have highlighted that large-scale cortical resting-state functional connectivity (rsFC) is altered in PD, possibly as a result of BG impairment effects on cortical-BG networks [148]. The striatum, a subcortical region significantly affected with dopamine depletion in PD, has altered FC with inferior parietal, temporal, and motor cortices [148], which supports that PD-induced connectivity changes can be seen beyond local subcortical regions. In addition to effects on BG-cortical FC, impairment in the BG can also alter cortico-cortical connectivity. Diminished interhemispheric connectivity in sensorimotor cortical regions [344] and reduced rsFC in widespread regions including inferior frontal, superior parietal, and occipital regions [95] have been shown to be implicated with disease duration and cognitive dysfunctions in PD.

Inferring pathological cortico-cortical connectivity in PD solely based on evidence from fMRI alone may not provide a complete picture, as fMRI has limited temporal resolution. Electrophysiology can provide complementary information as it measures spontaneous synchronous activity of a large population of neurons occurring on a millisecond time scale. A simultaneous LFP-electroencephalography (EEG) study reported that the dynamics of LFP synchrony in the STN is related to the dynamics of cortical synchrony [4], and BG DBS modulates cortical phase coupling measured with the EEG [351, 355].

One of the most widely-used method to quantify the coupling between oscillatory signals recorded at pairs of electrodes placed on the scalp in EEG is to look at their phase relationships [103, 184]. If cortical activities at two different regions are coupled, their phase angle differences tend to be consistent across time. Phase locking value (PLV) quantifies the strength of the phase coupling between two oscillatory signals, bounded between zero and one indicating a completely random and perfectly coupled relationship, respectively. Interregional phase synchronization has been shown to reflect specific neural activity coding different cognitive functions [141, 183], motor behaviours [13] (for a review, see [333]) and pathological brain states [207, 359, 394]. However, to date, only a few studies have examined phase-based rsFC across broad cortical regions and different frequency bands in PD [124, 144, 254, 351].

Most EEG connectivity studies to date have employed magnitude squared coherence. PD subjects exhibit excessive EEG coherence [124, 351], especially in the beta band, in the off-medication condition that is decreased by medication [124]. For PD subjects on-medication, enhanced coherence in the frontal regions in the theta (4–6 Hz), beta (12–18 Hz), and gamma (30–45

Hz) [254] and altered interhemispheric beta coherences in the midtemporal and frontal areas [144] can be observed, indicating the multifarious role of dopamine in the control of oscillatory activity, in and beyond the BG. However, coherence is different from PLV in that it relies on the assumption of linearity and stationarity in the signals and is calculated independently for each frequency, which is then scaled by the amplitudes of the signals. PLV-based connectivity, which do not rely on the strict assumptions underlying coherence, might be more suitable for nonlinear and non-stationary dynamics of neural oscillations, and sheds a new light on pathophysiological brain networks as it has not been explored yet in PD.

Recent progress in non-invasive brain stimulation (NIBS) has demonstrated its capability to modulate cortical oscillations [10, 147, 408] and interregional couplings, indicating its potential applications as an effective therapeutic technique for PD. EVS is a NIBS technique that delivers weak current to the mastoid processes and modulates firing rates of vestibular afferents, which then activates various cortical and subcortical regions including the BG and thalamus [30, 222, 392]. Similar to transcranial electrical stimulation (tES), EVS stimuli can take the form of direct current (DC), alternating current (AC) or random noise (RN) and stimulation effects vary according to stimulus types. While DC-EVS perturbs perception of orientation and locomotion and has been widely utilized in postural balance control research [362], RN-EVS has demonstrated its efficacy in motor functions [205, 278, 432] and modulation of EEG oscillatory rhythms across broad cortical regions in PD [177]. It is conceivable, therefore, that EVS may be able to modulate cortical couplings, which has not been explored yet.

To establish the potential of EVS as a therapeutic intervention to modulate cortical couplings in PD, we investigate resting-state cortical couplings measured as PLV that are altered in unmedicated PD patients and normalizing effects of EVS. Specifically, we applied three novel EVS stimuli bounded into specific frequency bands to PD and healthy subjects and examined whether EVS normalizes both the strength and temporal variation of aberrant couplings in PD and the effects are varying according to the stimulation frequencies.

Table 4.1: Demographic and clinical characteristics of the patients with Parkinson's disease (PD) and healhty controls (HC)

	PD	**HC**
Age (years), mean (SD)	67.3 (6.5)	67.6 (8.9)
Gender, n (male/female)	7/9	9/9
Disease duration (years), mean (SD)	7.4 (4.3)	-
UPDRS II, mean (SD)	14.8 (8.1)	-
UPDRS III, mean (SD)	22.1 (8.9)	-
Hoehn and Yahr scale, mean (range)	1.3 (1-2)	-
Levodopa Equivalent Daily Dose (mg), mean (SD) [383]	635.9 (356.4)	-

UPDRS II: Motor aspects of experience of daily living
UPDRS III: Motor symptoms

4.2 Materials and Methods

4.2.1 Participants

Twenty PD patients and 22 age- and gender-matched healthy controls (HC) participated in this study. Patients with atypical parkinsonism or other neurological disorders were excluded from the study, and all included PD patients were classified as having mild to moderate stage PD (Hoehn and Yahr Stage 1-2). Four PD and four HC subjects were excluded in the data analysis due to severe muscle artifacts in their EEG recordings. Therefore, 16 PD (7 males; age: 67.3 ± 6.5 years) and 18 HC (9 males; age: 67.6 ± 8.9 years) subjects were included in the analysis (Table 4.1). All subjects did not have any reported vestibular or auditory disorders and were right-handed. The study protocol was approved by the Clinical Research Ethics Board at the University of British Columbia (UBC) and the recruitment was conducted at the Pacific Parkinsons Research Centre (PPRC) in UBC. All subjects gave written, informed consent prior to participation.

Study Protocol

As individuals have inherently subjective perception of EVS, we utilized systematic procedures that have been previously used in determining subliminal current level [205]. The measured individual threshold level was in the range of 0.23–1.1 mA. After the threshold was determined, the subjects were comfortably seated in front of a computer screen and were instructed to focus their gaze on a continuously displayed fixed target while EEG was being recorded. EEG was first recorded without stimulation for 20 s and EVS were then delivered for a fixed duration of 60 s, followed by an EVS-off period for 20 s (post stimulation). During the stimulation period, EVS was applied at 90% of the individual threshold level.

EEG was recorded from the subjects in 4 different conditions: Sham (no stimulation), EVS1, EVS2 and EVS3 (for details, see 2.3 EVS). EEG recording was first performed in the sham condition and the EVS conditions were randomly ordered. We allowed a 2-minute break between each condition to prevent any potential post-stimulation effects carried over from the previous EVS conditions.

The HC subjects performed the protocol once, whereas PD subjects performed it twice in off-medication (PDMOFF) and on-medication (PDMON) conditions on the same day. The PD subjects stopped taking their normal L-dopa medication at least 12 hours, and any dopamine agonists 18 hours prior to the EEG recording. United Parkinsons Disease Rating Scale (UPDRS) Parts II and III were assessed in the off-medication condition. Immediately after finishing the EEG acquisition, they took their regular dose of L-dopa medication and rested for one hour. After the break, EEG was recorded in the on-medication condition. While this did not allow for counterbalancing between pre-medication and post-medication conditions, it was felt the variability induced by bringing people in on different days would actually be a greater source of variability than the ordering of PDMOFF and PDMON.

4.2.2 EVS

EVS was delivered through pre-gelled Ag/AgCl electrodes (BIOPAC Systems Inc., CA, USA) placed in bilateral, bipolar fashion over the mastoid process behind each ear. Nuprep^{TM} skin prep gel was used to clean skin for better electrode contact and to reduce resistance during stimulation. Stimulation waveforms were generated on a computer using MATLAB (R2018a, MathWorks, MA, USA) and converted to an analog signal using a NI USB-6221 BNC digital acquisition module (National Instruments, TX, USA). The

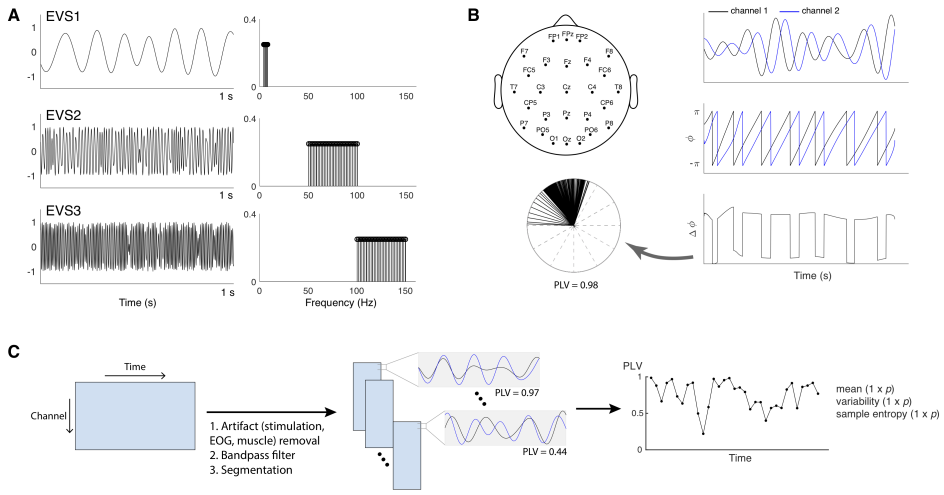

Figure 4.1: The multisine stimuli and the phase locking value (PLV) calculation. (A) Time and frequency plots of the three types of multisine stimulus given at 90% individual threshold level (EVS1: 4-8 Hz; EVS2: 50-100 Hz; EVS3: 100-150 Hz). (B) Placement of 27 EEG electrodes and PLV calculation. The Hilbert transform is applied to the two signals to extract instantaneous phases. The phase differences calculated at each time point are represented as unit vectors in the complex plane and PLV is computed to evaluate the spread of the distribution (Lachaux et al. 1999; Mormann et al. 2000). (C) The procedure to extract PLV time series. For each subject, preprocessing steps were first applied to the raw EEG data in order to remove high-voltage stimulation artifacts as well as cardinal artifacts caused by eye movements (electrooculography (EOG)) or muscle movement. The cleaned data were bandpass filtered into 4 different frequency bands (theta: 4–8 Hz; alpha: 8–13 Hz; beta: 13–30 Hz; gamma: 30–45 Hz) and segmented into epochs. PLV between a pair of electrodes in each epoch was computed to generate the time series, and its mean, variability, and sample entropy were calculated. Each subject has a $1 \times p$ vector for the mean, variability and sample entropy (p = 1,404 = 351 pairs x 4 frequency bands)

analog voltage signals were then passed to a constant current stimulator (DS5, Digitimer, UK), which was connected to the stimulating electrodes.

Three multisine signals in different frequency bands (EVS1: 4–8 Hz; EVS2: 50–100 Hz; EVS3: 100–150 Hz) were used (Fig. 4.1A). Multisine signals are designed to concentrate power at a precise number of frequencies within the bandwidth of interest, which is advantageous compared to other excitation signals (e.g., a white noise or swept sine) as there is no spectral leakage. Each multisine signals were designed to have the frequencies of sinusoids (f_i) uniformly distributed every 0.2 Hz and the phases (ϕ_i) chosen to minimize the crest factor using a clipping algorithm [401] in order to

generate a flat amplitude of the signal and thus improve subjects comfort:

$$x(t, \phi) = a \cdot \sum_{i=1}^{n} cos(2\pi f_i t + \phi_i) \tag{4.1}$$

where $x(t, \phi)$ is the multisine, a is the amplitude, and f_i and ϕ_i are the frequency and phase, and i is the index of each sinusoidal component (e.g., $f_1, f_2, ..., f_n = 4.0, 4.2, ..., 8.0$ Hz for EVS1).

4.2.3 EEG recording

Data were recorded from 27 scalp electrodes using a 64-channel EEG cap (Neuroscan, VA, USA) and a Neuroscan SynAmps2 acquisition system (Neuroscan, VA, USA) at a sampling rate of 1 kHz. Recording electrodes were positioned according to the International 10-20 placement standard with one ground and one reference electrode located between Cz and CPz (Fig. 4.1B). Impedances were kept below 15 $k\Omega$ using Electro-Gel (Electrode-Cap International, OH, USA). No clipping of EEG was observed during stimulation

4.2.4 EEG preprocessing

The EEG data were bandpass filtered between 3 and 45 Hz using a two-way finite impulse response (FIR) filter (the eegfilt function in EEGLAB). High-voltage stimulation artifacts during EVS2 and EVS3 were removed using the digital filters. The artifacts during EVS1 were removed using a quadrature-IVA method [206]. Data were then re-referenced to the average reference (linked earlobe) and ocular artifacts (EOG) were corrected based on cross-correlation with the reference EOG channels using the AAR toolbox included in EEGLAB. The cleaned EEG data were bandpass filtered into four conventional EEG frequency bands [132]: theta (4–8 Hz), alpha (8–13 Hz), beta (13–30 Hz) and gamma (30-45 Hz). The bandpass-filtered data were then segmented into non-overlapping epochs. Epoch sizes were determined such that the epochs include around 4 cycles at a centre frequency of the selected bandwidth, resulting in epoch sizes of 600, 400, 200, and 100 ms for the theta, alpha, beta, and gamma bands.

4.2.5 Phase Locking Value (PLV)

PLV evaluates the spread of the distribution of phase angle differences between pairs of electrodes over time [195, 256] (Fig. 4.1B). The connectivity

is measured from this spread such that strongly clustered phase differences between two electrodes result in the PLV value close to one, indicating a strong connectivity between the signals. If there is no phase dependence, PLV value becomes zero.

To calculate the PLV, instantaneous phase angles were obtained by applying the Hilbert transformation to the bandpass-filtered data. Then, the PLV between two signals A and B was computed as [54]:

$$PLV_{A,B} = \frac{1}{T} \left| \sum_{t=1}^{T} e^{i(\varphi_A(t) - \varphi_B(t))} \right| \tag{4.2}$$

where T is the number of time points and $\varphi(t)$ is the instantaneous phase angles of each EEG signal.

The PLV was computed for each epoch, resulting in times series of the PLV computed from all pairs of 27 electrodes and the 4 frequency bands (1,404 time series in total). Three temporal features were extracted from each PLV time series for further analysis: the mean, variability (standard deviation), and sample entropy. Sample entropy is a nonlinear measure to quantify the degree of complexity in a time series [315], and has been applied to EEG data for clinical application such as classification [52, 193] and epilepsy detection [358]. Tolerance (r) and window length (m) were specified to be 0.3 and 2, respectively, to compute the sample entropy based on [198] and characteristics of our data sets.

4.2.6 Sparce Discriminant Analysis

Linear discriminant analysis (LDA) is a classical supervised classification technique that finds the most discriminative projections of a $N \times p$ data in a p-dimensional space such that the data projected into the low-dimensional subspace can be well partitioned into K classes [228]. In biomedical research, it has become an increasingly important topic to perform classification on high-dimensional data where the number of variables far exceeds the number of samples. In such high-dimensional settings, LDA cannot be applied directly because of singularity of the sample covariance matrix. To overcome this limitation, various regularized versions of LDA have been proposed [326]. Sparse discriminant analysis (SDA) was proposed by Clemmensen and colleagues [70] where an elastic net penalty and an optimal scoring framework are applied to a high-dimensional data to generate a sparse discriminant vector. The authors demonstrated that SDA outperforms other regularized methods such as shrunken centroids regularized discriminant

analysis and sparse partial least squares regression. The details of the algorithm can be found in [70].

Here, we aim to classify the PDMOFF and HC groups in the baseline resting state (i.e., the sham condition) using the PLV features obtained above. The three data sets (mean, variability and sample entropy) have the same high-dimensional settings as each data set has the number of variables ($p = 1{,}404$) much greater than the number of samples (i.e., subjects). Therefore, we applied SDA to each data set to infer from the sparse discriminant vectors which combination of the electrode pairs and frequency bands are the most important features for the classification of the two groups. As in [70], we created the training set consisted of 26 subjects (12 PDMOFF and 14 HC) and the test set of 8 subjects (4 PDMOFF and 4 HC subjects) and the tuning parameters for SDA (i.e., λ and γ for regularization penalties) were chosen using leave-one-out cross-validation (LOOCV) on the training data. The models with the selected parameters were evaluated on the test data.

In the subsequent analyses, we investigated effects of L-dopa medication on the PLV features by applying the sparse discriminant vectors obtained from the above SDA to the data sets of the PDMON group in the sham condition. In the same manner, effects of EVS on the PLV features were evaluated by applying the same sparse discriminant vectors to the data sets in the EVS conditions.

4.2.7 Statistical Analysis

One-way ANOVA was performed to compare the PLV features between groups followed by post-hoc Tukey's honestly significant difference (HSD) test for multiple comparison correction. To evaluate effects of EVS on the PLV features within a group, repeated measures (rm) ANOVA with stimulation condition (*sham*, EVS1, EVS2 and EVS3) as the within-subject factor was performed followed by post-hoc Tukey's HSD test for multiple comparison correction. The rm ANOVA was performed for online and after-effect, respectively.

4.3 Results

4.3.1 SDA Classification Results and Selected Features

SDA was performed for the mean, variability, and entropy PLV data sets independently to discriminate the PDMOFF and HC groups. Since there are

two classes in the data, only one discriminant vector was obtained from each SDA. For the mean PLV data set, LOOCV on the training data resulted in the selection of 17 nonzero features (1.2 %) out of total 1,404 features (Fig. 4.2A). There were both negative and positive weights for the selected features in each frequency band. Since the transformed PLV mean was greater for the PDMOFF (Fig. 4.3A) than the HC group, the positive weights were interpreted as cortical couplings exaggerated in the PDMOFF group. 35% of the selected features were associated with Cz over a broad frequency bandwidth, and the PDMOFF group had a stronger coupling strength for the features. In contrast, the features related to C4 had negative weights, indicating that these couplings are attenuated in the PDMOFF group. In the gamma band, decreased long-distance connectivity in the left temporal region (T7-O1 and T7-P8) and increased short-distance connectivity in the parietal region (P3-PO5, P8-P4, and P8-PO6) were found to be related to the PDMOFF group. The training and test classification accuracy (fraction of correctly classified) were both 100%.

For the PLV variability data set, 12 nonzero features (0.85%) were selected and the largest number of the selected features was found in the theta band (Fig. 4.2B), followed by the alpha and gamma bands. Note that positive weights are associated with the lower connectivity variability of the PDMOFF group because the transformed variability is lower for the PDMOFF group (Fig. 4.3A). Decreased variability in the PDMOFF group was mostly associated with the frontal electrodes in the theta band and with F3-Cz, C3-Pz and P7-PO6 in the alpha band. The classification accuracy for the training and test data sets were 100% and 87.5%, respectively.

The SDA on the PLV entropy data set selected 17 nonzero features (1.2%) and most of them were long-distance connectivity. Note that positive weights are associated with the connectivity with lower entropy for the PDMOFF group. In the theta and alpha bands, the entropy of the selected features was lower whereas in the gamma band the entropy was higher for the PDMOFF group compared to the HC group. In the beta band, the PDMOFF group had a lower entropy for Fz-O2 and higher entropy for Pz-PO6 than the HC group. The training and test classification accuracy were 96% and 87.5%, respectively

4.3.2 Group Comparison of Baseline PLV Features

The SDA discriminant vectors were applied to the data sets obtained from the PDMON group, and the group means of the transformed data are compared in Fig. 4.3A. Significant group differences were found for the PLV

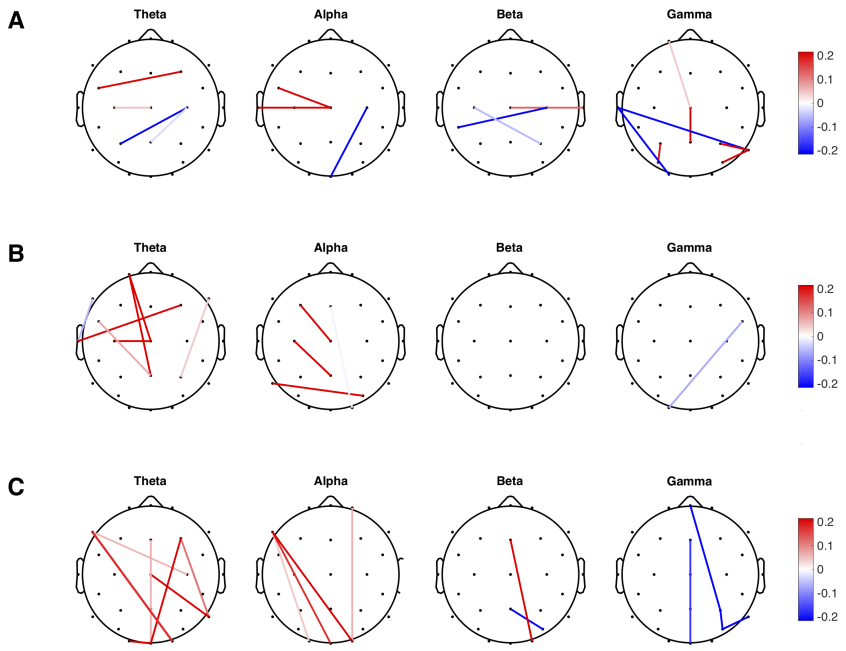

Figure 4.2: Nonzero features selected by sparse discriminant analysis (SDA). SDA was applied to the mean, variability and entropy data sets, respectively, to discriminate the PDMOFF and HC group. The nonzero weights in the sparse discriminant vectors are presented in the scalp maps. (A) Weights for the 17 selected features from the mean PLV data set. (B) Weights for the 12 selected features from the PLV variability data set. (C) Weights for the 17 selected features from the PLV entropy data set.

features (PLV mean: F(2, 47) = 41.68, $P < 0.001$; PLV variability: F(2, 47) = 23.46, $P < 0.001$; PLV entropy: F(2, 47) = 60.59, $P < 0.001$). The PLV mean for the PDMOFF group was significantly higher than the HC group ($P < 0.001$), which was decreased by L-dopa medication ($P < 0.001$). The PLV variability was significantly lower in the PDMOFF compared to the HC group ($P < 0.001$), and the lower variability was associated with higher UPDRS II scores (i.e., more severe difficulties of daily motor activities) ($r = -0.56$, $P = 0.025$). The medication slightly improved the variability in the PD subjects but the changes did not reach statistical significance ($P = 0.096$). The entropy of the PDMOFF group was lower than the HC group ($P < 0.001$) and the lower entropy was related to a longer disease duration ($r = -0.56$, $P = 0.038$). The medication did not improve the PLV entropy ($P = 0.21$).

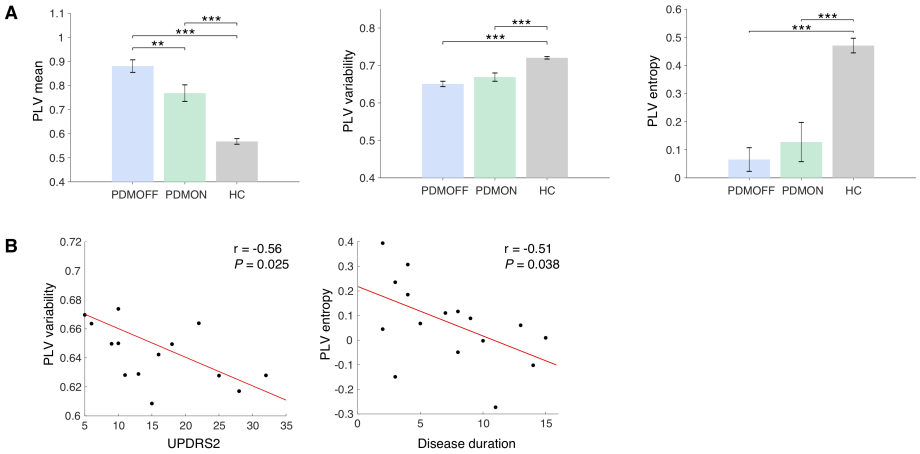

Figure 4.3: (A) Group comparison of the discriminant component obtained from the SDA. The discriminant components were obtained by multiplying the discriminant vectors to the data sets from the sham condition. Bars and error bars indicate group means and s.e. Significant P-values from one-sample/two-sample t-tests are indicated (***$P <$ 0.001). (B) Pearson correlations with clinical scores. The PLV variability and entropy of the PDMOFF subjects are significantly correlated with UPDRS2 and disease duration, respectively

4.3.3 Online- and after-effects of EVS

Next, EVS effects on the PLV features were investigated. Specifically, we examined whether the effects are dependent on the stimulus types and sustained even after the stimulation ceases. Fig. 4.4A–C show changes in the PLV mean for each group induced by EVS1, EVS2 and EVS3, respectively. The PLV mean was significantly modulated in PDMOFF (F(3, 45) = 11.16, $P < 0.001$) and HC (F(3, 51) = 3.81, $P < 0.05$) groups during stimulation. All stimuli decreased the PLV mean in the PDMOFF group compared to the sham condition (EVS1: $P < 0.001$; EVS2: $P < 0.01$; EVS3: $P < 0.01$), making it closer to the HC group, and the effects lasted in the post-stimulation period. EVS1 decreased the mean PLV greater than the other two stimuli and there was no continuing decrease in the post-stimulation period whereas EVS3 decreased the mean PLV less than EVS1 during stimulation and the effect continued in the post-stimulation period. In contrast, we found the opposite EVS effects for the HC group where EVS increased the PLV mean (EVS2: $P < 0.05$; EVS3: $P < 0.01$). No significant effects of EVS were found in the PDMON group (F(3, 45) = 0.77, $P = 0.52$).

EVS effects on the PLV variability are presented in Fig. 4.5A–C. There

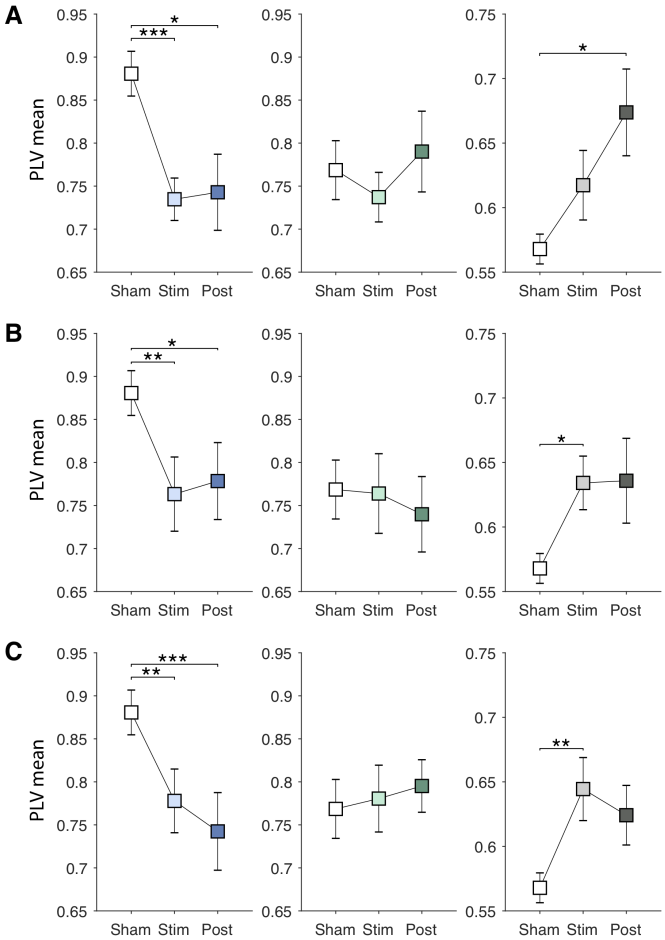

Figure 4.4: Effects of EVS on the PLV mean. The PLV mean values in the sham condition are identical to those in Fig. 4.3A. The PLV mean values in the stimulation (60 s) and post-stimulation period (20 s) were obtained in the same manner by multiplying the discriminant vector to the corresponding data sets. In each row, from the left, the results for the PDMOFF (blue), PDMON (green), and HC (grey) groups are presented in each panel. Significant P-values from the repeated measures ANOVA with post-hoc Tukey's HSD test are indicated (*$P < 0.05$; **$P < 0.01$; ***$P < 0.001$). (A) EVS1 effects. (B) EVS2 effects. (C) EVS3 effects.

were significant online effects of stimulation on the PLV variability in PDMOFF ($F(3, 45) = 4.43$, $P < 0.01$) and HC ($F(3, 51) = 4.62$, $P < 0.01$) groups. EVS1 and EVS2 were found to have positive effects on the PDMOFF group,

increasing the variability during stimulation (EVS1: $P < 0.01$; EVS2: $P < 0.05$). Similar to the effects on the PLV mean, EVS1 induced the greatest increase in the variability during stimulation and the increased value tends to return to the baseline after the stimulation ceased whereas the effects of EVS2 and EVS3 were less during stimulation but lasted longer than that of EVS1. In the HC group, we found decreases in the PLV variability induced by EVS (EVS1: $P < 0.01$; EVS2: $P < 0.05$; EVS3: $P < 0.05$). EVS1 decreased the variability during the stimulation and the effect lasted in the post-stimulation period. EVS2 and EVS3 appeared to further decrease the variability in the post-stimulation period. For the PDMON group, all stimuli increased the PLV variability but the effects did not reach statistical significance ($F(3, 45) = 1.13$, $P = 0.35$).

Fig. 4.6A–C show EVS effects on the PLV entropy. The PLV entropy was significantly modulated in PDMOFF ($F(3, 45) = 4.65$, $P < 0.01$), PDMON ($F(3, 45) = 3.12$, $P < 0.05$), and HC ($F(3, 51) = 4.25$, $P < 0.01$) groups during stimulation. We found that all stimuli increased the entropy significantly in the PDMOFF group (EVS1: $P < 0.01$; EVS2: $P < 0.05$; EVS3: $P < 0.05$), bringing it closer to the HC group. The effects were greatest during stimulation and diminished in the post-stimulation period, and EVS1 increased the largest amount of the entropy, followed by EVS2 and EVS3. For the PDMON group, EVS1 ($P < 0.05$) and EVS2 ($P < 0.05$) increased the entropy significantly. While not statistically significant, increases in the entropy were also found during and post EVS3 compared to the sham condition. The PLV entropy of the HC group changed in the opposite direction by EVS compared to the PD groups. Significant decreases in the entropy was observed with all stimuli (EVS1 ($P < 0.01$), EVS2 ($P < 0.05$) and EVS3 ($P < 0.01$)).

4.4 Discussion

We investigated phase-based cortical connectivity in resting EEG in PD. To our knowledge, this is the first study that examined connectivity dynamics in PD by characterizing temporally fluctuating cortico-cortical couplings over broad frequency bands. The results from the current study on the time-varying connectivity provide novel insights into altered cortical dynamics derived from pathological BG changes in PD.

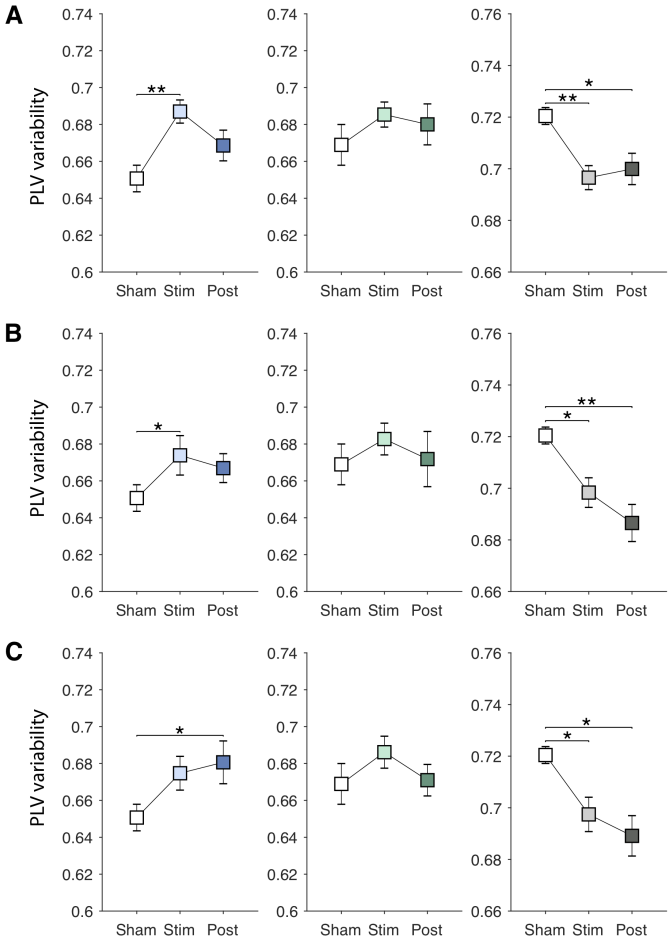

Figure 4.5: Effects of EVS on the PLV variability. The PLV variability values in the sham condition are identical to those in Fig. 4.3A. Descriptions for the arrangement of the plots and statistical significance are same as in the Fig. 4.4. (A) EVS1 effects. (B) EVS2 effects. (C) EVS3 effects.

4.4.1 Disrupted Cortical Coupling Strength in the Motor Regions

We found most changes in cortical coupling strength associated with PD (Fig. 4.2A; 11 out of 17) were in key motor and parietal regions, including over the primary motor cortex (M1), supplementary motor area (SMA), premotor area (PMA), and superior parietal regions, which was in line with

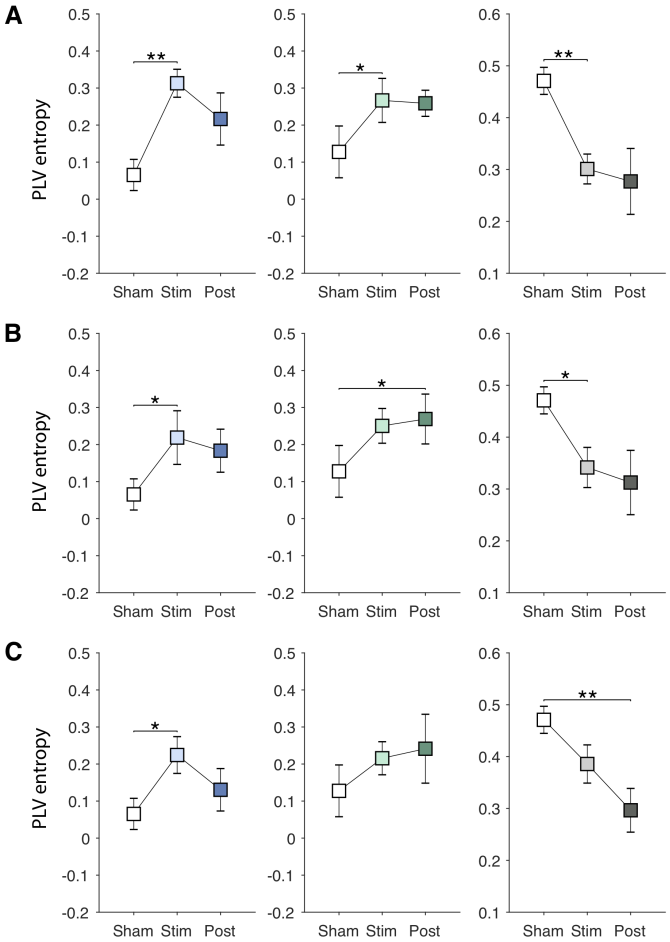

Figure 4.6: Effects of EVS on the PLV entropy. The PLV entropy values in the sham condition are identical to those in Fig. 4.3A. Descriptions for the arrangement of the plots and statistical significance are same as in the Fig. 4.4. (A) EVS1 effects. (B) EVS2 effects. (C) EVS3 effects.

previous findings [276]. Typically, a common finding of pathological synchronization in PD is hypersynchronization of the cortical regions in the beta range [124, 301, 351]. This appears to be related to exaggerated beta synchronization within the BG and between the BG and motor cortical regions [44, 48, 162]. However, growing evidence indicates that PD has more complex influences on motor networks beyond excessive beta synchronization [430, 431]. There is altered cortical oscillatory activity in other bands

beside beta [40, 370]. On the other hand, there is substantial agreement that therapeutic DBS [301] and dopaminergic medication [146, 374, 431] have normalizing effects on rsFC of motor networks in PD. Consistent with these findings, our results demonstrated that the altered connectivity found in the PDMOFF group was normalized by both medication and EVS to a similar extent.

4.4.2 Variablity and Entropy of PLV in the Theta Band

The altered variability and entropy of PLV in the PD group were mostly found in the theta band (Fig. 4.2B–C), which may reflect abnormalities in thalamocortical dynamics. The ventral anterior (VA) and anterior part of ventral lateral (VLa) thalamic nuclei are the major recipients from the globus pallidus internus (GPi) via pallidothalamic tracts that are crucially involved in motor disorders such as PD [120]. Simultaneously-recorded LFP in the VA and VLa nuclei and EEG on the scalp from PD subjects demonstrated the highest coherence in the theta band (4–9 Hz), in particular in the frontal region of both hemispheres [332]. Thalamocortical interaction may thus be a major influence in generation of frontal theta activity in PD, and possibly also healthy controls, but we typically do not have LFP recordings from healthy subjects. Multimodal functional imaging studies in healthy human and animal models suggest that the thalamus is critically involved in generating and modulating activities in the cortex [153, 182, 185, 343]. The enhanced synchronization in the theta band of the thalamus and frontal cortical region may be reflective of pathological changes in PD. Together, we conjecture that the increased mean and reduced variability in theta that we observed in PD subjects was a consequence of excessive synchronization between thalamocortical structures.

4.4.3 Variability and Entropy of PLV in the Alpha Band

The dominant frequency in the human EEG under rest is in the alpha frequency band (8–13 Hz). Alpha oscillations are known to be affected by visual and auditory stimuli [142] and change during voluntary movement [289]. A large body of evidence has also demonstrated the critical role of alpha rhythms in attention as well as various cognitive functions [182]. The dynamic change of alpha activity reflects a variability of states with enhanced and reduced cortical excitability, facilitating the brain's responses to surrounding stimuli [123]. Several studies have shown that brain signal variability/complexity can serve as an important discriminator for clinical com-

parisons. For example, EEG entropy is related to brain maturity, as adults have higher entropy compared to children and adolescents [218]. Higher entropy is also correlated with better performance on a working memory task [243]. Schlee and colleagues found reduced variability of alpha activity during rest over the temporal cortex for subjects with tinnitus compared to controls [337]. Similarly, the reduced variability and complexity of the cortical couplings of the PD groups we observed may be related to diminished motor and cognitive adaptability, as executive cognitive functions such as set shifting, divided or alternating attention and dual tasking (e.g., combining walking with another task) are impaired in PD [1, 258, 415]. Although the mechanisms responsible for these symptoms have not been fully accounted for, dopaminergic depletion in the striatum disrupts the parallel organization of cortico-striatal circuits, resulting in more widespread instead of domain-specific involvement of striatal activity and loss of the normally segregated circuits [31, 58, 263]. Our results together with the close relationships between cortico-striatal circuits and cortical alpha oscillations [202, 354] warrant future studies to further elucidate the functional implications of the impaired alpha dynamic couplings we have demonstrated here.

4.4.4 PLV sample entropy is higher in the long-range gamma activity in PD

We found that the connectivity in the gamma band was more irregular in the PD group than the HC group (Fig. 4.2C). The binding of cortical regions together via synchronization of gamma oscillations between neuronal populations, is implicated in numerous cognitive processes [116, 356]. In voluntary movement, for example, synchronization of cortical gamma oscillations prior to movement onset has been described as representing active information processing [292, 328] and considered to serve as a prokinetic signal [44]. Abnormal gamma oscillations in the motor cortex in PD have been reported [219, 270]. However, resting-state gamma oscillations and connectivity in PD remain largely unknown. The mechanism underlying generation of the gamma oscillations are known to be critically involved with excitatory postsynaptic potentials (EPSPs) of gamma-aminobutyric acid (GABA)ergic interneurons and their intact function of fast-spiking [117, 138, 410]. Thus, alterations in function of GABAergic interneurons could be inferenced from gamma-band oscillations at the macroscopic level. The fast-spiking interneurons are modulated by neurotransmitters including acetylcholine [116, 376, 385] and serotonin [116, 309], and there is robust evidence demonstrating deficits in the cholinergic and serotoninergic

systems in PD contributing to various aspects of parkinsonian pathophysiology including motor symptoms, gait dysfunction, cognitive decline, autonomic dysfunction (for review, see [288]). Therefore, it is likely that the disrupted neurotransmitter systems in PD cause alterations in the activities of fast-spiking interneurons, subsequently resulting in pathological cortical couplings in the gamma band in PD.

4.4.5 Normalizing Effects of EVS and Potential Mechanisms

In this study, we demonstrated that EVS normalizes the mean, variability and entropy of PLV in PD subjects during stimulation and the extent and duration of the effects were dependent on the stimulation frequencies (Fig. 4.4–4.6). Modulatory effects of EVS on the cortical oscillatory activity were reported in prior EEG studies that noisy stimulus (pink noise in 0.1–10 Hz) decreased gamma oscillatory activity in the lateral regions and increased the beta and gamma activity in the frontal region [177], and altered interhemispheric coherence [204]. To our knowledge, effects of high-frequency EVS ($>$ 50 Hz) on cortical activity have not been explored yet in humans and the results presented in this study provide valuable information on how the effects would differ from low-frequency EVS that has been used in prior behaviour and neuroimaging studies. We found two characteristics of effects induced by EVS2 and EVS3 on PLV. First, their effects were similar to EVS1 in the sense that the direction of changes (i.e., increase or decrease in the PLV features) was the same. We did not find a frequency specific increase or decrease in the PLV value in both the PD and HC groups. Second, the extent of changes was less compared to EVS1 during the high-frequency stimulation but lasted longer in the post-stimulation period. This was observed in the PDMOFF group for all the PLV measures and in the HC group for the variability and entropy. For the PDMON group, the EVS effects were less significant, indicating the processing of vestibular inputs in the thalamus and BG [221, 368, 421] is dependent on the dopaminergic level of the BG.

Modulating of firing rates of vestibular afferents by externally applied electrical current will alter directly the vestibular nuclei activities in the brain stem, and eventually multiple cortical areas through the thalamocortical vestibular system. Thus, understanding vestibular information processing regarding varying frequency contents at the vestibular nuclei and thalamus is critical to comprehend above findings. A prior study that examined spiking rates of the guinea pig medial vestibular nuclei (MVN) reported that two types of neurons having different characteristics of afterpotentials

responded to current inputs differentially according to the frequency content (1–30 Hz) [316]. It was shown that spontaneous firing rates of type A neurons was well modulated by only low-frequency (< 10 Hz) current inputs and the spiking rates becomes irrelevant to the current input at high frequencies whereas type B neurons tended to fire in synchrony better when the stimulation frequency was higher, which demonstrates existence of signal transformation at the vestibular nuclei level to a certain extent in that type A neurons act like a low-pass filter [94, 316] whereas type B neurons act as signal detectors with greater sensitivity to external stimuli at high frequencies.

Considering functional roles of the thalamic nuclei playing integrative and modulatory roles in sensorimotor processing [389], it is likely that further transformation of the modified signal transmitted from the vestibular nuclei occurs in the thalamus. The VA, VL, ventral posterior lateral (VPL), ventral posterior medial (VPM), intraminar nuclei and geniculate bodies of the thalamus receive primary afferents from the vestibular nuclei and play a critical role in processing vestibular information [30, 55, 247, 366, 421]. These thalamic nuclei also receive a range of different afferents from peripheral sensory, subcortical, and cortical regions, and process the different types of information before sending the refined signals to the cortex. This may also explain the interaction between EVS and L-dopa medication as observed in the PDMOFF and PDMON groups as the thalamic nuclei processing vestibular information would be receiving differential inputs from the BG according to dopaminergic state. Together, unlike transcranial electrical or magnetic stimulation that directly target cortical regions of interest, influences of EVS on cortical activities are much more indirect. Our results suggest that although the frequency contents of current input to the peripheral vestibular nerve vary considerably, alterations of the refined higher-level multisensory information transmitted from the thalamic nuclei to the broad cortical regions may be relatively consistent.

4.4.6 Limitations

The post-stimulation effects were evaluated for the first 20 seconds only after stimulation ceased and there may be potential confounding effects if the after effects persist much longer. After effects of EVS on cortical activation have not been fully investigated yet. Delayed responses in the beta and gamma power in frontal regions was reported to appear 20–25 s after 72-s EVS, but lasted only for several seconds. Based on prior studies reporting after effects of invasive [429] and non-invasive stimulation [372] and the short

duration of weak current EVS used here, we concluded that the break time and randomly-ordered trials were sufficient to avoid confounding effects.

We note that the PLV may be affected by volume conduction as in the case of EEG data several electrodes can simultaneously pick up activities from the same underlying sources. The propagation of the source signals can be assumed to be instantaneous due to the low capacitance of the skin tissues and the small distance that the currents have to travel [266, 364], and thus PLV at zero-phase differences are susceptible to the volume conduction [165]. Several alternative methods such as the phase lag index [364] and spatial filtering have been proposed to address the issue [377].

In conclusion, in this resting-state EEG study, we demonstrated that connectivity strengths in the sensorimotor region, and variability and complexity of the time-varying cortico-cortical connectivity are affected in PD, and improved by subthreshold EVS. Furthermore, the magnitude and duration of the improvement was found to vary depending on the stimulation frequency and the subjects' dopaminergic status. The findings from the current study provide valuable information that thalamic functions of integrating subcortical afferent inputs and thalamocortical projections to the cortex play a critical role in the mechanism of EVS effects, and warrant further investigation of EVS as a potential therapy in PD.

Chapter 5

Discriminant Correlation Approach to Joint Estimation of Maximal EVS Effects on Motor Behaviour and Cortical Beta Oscillations in PD

The previous chapter demonstrated that pathological cortical couplings in PD can be normalized by multisine EVS. Moving forward, in this chapter we investigated whether the multisine stimulus can also improve motor function in PD. Specifically, we focused to answer the fundamental questions 1) whether the EVS improves motor task performance in PD, 2) whether the EVS modulates movement-related cortical oscillations, and 3) how the changes in upstream cortical oscillations and downstream movements are related.

5.1 Introduction

Loss of dopaminergic neurons in the substantia nigra pars compacta (SNc) in PD gives rise to motor and functional changes in the basal ganglia (BG)-thalamo-cortical networks, affecting motor planning and control [83]. Some motor symptoms may arise because the functional networks in PD are stuck in a fixed state, leaving them in a characteristic exaggerated state of rhythms resonating in the beta range (13–30 Hz) [100, 210, 420]. Several studies have reported strong beta power in local field potentials (LFPs) recorded from the BG and cortex of PD patients associated with their poverty of movement [420]. PD therapies that restore movement deficits suppress these pathologically exaggerated, poorly-modulated beta oscillations. For example, ad-

ministration of levodopa medication [50, 191] and DBS [49, 429] attenuate highly synchronous beta oscillations in the subthalamic nucleus (STN).

Normal suppression of beta oscillations in the sensorimotor cortex before and during voluntary movement have long been investigated with EEG and MEG [161] (for review see [175]). This response, event-related desynchronization (ERD), has well-characterized temporal features: beta power starts to decrease just before movement onset, with sustained suppression during movement execution, and returns back to baseline often followed by post-movement beta rebound (PMBR), predominantly over primary sensorimotor regions [175, 290, 291]. PD patients demonstrate distinct ERD alterations, such as delayed onset [82], diminished ERD and PMBR [146], and different topographical patterns [146, 259] compared to controls.

Motivated by growing evidence of the functional role of synchronized neural oscillations in motor deficits and success of DBS in alleviating symptoms, recent studies have explored the use of non-invasive brain stimulation (NIBS) techniques as a potential therapeutic intervention for PD. Electrical vestibular stimulation (EVS) is a NIBS technique that applies electrical current over the mastoid processes to stimulate vestibular afferents that can activate numerous downstream cortical and subcortical regions [30]. Several studies have demonstrated beneficial effects of EVS on motor symptoms in PD [205, 278, 432] and modulatory effects on cortical oscillations [177], but a joint study linking changes in neural oscillations and behaviour induced by EVS is lacking.

Here, using EVS and simultaneously recorded EEG, we investigate modulatory effects of high-frequency EVS on movement-related beta oscillations and resultant changes in the motor behaviour of PD patients and healthy controls. Removing the stimulation artifacts in the EEG, online stimulation effects were investigated in this study without having to examine subtle post-stimulation remnants of influence as done in majority of NIBS studies. Three key findings are reported here. First, EVS augments beta ERD over the left motor region before right-handed movement onset and increases synchronization during motor execution, returning to baseline in broad frontal and medial parietal regions, resulting in improved motor task performance. Second, EVS not only modulates the magnitude of beta ERD but also influences its timing, resulting in an earlier onset of the ERD peak, and a faster recovery to baseline, suggesting increased fluidity of the motor network. Third, these stimulation effects were dependent on behavioural context as the beta oscillations were not significantly altered by EVS during rest. From the findings, we conjecture that strong vestibular inputs interact with movement-related signals (likely in the thalamus) as part of the

"motor integrative" hypothesis, making it easier to dynamically modulate motor systems.

5.2 Materials and Methods

5.2.1 Subjects

The subjects and study protocol are same as those in Chapter 4. Twenty PD and 22 age-matched healthy control (HC) subjects participated in this study. The PD subjects were classified as having mild to moderate stage PD (Hoehn and Yahr Stage 1-2) without atypical Parkinsonism or other neurological disorders. We excluded four PD and four HC subjects in the data analysis due to severe muscle artifacts irrelevant to the task such as excessive facial muscle activity and coughing (we note that clinical characteristics such as tremor and bradykinesia scores between included and excluded PD subjects were not significantly different). Therefore, sixteen PD (7 males, age 67.3 $\pm$ 6.5 years) and eighteen HC (9 males, age 67.6 $\pm$ 8.9 years) subjects were included in the analysis (Table 5.1). All subjects did not have any reported vestibular or auditory disorders and were right-handed.

The study protocol was approved by the Clinical Research Ethics Board at the University of British Columbia (UBC) and the recruitment was conducted at the Pacific Parkinsons Research Centre (PPRC). All subjects gave written, informed consent prior to participation.

5.2.2 EVS

EVS was delivered in bilateral, bipolar fashion through pre-gelled Ag/AgCl electrodes (BIOPAC Systems Inc., USA) placed over the mastoid process behind each ear using a constant current stimulator DS5 (Digitimer, UK). Two multisine signals were used for EVS (EVS1: 100–150 Hz; EVS2: 50–100 Hz). Each signal had the frequencies of sinusoids (f_i) uniformly distributed every 0.2 Hz, with the phases (ϕ_i) chosen to minimize the crest factor using a clipping algorithm [401] in order to improve subject comfort. We utilized systematic procedures previously used to determine individual threshold level [205], and the stimulus was applied at an imperceptible level (90% of sensory threshold) to avoid effects of placebo, general arousal and/or voluntary selective attention.

Table 5.1: Demographic and clinical characteristics of the patients with Parkinsons disease (PD) and healthy controls (HC)

	PD	**HC**
Age (years), mean (SD)	67.3 (6.5)	67.6 (8.9)
Gender, n (male/female)	7/9	9/9
Disease duration (years), mean (SD)	7.4 (4.3)	-
UPDRS II, mean (SD)	14.8 (8.1)	-
UPDRS III, mean (SD)	22.1 (8.9)	-
Hoehn and Yahr scale, mean (range)	1.3 (1-2)	-
Levodopa Equivalent Daily Dose (mg), mean (SD) [383]	635.9 (356.4)	-

UPDRS II: Motor aspects of experience of daily living
UPDRS III: Motor symptoms

5.2.3 Study protocol

Subjects were comfortably seated in front of a computer screen and instructed to focus their gaze on a continuously-displayed fixed target for 60 s. Then, a written instruction was given to press a key on the keyboard to start the motor task. Subjects were then instructed to respond to a visual cue ("Go") as fast as possible by squeezing a rubber bulb (Fig. 5.1). This motor task was adapted as it provides more descriptive behaviour measures than button-press tasks and prior studies on hypokinesia demonstrated motor control abnormalities of the PD subjects via their exerting pressure during a similar motor task as ours [236]. There were 10 trials in each stimulation condition and 12 different stimulation conditions (including *sham* (no stimulation) in total). The number of trials were selected such that the PD subjects can complete the entire study protocol without excessive tiredness (particularly in off-medication condition) and significant differences in task performance between conditions can still be detected. The order of the stimulation conditions was randomized across the subjects and we located the *sham* condition as far as possible from the EVS conditions by conducting it before any EVS conditions in order to avoid any potential effects carried over from EVS. We allowed a 2-min break between each condition to prevent any

confounding post-stimulation effects. In this work, we report results from *sham*, EVS1 and EVS2 conditions for which we could remove high-voltage stimulation artifacts and analyze the EEG data jointly with the behaviour data.

The PD subjects stopped taking their normal levodopa medication at least 12 hours, and any dopamine agonists 18 hours prior to the experiment (off-medication; PDMOFF). Unified Parkinson's Disease Rating Scale (UPDRS) Parts II and III were assessed in off-medication condition. After the first session, they took their regular dose of levodopa medication and rested for an hour before beginning the second session (on-medication; PDMON). There was one session for the HC subjects.

5.2.4 EEG Recordings and Preprocessing

EEG was recorded from 27 scalp electrodes with sampling rate of 1 kHz using Neuroscan SynAmps2 EEG acquisition system (Neuroscan, USA) and a standard electrode cap (64-channels Quik-Cap, Neuroscan, USA). EEG electrodes were positioned according to the international 10-20 placement standard with one ground and one reference electrode located between Cz and CPz. The electrodes were attached using Electro-Gel (Electrode-Cap International, USA) and impedances were kept below 15 $k\Omega$. For preprocessing, the EEG data were bandpass filtered between 3 and 55 Hz using a two-way finite impulse response (FIR) filter. The stimulation artifact could be removed using the digital filter as they were in the high-frequency range. Data were then re-referenced to the average reference (linked earlobe), and eye blinks, eye movements and muscle activities were removed using independent component analysis (ICA) available in EEGLAB.

5.2.5 Data analysis

Behaviour data analysis

We defined five landmarks in the water pressure recordings from the squeezable pressure-sensor bulb: P_{max} (peak grip pressure), t_1 (time when the visual cue was presented), t_2 (time when the pressure started to exceed 0.05), t_3 (time of P_{max}), t_4 (time when the pressure returns to 0.05 after P_{max}). They were used to extract six behavioural indices (Fig. 5.1).

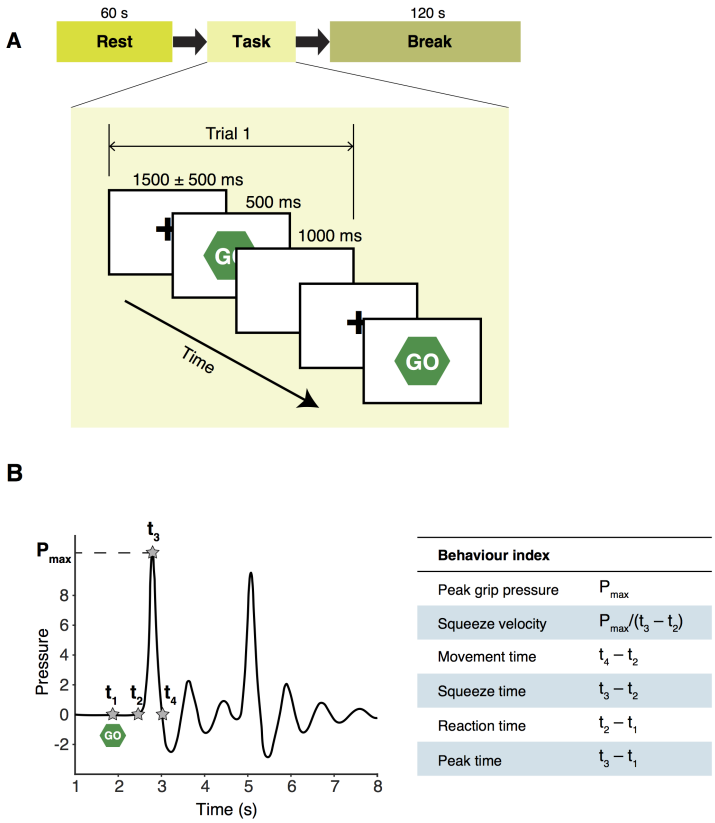

Figure 5.1: Schematic of study protocol and motor task performance. (A) Each subject performed the study protocol in *sham*, EVS1 and EVS2 conditions while EEG was continuously being recorded. In each condition, the subjects were comfortably seated and focused their gaze on a fixed target presented on a computer screen for 60 s (Rest). After pressing any key on a keyboard, they started a motor task consisting of 10 trials (Task). Each trial started with a hold phase in which a fixation cross was presented at the center for a randomized duration that ranged from 1000 to 2000 ms ($\mathcal{N}(1500, 500)$). Then, a visual cue ("Go") appeared for 500 ms followed by 1000-ms white blank screen. The subjects were instructed to squeeze a rubber bulb as fast as they could to respond to the visual cue. After finishing the motor task, they took a 120-s break. (B) Water pressure recorded from the squeezable pressure sensor bulb is plotted along the time in the x-axis. For each trial, a peak grip pressure (P_{max}) and four time points (t_1: the visual cue; t_2 movement onset; t_3 peak grip pressure; t_4: movement termination) were extracted to compute six behaviour measures shown in the table

ERD Analysis

With the visual cue onset as the reference time ($t = 0$ ms), the EEG data were epoched from -1000 to 1500 ms and then wavelet transformed using

complex Morlet wavelets (center frequency, $\Omega_c = 1$; bandwidth parameter, $\Omega_b = 2$; 30 frequencies logarithmically distributed from 7 to 50 Hz). The mean beta (13–30 Hz) power in the baseline interval (from -600 to 0 ms), P_{base}, was calculated as a reference value to evaluate ERD. Similar to the approach adopted in [99], we selected two distinct time windows to investigate the ERD at different movement phases based on 10th percentile of the reaction time of all subjects: 0–400 ms for motor preparation and 400–1000 ms for motor execution. In order to determine if our results were sensitive to the cut-off times, we repeated the analysis with 0–400 ms and 560–1000 ms windows (based on the 10th and 90th percentile respectively) and the results were unchanged (not shown). For each channel, beta ERD was calculated as

$$ERD = \frac{1}{N} \sum_{i=1}^{N} 10 \log_{10} \frac{P_i}{P_{base,i}} \tag{5.1}$$

where P is the mean beta power in the time window, i is the trial index, and N is the total number of trials ($N = 10$).

Joint analysis of behaviour and ERD data

In order to investigate maximal EVS effects across all subjects with regard to the task performance and the beta ERD, we used a feature fusion method, discriminant correlation analysis (DCA), that incorporates discrimination across classes into a canonical correlation analysis (CCA)-based algorithm. The basic concept of DCA is that it searches for transformation weights (W_X and W_Y) to project original data sets (X and Y) into a space where the new projected data (X' and Y') are correlated with each other and separation of different classes is achieved (for detailed description of the algorithm, see [137]). We created one data set (X) by concatenating the beta ERD from all subjects during *sham* (class 1) and EVS (class 2). Another data set (Y) was created by concatenating the behaviour indices (the peak time was excluded due to its collinearity with the squeeze time and reaction time). DCA were performed four times as there were two EVS conditions and two movement phases. The transformation weights and correlations between X' and Y' were examined to investigate EVS effects on the beta ERD and task performance as well as their interrelationship.

Statistical analysis

For each behaviour index, between-group task performance in the *sham* condition was compared using ANOVA with the results from 10 trials as the response variable and subjects and groups as the random and fixed factors. For EVS effects on task performance, ANOVA was performed for each behaviour index with the results from 10 trials as the response variable and subjects and EVS conditions as the random and fixed factors. The P values were corrected for multiple comparison using Tukey's honestly significant difference (HSD) test (multcompare.m in MATLAB). Students paired t-test were used for the DCA results. For investigation of potential accumulated and/or learning effects for the repeated stimulation and task, repeated measures ANOVA was performed for each behaviour measure using the task performance across the 11 stimulation conditions as the dependent variable, time as the within-subject factor, and group (i.e., PDMOFF, PDMON, HC) as the between-subject factor.

5.3 Results

5.3.1 Task Performance in the *Sham* Condition

Significant group differences in task performance were found in several behaviour indices (grip strength: $F(2, 497) = 8.87$, $P < 0.001$; squeeze velocity: $F(2, 497) = 3.42$, $P < 0.05$; movement time: $F(2, 497) = 4.74$, $P < 0.01$; squeeze time: $F(2, 497) = 10.45$, $P < 0.001$; reaction time: $F(2, 497) = 12.15$, $P < 0.001$; peak time: $F(2, 497) = 11.28$, $P < 0.001$). The PDMOFF group showed a significantly higher peak grip pressure compared to the PDMON ($P < 0.001$) and HC ($P < 0.01$) groups (Fig. 5.2), and a higher squeeze velocity than the PDMON group ($P < 0.05$). Both the movement time and squeeze time of the PDMOFF group were longer compared to the HC group whereas only the squeeze time was significantly longer than the PDMON ($P < 0.001$) group. The reaction time and peak time of the PDMON group were significantly shorter than the PDMOFF and HC groups.

5.3.2 EVS Effects on the Task Performance

There were significant effects of stimulation on the behaviour indices (Table 5.2) with greater effects in the PDMOFF group (Fig. 5.3). Compared to the *sham* condition, EVS1 significantly decreased the peak grip pressure ($P < 0.05$) in the PDMOFF group, and squeeze time, reaction time and peak time

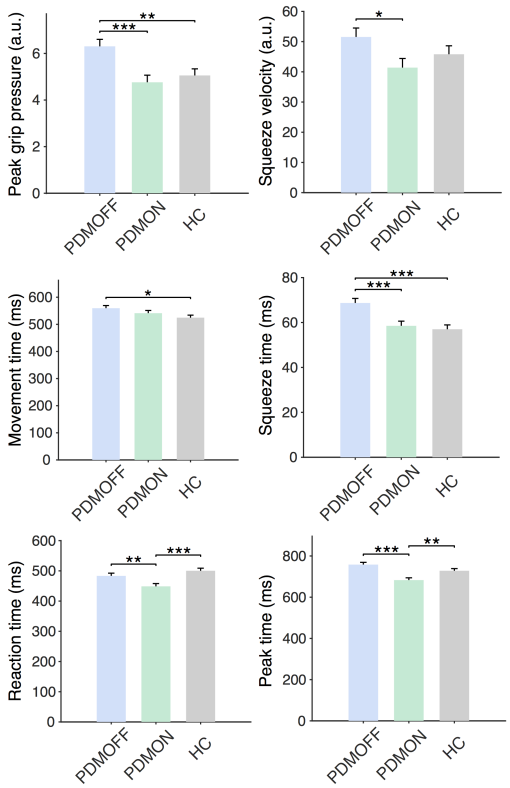

Figure 5.2: Motor task performance in *sham* condition. (A) Comparison of the task performance in the *sham* condition between the PDMOFF, PDMON and HC groups. Significant P values from ANOVAs are indicated (*$P < 0.05$; **$P < 0.01$; ***$P < 0.001$). Error bars indicate SEM.

in the PDMOFF and HC groups. For the PDMON group, the movement time was significantly reduced ($P < 0.01$). EVS2 changed the squeeze time and peak time in the PDMOFF and HC groups while no significant effects were found in the PDMON group (Fig. 5.3).

In order to determine if there is any interactino between EVS and L-dopa medication for the PD subjects, we carried out two-way repeated measures ANOVA with EVS and medication as within-subject factors and the six behaviour indices as dependent variables. The results showed a significant interaction between the EVS and medication (Wilks' Lambda = 0.487, F (10,52) = 2.251, P = 0.029).

Table 5.2: ANOVA results on the effects of stimulation condition on the behaviour indices

	df	Peak grip pressure	Squeeze velocity	Movement time	Squeeze time	Reaction time	Peak time
PDMOFF	2:477	F = 4.19 ($*P < 0.05$)	F = 2.73 ($P = 0.066$)	F = 7.77 ($***P < 0.001$)	F = 12.32 ($***P < 0.001$)	F = 3.9 ($*P < 0.05$)	F = 18.25 ($***P < 0.001$)
PDMON	2:477	F = 1.08 ($*P < 0.05$)	F = 1.42 ($P = 0.24$)	F = 4.37 ($*P < 0.05$)	F = 2.53 ($P = 0.08$)	F = 0.3 ($P = 0.74$)	F = 0.74 ($P = 0.48$)
HC	2:537	F = 0.47 ($P = 0.63$)	F = 1.29 ($P = 0.28$)	F = 3.6 ($*P < 0.05$)	F = 3.9 ($*P < 0.05$)	F = 29.04 ($***P < 0.001$)	F = 29.13 ($***P < 0.001$)

5.3.3 EVS Effects during Motor Preparation

Compared to the *sham* condition, the mean beta ERD during motor preparation was significantly lower during EVS1 (Fig. 5.4A), demonstrating that EVS1 augmented the ERD in the brain regions indicated in the weight (W_X). For better visualization of their spatial locations, W_X is presented on a scalp map (Fig. 5.4B). The largest positive weights were found at C3 and CP5, indicating EVS1 augmented the ERD primarily in the left motor regions. During EVS1, the behavioural index was lower compared to the *sham* condition (Fig. 5.4A) and was found to be associated more with movement time, squeeze time, and reaction time as indicated in W_Y in Fig. 5.4B, corresponding to the behavioural results that EVS1 had greater effects on these behaviour indices than the peak grip pressure and squeeze velocity.

To infer whether the changes in the ERD during EVS1 were positively or negatively related to task performance, we examined its correlation with the behaviour index and found a positive correlation ($r = 0.23$, $P = 0.019$). Given that the lower behaviour index is associated with shorter movement time, squeeze time and reaction time, a more negative ERD is thus related to better task performance. Therefore, the results that EVS1 augments the

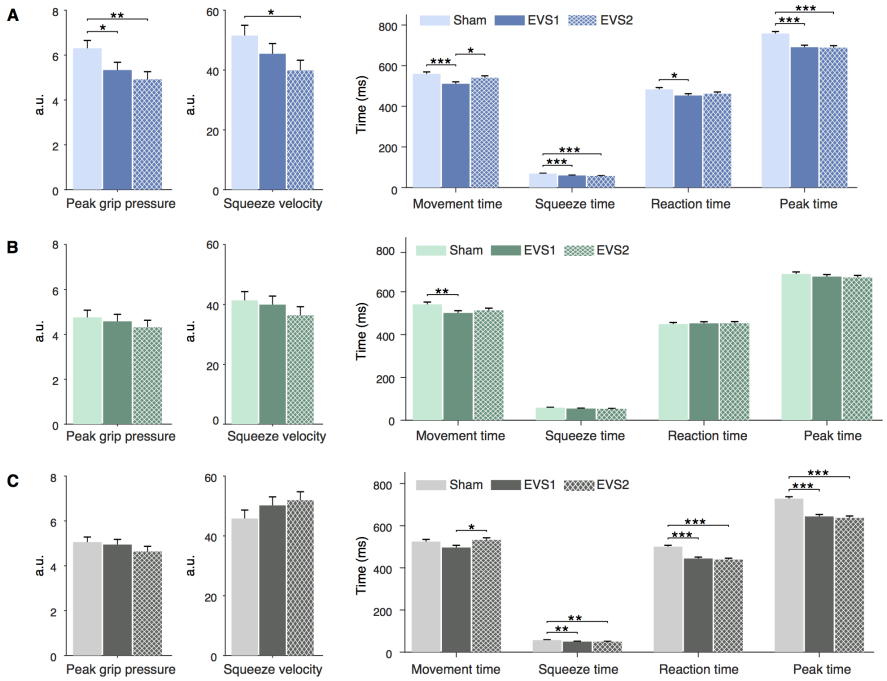

Figure 5.3: EVS Effects on the motor task performance. Experiment conditions are indicated by the light color (*sham*), dark color (EVS1), and hatch pattern (EVS2). (A) the PDMOFF group (blue). (B) the PDMON group (green). (C) the HC group (grey). Significant P values from ANOVAs are indicated (*$P < 0.05$; **$P < 0.01$; ***$P < 0.001$). Error bars indicate SEM.

ERD and decreases the behaviour index can be interpreted as facilitating motor function.

In *post-hoc* analyses of the DCA results, we found that the ERD was significantly augmented by EVS1 in the PDMOFF ($P < 0.05$) and HC ($P < 0.001$) groups (Fig. 5.4C). Particularly, in the PDMOFF group, the degree of the augmented ERD by EVS1 was positively correlated with disease severity (r = 0.59, p = 0.015; Fig. 5.4D). For the behaviour index, significant improvement by EVS 1 was observed for all groups (PDMOFF: $P < 0.001$; PDMON: $P < 0.01$; HC: $P < 0.05$). As there was no correlation between the ERD and behaviour index ($r = -0.075$, $P = 0.46$) from DCA results of the EVS2 condition, we did not draw inferences about the EVS2 results.

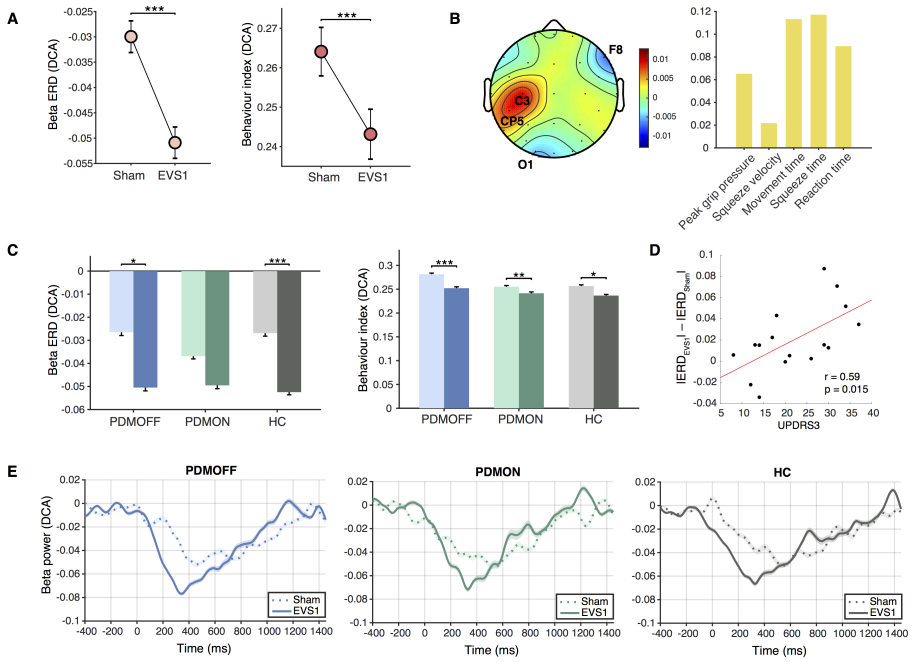

Figure 5.4: DCA results demonstrating EVS1 effects on the beta ERD and task performance during motor preparation. (A) The beta ERD was significantly augmented and the behaviour index was significantly decreased by EVS1 compared to the *sham* condition (***$P < 0.001$; paired t-tests). (B) The weight (W_X) associated with the beta ERD is presented on the scalp map (left), demonstrating that the augmentation of the beta ERD occurred predominantly in the left motor region. The weight (W_Y) for the behaviour index presented in a bar graph (right) shows that EVS1 decreased the movement time, squeeze time, and reaction time more than the other behavioural measures. (C) *Post-hoc* analyses with Wilcoxon signed-rank tests revealed EVS1 decreased the beta ERD in the PDMOFF and HC groups and the behaviour index in all groups compared to the *sham* condition (*$P < 0.05$; **$P < 0.01$; ***$P < 0.001$). Light and dark colours represent the *sham* and EVS1 conditions, respectively. (D) Correlation between the degree of augmented beta ERD by EVS1 with UPDRS Part III scores. (E) Temporal evolution of the beta ERD averaged across the subjects in each group (lines: mean; shaded area: SEM of leave-one-out cross-validation). Compared to the *sham* condition, the suppression of the beta power was greater and the timing of the negative peak was earlier in the EVS1 condition.

5.3.4 EVS Effects during Motor Execution

The beta ERD during motor execution was higher during EVS1 compared to the *sham* condition (Fig. 5.5A), and the difference was most prominent in the frontal and medial parietal regions (Fig. 5.5B). A negative correlation

was found between the ERD and behaviour index ($r = -0.39$, $P < 0.001$), indicating that a better task performance related to a higher ERD value. In post-hoc analyses, considerable increases in the ERD and behaviour index by EVS1 were found in the PDMOFF ($P < 0.01$) and HC ($P < 0.001$) groups (Fig. 5.5C).

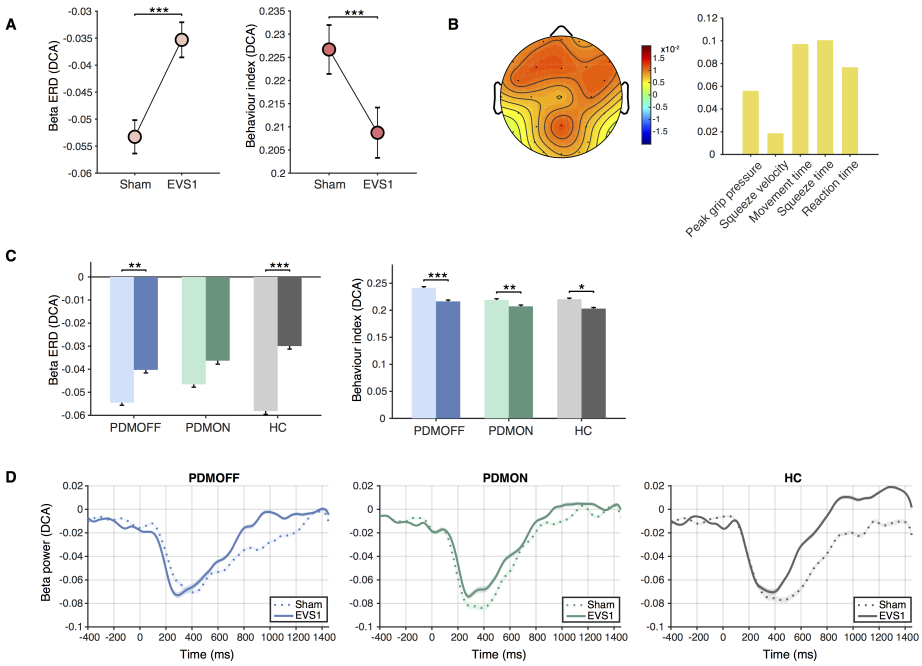

Figure 5.5: DCA results demonstrating EVS1 effects on the beta ERD and task performance during motor execution. (A) The beta ERD value was significantly increased and the behaviour index was significantly decreased by EVS1 compared to the *sham* condition (***$P < 0.001$; paired t-tests). (B) The weight (W_X) associated with the beta ERD is presented on the scalp map (left), demonstrating the increase occurred in the frontal and medial parietal regions. (C) *Post-hoc* analyses with Wilcoxon signed-rank tests revealed EVS1 increased the beta power during motor execution in the PDMOFF and HC groups and the behaviour index in all groups compared to the *sham* condition (*$P < 0.05$; **$P < 0.01$; ***$P < 0.001$). Light and dark colours represent the *sham* and EVS1 conditions, respectively. (D) Temporal evolution of the beta ERD averaged across the subjects in each group (lines: mean; shaded area: SEM of leave-one-out cross-validation). Compared to the *sham* condition, the rate of the beta power returning to the baseline ($t > 400$ ms) is faster in the EVS1 condition.

In the EVS2 condition, similar to the aforementioned results, positive weights were found in the left frontal and right central regions with some extension to the medial parietal region (Fig. 5.6B), and the ERD over

these regions was higher during EVS2 compared to the *sham* condition (Fig. 5.6A). A negative correlation was found between the ERD and behaviour index ($r = -0.36$, $P < 0.001$). In *post-hoc* analyses, significant increases in the ERD by EVS2 was observed for all three groups (PDMOFF: $P < 0.05$; PDMON: $P < 0.01$; HC: $P < 0.001$ in Fig. 5.6C). The behaviour index was reduced by EVS2 in the PDMOFF ($P < 0.001$) and PDMON ($P < 0.01$) groups.

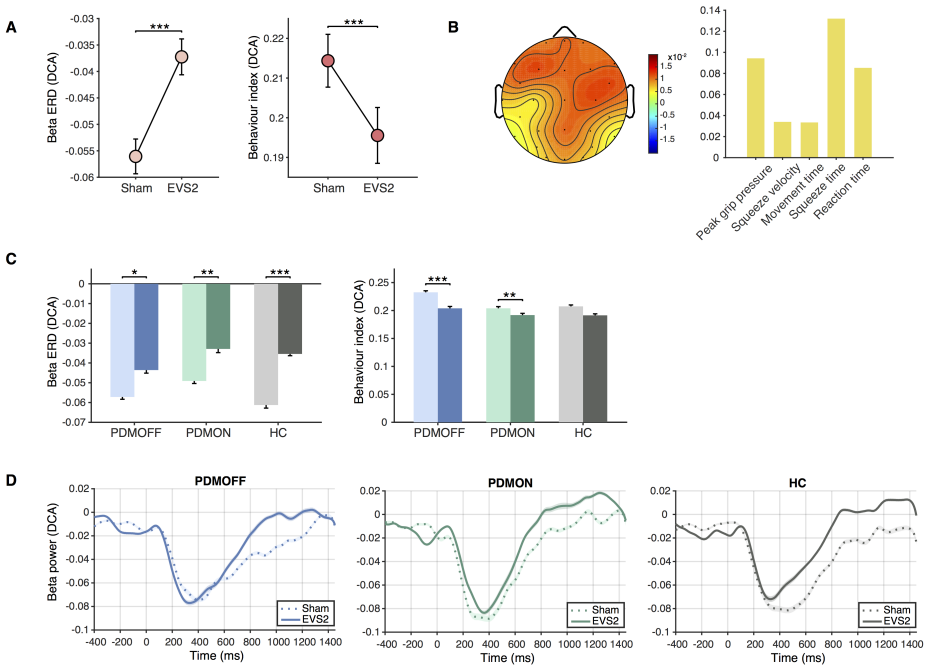

Figure 5.6: DCA results demonstrating EVS2 effects on the beta ERD and task performance during motor execution. (A) The beta ERD value was significantly increased and the behaviour index was significantly decreased by EVS2 compared to the *sham* condition (***$P < 0.001$; paired t-tests). (B) The weight (W_X) associated with the beta ERD is presented on the scalp map (left), demonstrating the increase occurred in the frontal and medial parietal regions. The weight (W_Y) for the behaviour index presented in a bar graph (right) shows that EVS2 decreased the peak grip pressure, squeeze time, and reaction time more than the other behavioural measures. (C) *Post-hoc* analyses with Wilcoxon signed-rank tests revealed EVS2 increased the beta power during motor execution in all groups and the behaviour index in the PDMOFF and PDMON groups compared to the *sham* condition (*$P < 0.05$; **$P < 0.01$; ***$P < 0.001$). Light and dark colours represent the *sham* and EVS2 conditions, respectively. (D) Temporal evolution of the beta ERD averaged across the subjects in each group (lines: mean; shaded area: SEM of leave-one-out cross-validation). Compared to the *sham* condition, the rate of the beta power returning to the baseline ($t > 400$ ms) is faster in the EVS2 condition.

5.3.5 EVS Effects on Temporal Patterns of the Beta ERD

Since EVS had opposite effects on the beta ERD when we divided the motor task into discrete "preparation" and "movement" phases, we probed the origin of the differential effects by examining the entire time courses of the ERD (Fig. 5.4E) (note that the ERD lines represent time courses of the beta power over the brain regions indicated in the DCA weights (W_X) shown in Fig. 5.4B). Compared to the *sham* condition, distinct features in the EVS1 condition were found at the time when the curve reaches the minimum: suppression of the beta power was greater and the timing of the negative peak was earlier.

For movement execution, differences between the *sham* and EVS1 conditions were observed after the negative peak appeared (Fig. 5.5D). The beta power started to return to baseline around 400 ms after the visual cue onset, and the recovery rate was faster during EVS1. In addition, towards the termination of the movement, beta power was higher, suggesting a greater PMBR. Similar results were found in the EVS2 condition (Fig. 5.6D). Based on these observations, we conclude that the overall increased ERD by EVS during motor execution is ascribed to this temporal feature of the beta power recovery rather than the magnitude of the ERD itself being small.

5.3.6 EVS Effects on the Beta Oscillations in the Resting Condition

There were no significant changes induced by EVS in both the mean and SD of the beta power the left motor, frontal and medial parietal regions during rest (Figs. 5.7 and 5.8).

5.4 Discussion

We demonstrated EVS elicits a range of changes in task performance, with the most remarkable results in the PDMOFF, followed by HC and PDMON groups. The improvement was greater with EVS1 than EVS2 overall and correlated with more pronounced beta ERD in the left motor region during motor preparation and faster recovery of the beta power in the frontal and medial parietal regions during motor execution. Finally, the modulatory effects on the beta oscillations were specific to performing the motor task.

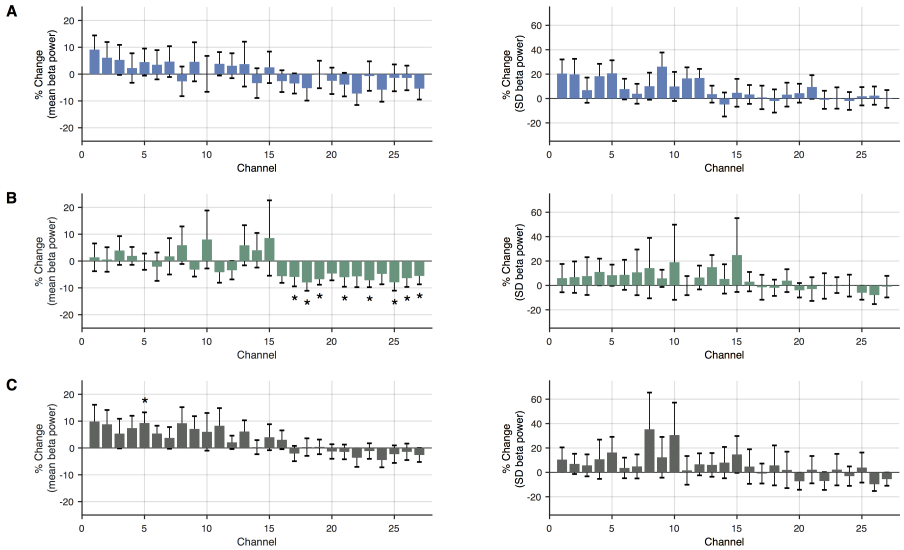

Figure 5.7: Effects of EVS1 on the beta power during the 60-s resting condition. The beta power in each of the 2-s epochs was computed using the multi-taper method (seven Slepian sequences; frequency resolution = 0.5 Hz), and then the temporal mean and SD across the epochs in the EVS1 condition were compared to those in the *sham* condition. Bar graphs represents the % change in the temporal mean (left) and the SD (right) induced by EVS1 for subjects in each group and error bars indicate SEM. Significant P values from one-sample t-tests are indicated (*$P < 0.05$ before multiple correction). To account for multiple comparisons, false discovery rate (FDR)-corrected P values were calculated using the method introduced by Benjamini and Hochberg [27] (mafdr.m in MATLAB). After the multiple correction, none of the P values reached significance level. (A) The PDMOFF group. (B) The PDMON group. (C) The HC group

5.4.1 Abnormalities in Motor Control in PD

We found greater peak grip pressure and squeeze velocity in the PDMOFF group. This may seem counterintuitive at first, because impairment of motor function in PD would make one believe the patients might have a weaker grip force. However, PD patients have comparable overall muscle strength to control subjects [404]. In addition, *de novo* PD patients use abnormally large grip forces when they are lifting and static-holding an object [104], suggesting this may be an intrinsic feature of PD.

In linear regression analyses (Table 5.3), another pathological characteristic of the grip force was found in the PDMOFF group. For the PDMON and HC groups, the grip force and squeeze velocity were negatively related with reaction time, indicating they tend to produce more ballistic move-

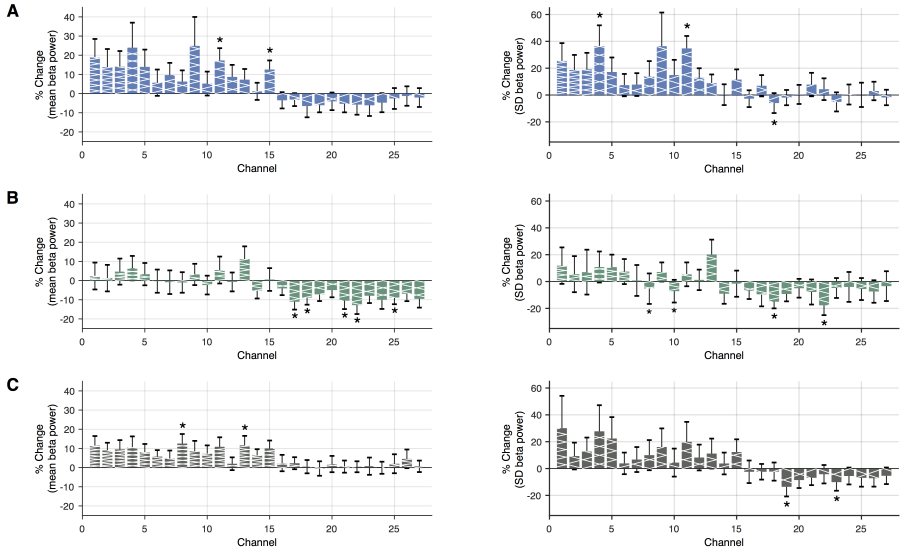

Figure 5.8: Effects of EVS2 on the beta power during the 60-s resting condition. The beta power in each of the 2-s epochs was computed using the multi-taper method (seven Slepian sequences; frequency resolution = 0.5 Hz), and then the temporal mean and SD across the epochs in the EVS2 condition were compared to those in the *sham* condition. Bar graphs represents the % change in the temporal mean (left) and the SD (right) induced by EVS2 for subjects in each group and error bars indicate SEM. Significant P values from one-sample t-tests are indicated (*$P < 0.05$ before multiple correction). After multiple correction, none of the p-values reached significance level. (A) The PDMOFF group. (B) The PDMON group. (C) The HC group.

ments when the responses are faster. In contrast, this relationship was lost in the PDMOFF group. PD subjects tended to squeeze harder independent of reaction time, supporting the view that modulation of vigour is impaired in the PD subjects [129, 236].

Table 5.3: Linear regression analysis to demonstrate a relationship between fast responses and vigorous movements. P-values represent statistical significance of the slopes.

	PDMOFF	**PDMON**	**HC**
y (reaction time, ms) x (peak grip pressure, a.u.)	$y = 473.0 - 1.2x$ ($P = 0.52$)	$y = 468.3 - 4.6x$ ($P < 0.01$)	$y = 518.4 - 5.4x$ ($P < 0.05$)
y (reaction time, ms) x (squeeze velocity, a.u.)	$y = 475.8 - 0.2x$ ($P = 0.24$)	$y = 468.0 - 0.5x$ ($P < 0.01$)	$y = 537.5 - 1.0x$ ($P < 0.01$)

5.4.2 EVS effects on the behavioural indices

To the best of our knowledge, there is only one prior study that reported EVS effects on reaction time in a motor task [432]. In that study, the reaction time of the PD patients was decreased by EVS without changes in omission or commission errors, suggesting cognitive processes were not affected by the stimulation. Considering the task was rudimentary, the authors suggested EVS may have improved bradykinetic motor execution. We found EVS improved the reaction time in both PDMOFF and HC groups, suggesting the underlying neural mechanism may be common across the groups rather than specific to the disease. EVS effects were mild for the PDMON group compared to the other groups, suggesting interactions between the medication and EVS. Possibly this was due to ceiling effects, as levodopa is already known to suppress pathological beta-band oscillations in PD [93, 126].

We carefully evaluated whether or not there was an accumulated and/or learning effect due to repetitive stimulation and task using repeated-measures ANOVA, and none of the behaviour measures showed a systematic difference across trials (Table 5.4). We conclude that our observations were consistent with a stimulus-specific effect that was robust and repeatable as compared to insignificant behaviour changes found using the other stimuli (not reported here). However, there were differences across sham trials, suggesting that although the stimulation trials did not show any accumulated effect, there may have been some carryover during rest. More work is required to determine the duration of any possible carryover effect at rest.

5.4.3 Functional significance of beta ERD in voluntary movement

The correlation between better performance and greater beta ERD is in line with the concept that augmented ERD reflects involvement of a larger neural network in information processing, which facilitates more efficient task performance [291, 367]. The reduced development time and enhanced magnitude of the ERD in the motor preparation period is similar to effects of levodopa on PD subjects [90, 227], which may indicate facilitation of readiness of motor network for the upcoming movement [14, 15, 97, 127]. In accordance with this view, at the subcortical level, the early timing of beta ERD onset in the STN is correlated with shorter reaction times [426].

In the motor execution period, EVS was found to facilitate more rapid beta power recovery in the frontal and medial parietal regions belonging to the frontoparietal network. The frontoparietal network is important in

Table 5.4: Results of the repeated measures ANOVA to investigate accumulated and/or learning effect on the behaviour measures.

		SS	**df**	**MS**	**F**	***P* value**
Peak grip pressure	Time	5.976	10	0.598	1.097	0.369
	Group × Time	12.7	20	0.635	1.166	0.279
	Error (Time)	250.59	460	0.545		
Squeeze velocity	Time	629.72	10	62.97	0.752	0.675
	Group × Time	1716.8	20	85.84	1.025	0.430
	Error (Time)	38510	460	83.72		
Movement time	Time	6799	10	679.9	0.244	0.991
	Group × Time	59016	20	2950.8	1.061	0.388
	Error (Time)	1.279×10^6	460	2780.4		
Squeeze time	Time	681.2	10	68.12	1.275	0.242
	Group × Time	641.5	20	32.08	0.600	0.913
	Error (Time)	24570	460	53.41		
Reaction time	Time	8040.2	10	804.02	0.921	0.514
	Group × Time	19422	20	971.11	1.112	0.333
	Error (Time)	401690	460	873.23		
Peak time	Time	16165	10	1616.5	1.808	0.057
	Group × Time	27385	20	1369.3	1.531	0.066
	Error (Time)	411330	460	849.2		

conscious motor intention and movement awareness [88], facilitating motor preparation and execution through information flow between the parietal and frontal cortices [419]. In addition, the frontal region includes supplementary motor area (SMA) and premotor areas (PMA) where beta oscillations are known to play a critical role in motor control [290, 371]. The functional significance of the rate of beta power recovery in these regions, however, still remains incompletely understood as most effort has been devoted to understanding the magnitude and spatial distribution. Nevertheless, we suggest that it might be associated with post-movement resetting for the next movement [365].

5.4.4 Modulation of beta ERD via NIBS

Several tACS studies have demonstrated changes in the beta oscillations are causally linked to motor behaviour (for review see [403]). Entraining beta oscillations in the motor cortex by 20-Hz tACS affected motor-evoked potentials (MEPs) [107] and slowed down voluntary movements [169, 298]. Our results extend these studies and show that modulating beta ERD appears causally related to motor responses in the PD and HC subjects.

A significant contribution of this work is to provide evidence of online effects of EVS on beta ERD, which was not demonstrated in prior NIBS studies presumably due to high-voltage artifacts from electrical stimulation severely corrupting EEG. Here, we used stimulation frequencies beyond the range of cortical oscillations of interest in typical EEG studies (1–50 Hz) and multisine signals that keep excitation power within specific frequency components [294], so stimulation artifacts in the EEG data could be effectively removed by applying a digital filter.

5.4.5 Beyond the modulation of cortical oscillations —potential mechanisms of EVS

We had two competing hypotheses for the EVS effects on the beta ERD. The first hypothesis was EVS reduces beta power overall, not necessarily during a motor task. This will facilitate movement as one must suppress the beta power below a certain threshold before movement can commence [145]. The second hypothesis was EVS effects are dependent on behavioural context so that vestibular inputs interact with movement-related signals in the ventral thalamic region, the motor areas of the thalamus. The ventral thalamic region integrates multiple motor-related inputs and projects highly refined motor plans back to the motor cortex. We did not find any significant changes in both the mean and SD of the beta power in during rest (Figs. 5.7 and 5.8), supporting the latter hypothesis—namely involvement EVS effects were integrated with motor task commands rather than nonspecifically reducing overall beta oscillations.

Previous studies support the notion of thalamic nuclei playing integrative and modulatory roles in sensorimotor processing. Vestibular nuclei in the brainstem have multiple ascending projections directly to the thalamus, primarily targeting the ventral anterior (VA), ventral lateral (VL), ventral posterior lateral (VPL), ventral posterior medial (VPM), intraminar nuclei and the geniculate bodies (Fig. 5.9A) [221, 247, 286], and strong activations in these regions by vestibular stimulation have been reported

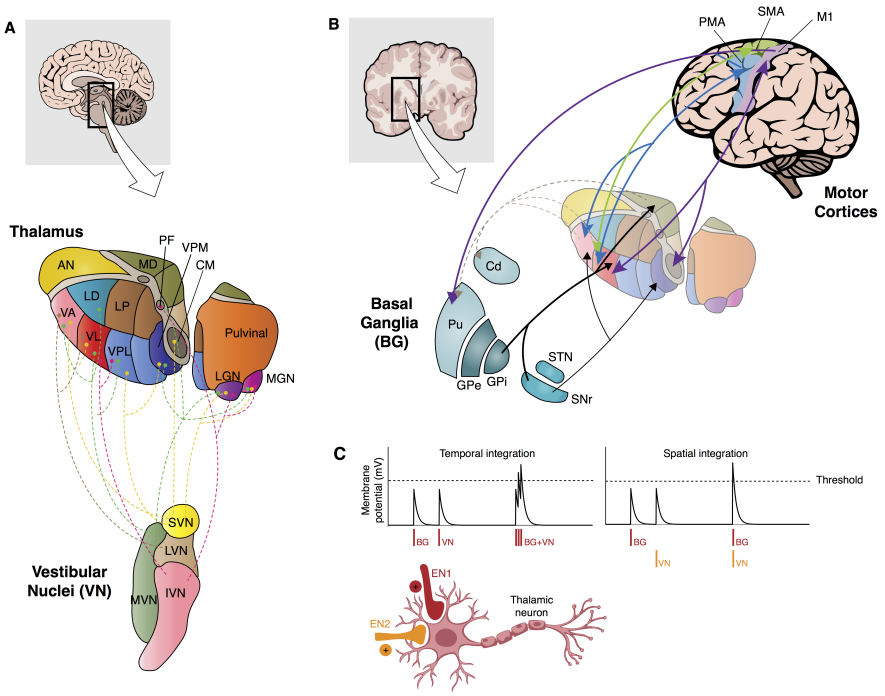

Figure 5.9: Schematic representation of the major projections involved with motor functions. (A) Projections from the four vestibular nuclei to thalamic nuclei. The projections primarily target at the ventral part of the thalamus, a region also known as the motor thalamus. The figure was adapted from [421] and modified based on [221, 368]. (SVN: superior vestibular nucleus; MVN: medial vestibular nucleus; LVN: lateral vestibular nucleus; IVN: inferior vestibular nucleus; AN: anterior nucleus; LD: lateral dorsal nucleus; LP: lateral posterior nucleus; VA: ventral anterior nucleus; VL ventral lateral nucleus; VPL: ventral posterior lateral nucleus; VPM: ventral posterior medial nucleus; MD: mediodorsal nucleus; CM: centromedian nucleus; PF: parafascicular nucleus; LGN: lateral geniculate nucleus; MGN: medial geniculate nucleus) (B) Projections between the thalamus, BG and motor cortices. The thalamus and layer V neurons in the motor cortices have reciprocal connections [41]. The VA, VL and MD project to the putamen and caudate, and the VL and MD receive the bulk of BG outputs [136]. (Cd: caudate; Pu: putamen; GPe: globus pallidus externus; GPi: globus pallidus internus; STN: subthalamic nucleus; SNr: substantia nigra pars reticulata; PMA: premotor cortex; SMA; supplementary motor cortex; M1: primary motor cortex) (C) An illustration of vestibular inputs influencing integrative processes of a motor thalamic neuron. Inputs from the vestibular nuclei (VN) can be temporally and/or spatially integrated with thalamic afferents from other motor-related structures such as the BG, modulating the neuronal activity.

[30, 55, 247, 366, 421], indicating a critical thalamic contribution to processing vestibular information [221, 421]. In particular, the ventral part of the thalamus has strong connections with motor-related structures such as M1, PMA, and BG (Fig. 5.9B) [41, 55, 286, 368] and its neural activities are associated with a range of aspects in motor control [158, 194, 405], suggesting it serves as the motor thalamus. Recent studies highlight the functional role of the motor thalamus as a critical hub region to temporally and specially integrate information required for controlling movement by efficiently assigning weights to afferent inputs depending on the context and desired motor outcome and send this highly refined information to the motor cortices [41, 156, 421]. Thus, precise temporal and spatial pattern of the neural activation in the motor thalamus is critically involved with motor preparation and execution, and we surmise that strong vestibular inputs to the motor thalamus had strong influence on the integrative process (Fig. 5.9C). This may also explain the mild EVS effects in the PD subjects on medication as the inputs from the BG afferents to be integrated in the motor thalamus are a function of dopaminergic tone.

We note that EVS might also affect the striatum, a region described as an integrative centre for sensory information and involved in planning and execution of movements. Although the largest inputs to the striatum are from the cortex, recent studies have shed light on its subcortical pathways critical to interpret and respond to environmental stimuli appropriately [109, 242]. Electrophysiological studies in animal models and neuroimaging studies in humans have shown vestibular stimulation activates the head of the caudate nucleus and putamen [30, 42, 178, 234, 366], likely through the parafascicular thalamic nucleus [196, 368].

Understanding the neural mechanisms behind EVS effects will provide deeper insights into brain functioning and brain-behaviour relationships and be crucial to improve neurotherapuetic effects. Although this study reports electrophysiological evidence for its efficacy, findings from various neuroimaging modalities together will allow for a more refined description of EVS effects.

Chapter 6

Spectral Clustering and Discriminant Correlation Approach to Estimation of EVS Effects on Functional Thalamic Subregions and BG–thalamic Connectivity in PD—fMRI Study

The previous chapters have demonstrated therapeutic effects of EVS on cortical oscillations and motor behaviour in PD, which leads us to the next question, "how does the modulation of vestibular nerve activity results in the changes? What are the pathways and mechanisms underlying EVS effects?". Evidence from recent studies suggests that the thalamus may be a key region involved in EVS effects as it has dense connections with both the vestibular nuclei in the brain stem and basal ganglia and serves as a hub region to integrate and modulates sensorimotor information. In this chapter, we addressed the questions by investigating effects of EVS on thalamus activity and connectivity between the thalamus and basal ganglia in PD.

6.1 Introduction

PD is a neurological movement disorder characterized by several cardinal motor symptoms (bradykinesia, rigidity, tremor, and postural instability) that are caused by substantial loss of dopamine in the substantia nigra pars compacta (SNc) located in the midbrain. Afferents from the SNc to the

basal ganglia (BG) supply the striatum with dopamine [262], which is intimately linked to mediating signals transmitted from the cerebral cortex to the thalamus, which, in turn, project back to the cerebral cortex (the cortical-BG-thalamic loops) via direct and indirect pathways [6, 199]. Degeneration of the dopaminergic system results in striatal dopamine depletion of ∼44–98% in PD [313, 428], with changes found in various sub-regions of the striatum including not only the motor regions of the striatum (posterior and ventral putamen) receiving projections from the motor and premotor cortex but also the head of the caudate nucleus, the anterior putamen and the ventral striatum connected to the cerebral cortex, in particular the frontal lobe [68, 271, 412].

The BG work in conjunction with the thalamus and cortex to carry out a number of segregated functions such as motor, oculomotor, cognitive, working memory, and limbic processes in parallel [7, 135]. The primary role of the thalamus has been assumed to be the relaying of information, transferring the signals from the output structures of BG (the internal segment of the globus pallidus (GPi) and substantia nigra pars reticula (SNr)) to the cortex, but recent evidence suggests a much more active functional role of thalamic cell groups in processing BG information and subsequently modulation of the dynamics of cortical processing [135]. In PD, significant pathology in the thalamus can be detected and contribute to parkinsonian motor dysfunction [139]. In parkinsonian rodent models, administration of MPTP or 6-hydroxydopamine has been shown to induce degeneration of thalamic neurons projecting to the striatum as well as the loss of dopaminergic neurons in the SNc [19]. In addition, a range of intrinsic thalamic changes such as bilateral morphological alterations [245], thalamic nuclei degeneration [46, 140, 149], and substantial deposition of α-synuclein [46, 149] have been reported in PD patients. The thalamic changes consequently contribute to alterations in the dynamics of the cortico-BG-thalamic circuits [19] and can result in aberrant connectivity patterns such as decreased connectivity of the thalamus with the GP, SN and the sensorimotor cortices [347].

One promising way to modulate the cortico-BG-thalamic loop altered in PD is through brain stimulation. Deep brain stimulation (DBS) of the thalamic ventral intermediate (Vim) nucleus, internal segment of the GPi or the subthalamic nucleus (STN) has been shown to be effective in treating parkinsonian tremor, dystonia and bradykinesia in PD [76, 310] with minimal effects on akinesia and gait disturbance [253]. One mechanism underlying Vim DBS effects may be that the stimulation inhibits incoming afferent inputs carrying pathological signals or alters the excitability of thalamic nuclei [12]. The success of DBS has led to strong interest in non-

invasive brain stimulation (NIBS), which is particularly attractive due to its easy accessibility and lower cost compared to DBS.

EVS is a NIBS technique where electrical current is applied to mastoid process behind the ear to alter firing rates of vestibular afferents. Several studies have reported beneficial effects of random noise EVS on PD subjects including improved motor performance [205, 278, 330, 432], enhanced pedunculopontine nucleus (PPN) connectivity [57], and modulation of cortical oscillations and connectivity strength [177, 204]. Such effects seem to be ascribed to changes in neural dynamics in the brain by manipulation of ascending pathways from the vestibular nuclei located in the brainstem to the cerebral cortex via thalamocortical vestibular system [221, 392, 421], which has been evidenced in simultaneous fMRI and alterating current EVS studies [30, 220, 366]. The vestibular nuclei have multiple projections to thalamic nuclei including the ventrobasal nuclei that receive strong inputs from the BG and project to primary and motor cortices [421] and the intralaminar nuclei that projects to the striatum [196, 368], suggesting that EVS may be capable of modulating functional connectivity between the thalamus and BG structures.

Here, we investigated the effects of noisy EVS (nEVS) and 1-Hz sine EVS (sEVS) on activity of thalamic subregions obtained from connectivity-based parcellation and their connectivity with BG structures using resting-state fMRI (rsfMRI) data recorded from PD and age-matched control subjects. We demonstrate that the sizes of thalamic functional subregions are altered in the PD subjects, and both nEVS and sEVS "normalize" them, i.e. makes them closer to that of control subjects. We found the connectivity between the left thalamus and left BG is attenuated in the PD subjects off-medication compared to controls and PD subjects on-medication. This alteration was normalized by EVS in a stimulus dependent manner.

6.2 Materials and Methods

6.2.1 Subjects

Fifteen PD subjects (11 males, age: 65.7 ± 8.8 (mean $\pm$ SD) years) and 15 age-matched healthy controls (12 males, age: 63.7 ± 9.6 years; HC) participated in the study (Table 6.1). All subjects did not have any reported vestibular or auditory disorders. The PD subjects were classified as having mild to moderate PD state (Hoehn and Yahr stage I–III) without atypical Parkinsonism or other neurological disorders. The PD subjects stopped taking their normal levodopa medication at least 12 hours, and any dopamine

Table 6.1: Study cohort demographics

Measure	**PD**	**HC**
Age (years)	65.7 ± 8.8	63.7 ± 9.6
Gender (n), male:female	11:4	12:3
Disease duration (years)	3.5 ± 2.0	N/A
Hoehn and Yahr scale	1.6 ± 1.0	N/A
UPDRS III	17 ± 13	N/A
Levodopa Equivalent Daily Dose (mg) [383]	741.7 ± 564.2	N/A
Handedness	all right-handed	all right-handed
Affected side, right:left	9:6	N/A

Affecte side was defined as summed left and right scores of UPDRS III 3.3-3.8 and 3.15-3.17. Subjects with equal scores for the left and right were not counted.

agonists 18 hours prior to the experiment (off-medication; PDMOFF). Unified Parkinsons Disease Rating Scale (UPDRS) Part III was accessed in off-medication condition. After the first fMRI scan in off-medication condition, they took their regular dose of levodopa (L-dopa) medication and rested for an hour before beginning the second scan (on-medication; PDMON). There was one scanning session for the HC subjects.

All subjects were recruited from the Pacific Parkinsons Research Centre (PPRC) at the University of British Columbia (UBC) and provided written, informed consent prior to participation. The study was approved by the UBC Ethics Review Board.

6.2.2 EVS

A bipolar constant current DS5 stimulator (Digitimer Ltd., Hertfordshire, UK) was used to deliver an alternating current via two MR-compatible pre-gelled Ag/AgCl electrodes (Biopac Inc., Montreal, Canada) placed over the mastoid process behind each ear. Digital signals of the EVS stimuli were first generated on a PC with MATLAB (MathWorks, MA, USA) and were converted to analog signals via a NI USB-6221 BNC digital acquisition module

(National Instruments, TX, USA), which subsequently passed to the stimulator in the console room with the output cable leading into the scanning room through a waveguide. The twisted coaxial output cable included four custom-built inductance capacity filters spaced 20 cm apart and tuned for the Larmor frequency (128 MHz).

Two different stimuli were tested in the study. nEVS was pink noise with zero-mean and $1/f$-type power spectrum between 0.1–10 Hz, and sEVS was a 1 Hz sine wave. Since individuals have an inherently subjective perception of EVS, prior to scanning, we determined the individual sensory threshold level (cutaneous sensation at the electrode site) utilizing systematic procedures used in prior EVS studies [205, 424] and delivered EVS at 90% of the individual threshold level. Before conducting the real experiment, we carried out a pilot study and recorded the current actually delivered to the subjects. We confirmed that the delivered current matched with the designed stimulus and device was compatible with MRI.

6.2.3 MRI acquisition and preprocessing

Imaging data were acquired using a Philips Achieva 3.0T R3.2 scanner (Philips Medical Systems, Netherlands). Before scanning, all the subjects were instructed to lie on their back in the scanner and had several minutes to acclimatize themselves to the scanner environment with the eyes closed. Before the functional scans, high-resolution T1-weighted images of the entire brain were acquired (repetition time = 7.9 ms, echo time = 3.5 ms, flip angle = 8). For functional scans, BOLD contrast echo-planar (EPI) T2*-weighted images (repetition time = 1985 ms, echo time = 37 ms, flip angle = 90, field of view = 240 mm × 240 mm, matrix size = 128 × 128, pixel size = 1.9 mm × 1.9 mm) were acquired after 4 initial dummy scans. The scan order was kept consistent for all subjects as *sham*, nEVS, and sEVS, and there was a 2-min break between each condition to avoid any possible post-stimulation effects. The *sham* condition was 8-min resting state and 5-min continuous stimulation was applied in the EVS conditions.

6.2.4 Data preprocessing

Functional MRI data were preprocessed using DPABI version 3.0 [433] and SPM8 software package (https://www.fil.ion.ucl.ac.uk/spm). The first 5 time points were discarded to allow the magnetization to approach a dynamic equilibrium and to allow participants to get used to the scanning noise. Then the images were corrected for slice timing effects, resliced to

$3.0 \times 3.0 \times 3.0$ mm isotropic voxels, movement corrected using rigid body alignment, normalized into standard MNI space. The fMRI data were then spatially smoothed with a 6-mm Gaussian kernel to increase its signal-to-noise ratio. To reduce the potential confounds of head motion and possible effects of physiological artefacts, nuisance time courses were voxel-wise regressed from the processed data to remove sources of variance including head-motion parameters, their temporal derivatives and their squares, white-matter signal and CSF signal. Any linear or quadratic trends were removed from fMRI signals. The fMRI data were finally bandpass filtered at 0.01 Hz to 0.08 Hz as recommended.

6.2.5 Connectivity based parcellation of thalamus

To determine the regional specificity within the thalamus associated with the disease and investigate their regional alterations by EVS, we performed connectivity based subregional parcellation using Normalized Cut Spectral Clustering (NCUT) algorithm that is robust to outliers [166], can easily incorporate spatial constraints, and performs well on fMRI data [74].

Suppose the number of voxels in the thalamus is N, and we construct a graph $G = \{V, E\}$, where the vertex set V represents all N voxels, and E is the edge set. Let W denotes the weight matrix between vertices, and $W(i, j)$ is defined as a function of correlation between nodes i and j. To divide the graph into two disjoint sets A and B, we try to minimize the connections between two sets while maximizing the connections within each set, and the objective function of NCUT is defined as,

$$NC(A, B) = \frac{cut(A, B)}{assoc(A, V)} + \frac{cut(A, B)}{assoc(B, V)} \tag{6.1}$$

where $cut(A, B) = \sum_{i \in A, j \in B} W(i, j)$ is the sum of weighted connections between sets A and B, and $assoc(A, V) = \sum_{i \in A, j \in V} W(i, j)$ is the total weights of connections from nodes in A to all other nodes in the graph.

The NCUT algorithm can be further extended to the K-way partition with K representing the number of partitions [38]. Let D be an $N \times N$ diagonal matrix with $D(i, i) = d_i = \sum_{j=1}^{N} w(i, j)$, and indicator matrix $Y \in \{0, 1\}^{N \cdot K}$ represents the partition of graph G. Then, if node i belongs to partition set j, $Y(i, j) = 1$, otherwise, $Y(i, j) = 0$. This optimization problem can be efficiently solved as a generalized eigenvalue problem,

$$NC = K - Tr(Z'(D^{-\frac{1}{2}} W D^{\frac{1}{2}})Z) \tag{6.2}$$

where $Z'Z = I_K$, and I_K is the identity vector with length K. The solution of Z is the matrix with the k eigenvectors associated with the first K eigenvalues of matrix $D^{-\frac{1}{2}}WD^{\frac{1}{2}}$. Z can be considered as the new set of coordinates for the graph and we further apply the K-means to obtain the cluster indicator matrix Y.

As we were interested in the spatially confluent parcellations, we incorporated spatial information into the subregion parcellation of the thalamus where only spatially continuous voxels were allowed to be connected with each other in the similarity matrix W. In addition, negative correlations were removed from the network, resulting in the symmetric, positive and spatially continuous time-dependent similarity matrices for spectral clustering. After the parcellation, the number and mean time course of the voxels in each subregion were computed.

6.2.6 Subregion size analysis

Multivariate logistic regression analysis was used to compare sizes of the thalamic subregions between PDMOFF and HC groups (independent variables: the sizes of the bilateral thalamic subregions; dependent variable: group). The weights (w_{logit}) obtained from the logistic regression model were then further utilized to compute thalamic subregion sizes of the PDMON subjects (*sham*) and PDMOFF subjects during stimulation to evaluate L-dopa and EVS effects.

6.2.7 Thalamus-BG connectivity analysis

Functional connectivity between the thalamic subregions and BG structures including the bilateral caudate, putamen and pallidum were computed using Pearson correlation and normalized between zero and one for each subject. We examined the ipsilateral and contralateral functional connectivity between the thalamus and BG that is maximally different across the PDMOFF, PDMON, and HC by utilizing discriminant correlation analysis (DCA), a feature fusion method that incorporates discrimination of different classes into a canonical correlation analysis (CCA)-based algorithm. The basic concept of DCA is to search for transformation matrices (W_X and W_Y) to project original data sets (X and Y) into a space where the new projected data (X' and Y') are correlated with each other while simultaneous class separation is achieved (for detailed description of the algorithm, see [137]). Here, we created one data set, X ($n \times p$ matrix; n = number of subjects; $p =$

number of ipsilateral connectivity), by concatenating the functional connectivity between the left BG structures and left thalamic subregions across all subjects in the *sham* condition. Another data set, Y ($n \times q$ matrix; q = number of contralateral connectivity), was created by concatenating functional connectivity between the left BG structures and right thalamic subregions across all subjects in the *sham* condition. The DCA model is therefore,

$$\begin{aligned} X' &= XW_X \\ Y' &= YW_Y \end{aligned} \tag{6.3}$$

where W_X ($p \times k$) and W_Y ($q \times k$) are the weight vectors, and X' ($n \times k$) and Y' ($n \times k$) are the transformed ipsilateral and contralateral connectivity, respectively. We used the first columns of X' and Y' that have the maximum correlation and the corresponding weights in further analyses.

The obtained weights and transformed connectivity were used to examine discriminant connectivity patterns and differences in the connectivity strengths between the PD and HC groups at baseline. Likewise, DCA was applied to the functional connectivity matrices between the right BG structures and subregions in the right and left thalamus, and the weights and transformed ipsilateral and contralateral connectivity were further analyzed. Finally, the computed weights (W_X and W_Y) were used in the subsequent analyses to infer EVS effects. That is, functional connectivity matrices were created in the same manner as the above using the fMRI data acquired in the EVS conditions and multiplied by the transformation weights obtained from the *sham* condition. The transformed connectivity (X' and Y') during each EVS were then compared with those obtained from the *sham* data.

6.2.8 Statistical analysis

Differences between groups in the thalamus functional subregion size and the BG-thalamic connectivity from the DCA were assessed using one-way ANOVA. EVS effects on the subregion size and the BG-thalamic connectivity within a group were evaluated using repeated measures ANOVA with stimulation condition (*sham*, nEVS and sEVS) as the within-subject factor. Statistical significance was considered when P values were < 0.05 after Bonferroni correction for multiple comparison.

6.3 Results

6.3.1 Thalamus Parcellation

Each thalamus was segmented into five subregions by applying the spatially constrained normalized cut approach (Fig. 6.1). According to the variance ratio criterion, the data-driven averaged optimal number of clusters was three. However, anatomically, the thalamus is classically segmented into a number of relay, association, and nonspecific nuclei, including the medial dorsal nucleus, an anterior nuclear group, the ventral nuclear group (ventral anterior, ventral lateral, ventral posterolateral and ventral posteromedial nuclei), the lateral nuclear group and the pulvinar nucleus, however at the relatively coarse spatial resolution of fMRI, these may not be individually discriminable. In a previous rsfMRI study, five distinct regions, including ventral anterior nuclei, ventral lateral nuclei, pulvinar, anterior nuclei and medial dorsal nuclei were identified based on independent component analysis [176]. Using diffusion tensor parcellation approach, Kumar and colleagues [192] also selected five stable subunits in the anterior, medial, lateral-anterior, lateral-posterior and posterior thalamus. Six subunits have also been chosen to investigate their subregional connectivity [35, 164]. Here, we chose the number of subregions in thalamus to be five as an optimal balance between ease of interpretation of the results and complexity of the subregional structures consistent with anatomical prior knowledge and previous studies. The identified functional subregions we segmented were related to the following anatomical thalamic nuclei as follows (Fig. 6.1): pulvinar and lateral posterior nuclei (PU+LP; subregion 1), anterior nuclear group and lateral dorsal nuclei (AN+LD; subregion 2), ventral postero-lateral nuclei (VPL; subregion 3), medial nuclei (MN; subregion 4), and ventral anterior and ventral lateral nuclei (VA+VL; subregion 5).

6.3.2 Thalamic subregion sizes

A significant difference in the thalamus functional subregion size was found across the groups ($F(2, 42) = 12.37$, $P < 0.001$; Fig. 6.2A). The subregion size was significantly different between the PDMOFF and HC groups ($P < 0.001$), which was normalized by L-dopa medication ($P < 0.001$). The weights from the logistic regression analysis (w_{logit}) indicated that the PDMOFF group particularly had decreased sizes of the PU+LP in the left thalamus and MN in the right thalamus (L1 and R4 in Fig. 6.2B) compared to the other groups.

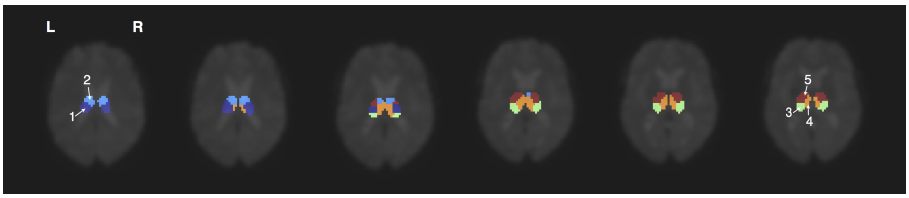

Figure 6.1: An example of thalamus parcellation results from a subject is displayed on the horizontal slices arranged from superior to inferior (from left to right). The identified subregions are colour coded and labeled with numbers (1: pulvinar and lateral posterior nuclei (PU+LP); anterior nuclear group and lateral dorsal nuclei (AN+LD); 3: ventral postero-lateral nuclei (VPL); 4: medial nuclei (MN); 5: ventral anterior and ventral lateral nuclei (VA+VL))

The stimulation condition showed significant effects on the subregion size in the PDMOFF subjects (F(2, 28) = 3.85, $P < 0.05$; Fig. 6.2C). Both stimuli normalized the thalamic subregion size in the PDMOFF subjects ($P < 0.05$) and the effect of nEVS was greater compared to sEVS. In contrast, the stimulation did not show significant effects on the subregion size for PDMON (F(2, 28) = 2.03, $P = 0.15$) and HC (F(2, 28) = 3.12, $P = 0.06$) groups.

6.3.3 Connectivity between the left BG and thalamic subregions

The ipsilateral connectivity between the left BG and left thalamus showed a significant difference across the groups (F(2, 42) = 3.6, $P < 0.05$; Fig. 6.3A). The PDMOFF subjects demonstrated decreased ipsilateral connectivity compared to the HC group ($P < 0.01$), and L-dopa medication did not induce a significant normalizing effect. The DCA weights indicated the following ipsilateral connectivity is primarily reduced in the PDMOFF group: AN+LD region and putamen, AN+LD region and pallidum, VA+VL region and pallidum, VA+VL region and putamen, and PU+LP region and putamen. In contrast, the contralateral connectivity between the left BG and right thalamus did not show a significant difference across the group (F(2, 42) = 1.87, $P = 0.17$).

EVS significantly modulated the ipsilateral connectivity in the PDMOFF (F(2, 28) = 3.76, $P < 0.05$) and HC (F(2, 28) = 4.65, $P < 0.05$) groups (Fig. 6.3B) whereas no significant EVS effect was found in the PDMON group (F(2, 28) = 1.23, $P = 0.31$). nEVS increased the ipsilateral connectivity in the PDMOFF group ($P < 0.05$) while both nEVS and sEVS reduced the ipsilateral connectivity in controls ($P < 0.05$ and $P < 0.01$, respectively).

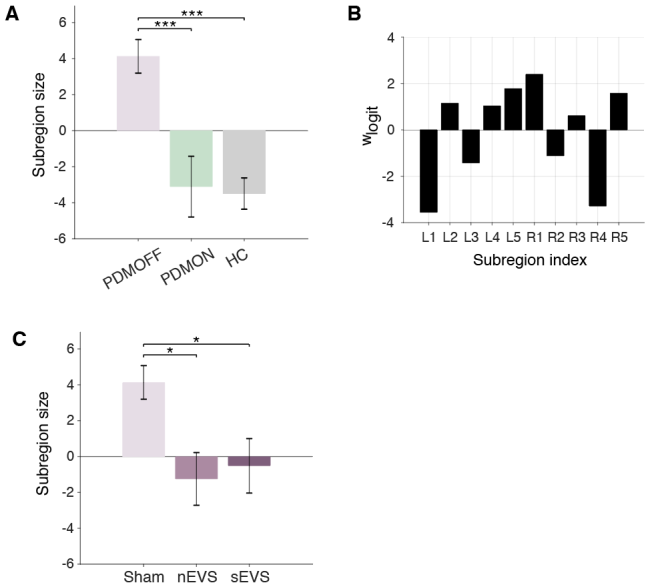

Figure 6.2: Comparison of the transformed subregional size obtained from the logistic regression and EVS effects. (A) Comparison of the baseline (i.e., *sham* condition) subregion sizes between the PDMOFF, PDMON and HC. (B) The weights (w_{logit}) from the logistic regression analysis (L/R: left/right thalamus; 1–5: subregion index shown in Fig. 6.1). (C) Normalizing effects of EVS on the thalamic subregion size in the PDMOFF group. Significant P values are indicated (*$P < 0.05$; ***$P < 0.001$).

The difference between the ipsilateral and contralateral connectivity strength was computed for each subject to examine symmetry of the left BG and thalamus interactions. We found a significant difference in the baseline symmetry across the groups (F(2, 42) = 4.24, $P < 0.05$; Fig. 6.3C). The PDMOFF group had a significantly weaker ipsilateral connectivity than the contralateral connectivity compared to the HC group ($P < 0.01$). This asymmetry was normalized by EVS ($P < 0.001$ and $P < 0.01$ for nEVS and sEVS, respectively; Fig. 6.3D). For the 15 PD subjects, we found improvement in the asymmetry for 12 subjects by L-dopa medication (binomial test, $P < 0.01$), 13 subjects by nEVS (binomial test, $P < 0.001$), and 12 subjects by sEVS (binomial test, $P < 0.01$) (Fig. 6.3E).

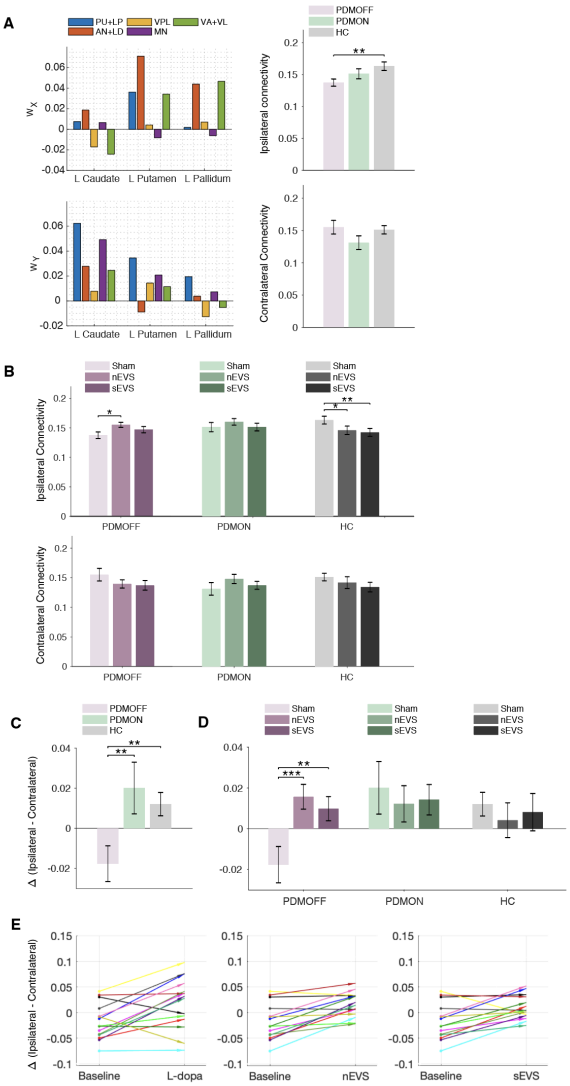

Figure 6.3: DCA results for the connectivity between left BG and bilateral thalami and EVS effects. (A) The weights and transformed data for the ipsilateral (left BG-left thalamus; top) and contralateral (left BG-right thalamus; bottom) connectivity in the sham condition. (B) EVS effects on the ipsilateral connectivity. (C) Ipsilateral and contralateral connectivity difference in the sham condition. (D) Effects of EVS on the ipsilateral and contralateral connectivity difference. (E) Effects of L-dopa medication and EVS on the connectivity difference for the 15 PDMOFF subjects. Significant P values are indicated ($^*P < 0.05$; $^{**}P < 0.01$; $^{***}P < 0.001$)

6.3.4 Connectivity between the right BG and thalamus subregions

There was no significant difference in the ipsilateral connectivity (right BG and right thalamus F(2, 42) = 1.22, $P = 0.31$) and the contralateral connectivity (right BG and left thalamus; F(2, 42) = 1.62, $P = 0.21$) between PDMOFF, PDMON and HC groups in the *sham* condition. The stimulation did not induce significant effects on the ipsilateral connectivity for all three groups (PDMOFF: F(2, 28) = 0.71, $P = 0.50$; PDMON: F(2, 28) = 0.05, $P = 0.96$; HC: F(2, 28) = 3.10, $P = 0.06$). The contralateral connectivity for PDMOFF and PDMON groups did not change by the stimulation (PDMOFF: F(2, 28) = 1.12, $P = 0.34$; PDMON: F(2, 28) = 0.70, $P = 0.50$) whereas both nEVS and sEVS decreased the contralateral connectivity in HC group (nEVS: $P < 0.05$; sEVS: $P < 0.01$).

6.4 Discussion

The main results of this study are threefold. We demonstrate that: 1) functional subregions of the thalami are subdivided differently between PD groups on and off dopaminergic medication and healthy controls; 2) a significant asymmetry exists in thalamic/BG interactions in the left BG, and, 3) these alterations are partially ameliorated with EVS in a stimulus-dependent manner. Thus, this work provides additional mechanisms through which EVS may prove beneficial in PD.

6.4.1 Functional thalamic subregion sizes altered in PD

Structurally, the overall volume of the thalamus as a whole appears to be relatively spared in PD, while microscopically, there can be selective degeneration and structural changes of particular thalamic nuclei [122, 245]. We demonstrated that the PDMOFF group had a decreased size of the functional PU+LP subregion than the other groups. The PU plays an important role in visual perception, visual attention and visual target selection [98] and is critically involved in maintaining and modulating dynamics of neuronal oscillations in the visual cortex [197], which may be implicated in visual dysfunctions in PD [349, 373, 416]. Impaired visual functions in PD are reflected by deficits in sensitivity to visual stimuli such as colour-contrast and luminance and reduced attentive visual processing [201, 216, 304]. Delays in visually evoked potentials in PD have been also reported in electrophysiological studies [143]. The LP region is important in sensory perception as

it integrates sensory information and projects to superior parietal region in concert with the PU. Recently, a voxel-based morphometry study has shown that PD patients have reduced functional connectivity between the parietal region and thalamus involved in visual and sensorimotor networks compared to healthy controls [133], which may be associated with the reduced size of PU+LP found in our results.

We demonstrated that PDMOFF subjects also had a decreased functional size of the MN region. The MN region is known to have substantial reciprocal interconnections with the prefrontal cortex (PFC), playing a critical role in memory and various cognitive tasks [251]. Causal relationships between the MN and PFC have been demonstrated in lesion studies in human and animal models (for reviews, see [280]) and recently it was demonstrated that decreased MN activity disrupts modulation of MN-PFC synchrony required for working memory [281]. Although the MN plays a key role in working memory and behaviour flexibility that are recognized as common non-motor complications of PD [415], there is a lack of prior studies that studied the functional role of the MN in PD. There are currently only two studies available that reported significant white matter changes of the MN in PD patients, in relation to depression [59, 215]. Further studies are required to elucidate implications of the volumetric changes of the MN region in PD for cognitive functions.

6.4.2 Asymmetric connectivity of left BG and thalamus

Anatomical connectivity between the BG and bilateral thalami has been demonstrated in animal models of PD where contralateral projections of the GP (primarily targeting the VM) and SNr (primarily targeting intralaminar nuclei) were found [61, 157]. Bilateral GABAergic and glutamate pathways have been reported [239], and a recent optogenetic study demonstrated that stimulation of D1 and D2 dopamine receptors in the striatum activates bilateral thalami [203]. Our results showed reduced connectivity between ipsilateral left BG and thalamus connectivity in the PD group, which is in accordance with prior studies demonstrating the SN and ipsilateral thalamus connectivity is decreased in PD [248, 311, 347].

We found significantly greater asymmetry in the connectivity between the left BG and bilateral thalamus in the PDMOFF group, which became more symmetric with dopaminergic medication. This asymmetry was not observed with the right BG, suggesting the left BG connectivity with the thalamus is more susceptible to disease effects. Prior studies have implied that left nigrostriatal pathway is more affected by the disease than the

right [303, 336], increasing the susceptibility of the left nigrostriatal network [53, 229]. This may be due to the handedness [22, 32, 69, 235, 338, 391, 399] although there may be other confounding factors. In our subjects, all PD subjects were right-handed, whereas the obvious clinical asymmetry (defined as the difference between the summed UPDRS scores of the left and right extremities with respect to rigidity, bradykinesia and tremor [39]) was not found (left worse: 40%; Table 6.1). While our results are consistent with the notion that the asymmetric left BG-thalamus connectivity is due to handedness, we do not have sufficient evidence to prove/disprove this hypothesis.

6.4.3 Potential mechanism of EVS

We demonstrated that nEVS and sEVS both significantly normalized functional subregion size in the PDMOFF group. Additionally, nEVS enhanced the diminished ipsilateral connectivity between the left BG and thalamus in the PDMOFF group. The $1/f$ type power spectrum of nEVS reflects the power distribution found in cortical and subcortical functional networks [56], and its beneficial effects in PD have been demonstrated in previous studies [205, 278, 424, 432]. The stochastic resonance phenomena (also known as "stochastic facilitation" in biological and medical fields) where a sub-threshold random stimulus elicits functional benefits in a non-linear system [238] such as the nervous system has been proposed as a mechanism to explain how the randomly-varying stimuli may provide beneficial effects.

Anatomically, the vestibular nuclei in the brainstem have multiple projections directly to the thalamus including the VA, VL, VPL, VPM, intralaminar nuclei, and geniculate bodies [221, 247, 286]. Prior fMRI-EVS studies have shown that vestibular stimulation induces strong activation in the thalamus [30, 55, 247, 366, 421]. However, neither effects on the thalamic subregions nor modulatory influences on the BG-thalamic functional connectivity have been previously described. Our findings provide evidence that EVS modulates subgroups of thalamic nuclei and interaction with the BG in a stimulus-dependent manner. We elucidated the EVS effects focusing on the thalamus and BG based on their anatomical importance in both PD and vestibular information processing. Further studies to investigate effects at the cortical level with respect to the changes at the subcortical level shown here will provide deeper understanding in the neurotherapeutic mechanism of EVS. The results from the current study suggests that "normalization" of disrupted BG-thalamus connectivity may be a key mechanism through which EVS induces beneficial effects in PD.

Chapter 7

Conclusion and Future Work

In this dissertation, in an effort to advance application of EVS as a potential therapeutic intervention for PD, we utlized new multisine EVS stimuli and investigated effects of the different stimuli on brain activity and motor function in PD and healthy subjects. In addition, we investigated effects of noisy EVS, the stimulus type used in the majority of prior EVS studies on PD, on motor function in PD subjects. By utilizing a new motor task and analytical methods, we have added valuable new information on top of existing findings. Furthermore, we conducted simultaneous EVS-fMRI experiments to probe the fundamental mechanisms of EVS utilizing the excellent spatial resolution of the fMRI data. This is the first fMRI study to investigate effects of EVS in PD, and we believe the outcomes from the study will significantly increase our understanding of the EVS mechanisms. Finally, we developed a novel denoising method to remove stimulation artifacts in EEG, which has been identified a critical challenge to resolve in order to be able to investigate immediate stimulation effects on brain oscillations.

7.1 Conclusion and Summary

7.1.1 Conclusion and Summary

In Chapter 2, subthreshold noisy EVS was applied to PD subjects while they performed a visuomotor joystick tracking task, which alternated between 2 task conditions depending on whether the displayed cursor position underestimated the actual error by 30% ('Better') or overestimated by 200% ('Worse'). Coefficients from LDA indicated that noisy EVS had significantly affected the perceived error between the target and the displayed cursor position, displayed cursor velocity and acceleration. It was also found that EVS made the subject more smoothly track the target as observed in SNR and less overshoot in the tacking. These results in accordance with previous findings that noisy EVS has effects on modulating motor functions in PD, and raises the additional question as to whether the effects are specific only to the type of stimulus used in this study (0.1–10 Hz, pink noise) or can

be induced, through modulation of the sensorimotor system via stochastic facilitation or other neural mechanisms, with other types of stimuli (e.g., sine waves, white noise).

In Chapter 3, a new framework was proposed for removal of stimulation artifacts in EEG recordings using a JBSS technique. As opposed to conventional methods (PCA and ICA), which decompose a single dataset into individual components, this new approach is able to simultaneously accommodate multiple datasets and identify source components using their correlation or independence within and between datasets. It was demonstrated that the proposed method, q-IVA, outperforms the conventional methods, MCCA and IVA in simulations. When examining real data, q-IVA successfully attenuated the stimulation artifact and enabled detection of physiological changes in the cleaned EEG data. The results suggest that q-IVA is an effective denoising method for the investigation of neurophysiological online effects of EVS and the method is utilized in the simultaneous EVS-EEG study in Chapter 4.

For the evaluation of multisine EVS stimuli on brain oscillations, in Chapter 4 discriminant features in widespread cortico-cortical couplings between PD and HC groups were first identified using SDA and the changes in the direction and magnitude of the discriminant features induced by the EVS stimuli were examined. It was demonstrated that the discriminant features are associated with the strength of cortical couplings in the sensorimotor region, and variability and complexity of the coupling dynamics in predominantly theta and alpha bands. The discriminant features in the PD subjects were found to modulated by 4-8 Hz, 50-100 Hz and 100-150 Hz EVS such that during and after each stimulation the features were brought close to those of the HC subjects. The direction of the changes (normalizing or worsening) induced by the stimulation was same across the different stimuli while the magnitude and duration of the aftereffects were stimulus-dependent.

In Chapter 5, effects of multisine EVS stimuli on motor functions were examined using joint analysis (DCA) of the EEG and behaviour data that were recorded simultaneously from PD and HC subjects while they were performing a squeeze-bulb motor task. First, it was demonstrated that both 50-100 Hz and 100-150 Hz multisine EVS improved task performance of the PD subjects when they were off-medication and induced less improvement when they were on medication, suggesting interaction between the medication and EVS. The results derived from the DCA demonstrated that the improvement in the task performance was correlated with the EVS-induced changes in the magnitude and dynamics of beta ERD in the left motor,

broad frontal and medial parietal regions. The effects of EVS were found greater with the 100-150 Hz stimulation in the PD subjects off medication and HC subjects as compared to the 50-100 Hz stimulation and the PD subjects already on optimal medication.

The focus of Chapter 6 was to provide a deeper understanding of the fundamental mechanisms underlying the EVS effects shown in PD, focusing on the thalamus based on its anatomical importance in both motor networks and vestibular information processing. FMRI data were collected from the PD and HC subjects while 0.1-10 Hz noisy EVS (same as in Chapter 2) and 1-Hz sinusoidal EVS were continuously being applied for 5 minutes. The results demonstrate that both EVS significantly normalized the size of PU+LP functional subregions in the PDMOFF group and the size of VPL subregion in the PDMON group. In addition, the noisy EVS was effective in improving the connectivity strength between the left BG and bilateral thalami such that the strength of the ipsilateral and contralateral connectivity, was less asymmetric, as would be seen in HC subjects. The findings suggest that modulation of thalamo-BG connectivity may be one potential mechanism underlying EVS effects on motor improvement in PD.

In conclusion, this dissertation aims to improve our understanding of EVS technique as a potential therapeutic intervention for PD. The results demonstrated that EVS is effective in modulating brain oscillations, activity and functional connectivity of the thalamus and improving motor behaviours in PD, and by varying stimulation waveforms the effect size and duration can be further improved. The presented work lays the groundwork and demonstrates a potential to further develop EVS for a patient-specific neuromodulation tool to improve motor functions in PD.

The contributions of this dissertation are summarized as follows:

1. Based on approaches used to describe behaviour of the system in the field of system identification, novel multisine stimuli for EVS were developed such that they have advantages over conventional noisy EVS in that they can excite specific components of responses, minimize unwanted loss of accuracy (leakage) in the frequency domain, apply maximum power to the system and improve subjects discomfort.

2. Multisine EVS signals were tested for the first time with neuroimaging modality tol their investigate effects on electrical brain activities.

3. It was first demonstrated that EVS can modulate phase-based cortical couplings. Results indicated that EVS improve both strength and temporal dynamics of cortical couplings in PD.

4. Results demonstrated that EVS significantly improves motor task performance of PD subjects off-medication.

5. The correlation between changes in brain oscillations and motor behaviours induced by EVS was demonstrated for the first time. Results indicated that EVS can modulate the magnitude and dynamics of movement-related desynchronization of beta oscillations, which are correlated with improvement of the motor task performance.

6. Comparison of EVS effects on cortical couplings, movement-related beta desynchronization, and motor task performance between off- and on-medication conditions of the PD subjects indicated interactions between L-dopa medication and EVS. It was found that, in general, improvements by multisine EVS is greater in the off-medication condition compared to the on-medication condition.

7. It was found that EVS effects can be dependent on brain states. Results demonstrated that EVS modulated the power of beta oscillations when the subjects were engaged in the motor task but did not change the beta power when subjects were at rest.

8. EVS was shown to change activities of the functional thalamic subregions and the connectivity between the thalamus and BG in PD. This provides a potential mechanism of how EVS can affect motor systems in PD.

9. A novel method was devised for removal of stimulation artifacts in EEG. The results demonstrated a robust artifact removal performance of q-IVA method through the simulation and real-data studies. Thus, the method could be a promising tool to properly analyze the EEG acquired during electrical brain stimulation in future studies.

7.1.2 Limitations and suggestions for future work

Development, implementation and evaluation of EVS is highly multidisciplinary work, and accordingly a number of interesting areas of research can be suggested to further improve the current EVS technique as follows:

1. **Comparison of the noisy EVS and multisine EVS**: In Chapters 4 and 5, the results demonstrated promising efficacy of multisine EVS to improve motor functions in PD. As most prior EVS studies in PD have used a noisy stimulus, it would be informative to know how multisine EVS compares to a noisy stimulus in the investigated results or

in future studies. Synchronous neuronal activities between brain regions at specific frequencies are involved to carry out particular brain functions, and it has been shown that changes in brain activities and resultant outcomes are dependent on the frequency of the stimulation applied. Therefore, multisine EVS bounded in a specific frequency band would be likely to bring about changes in particular brain regions or network compared to a noisy stimulus. What would happen if the frequency band of a multisine signal is a subset of the one of the noisy signal like as in this study? (e.g., the 4–8 Hz multisine and 0.1–10 Hz pink noise). Would be the effect size greater with the multisine compared to the pink noise? To be able to answer this question in the future would be critical to for providing rationales for building optimized stimulation signals that can enhance the effect size of the stimulation.

2. **Further validation of q-IVA method**: Q-IVA method was tested in the simulation study where the stimulation artifacts were derived from the multisine signal in 4-8 Hz. In practice, stimulation signals can be in various waveforms (e.g., sine waves, chirps, multisines, pulses) and it is recommended to test out the method with different types of stimulation artifacts and identify when q-IVA works the best and when it is less successful. This information will help promote the NIBS field by providing more freedom for selecting stimulation parameters that have the available denoising option to probe online stimulation effects.

3. **Investigation of relationship between brain states and responses to EVS:** Although this research has focused on the EVS effects at group levels (e.g., PD patients vs. healthy controls), it is of great interest to determine how and why the effects vary across different individuals. This has partially done in this thesis by looking at the correlation between effect sizes of EVS and clinical characteristics of the PD subjects such as disease duration, severity and the amount of dopaminergic medication taken. Nevertheless, relationships between characteristics of individual brain activities at the baseline and EVS effect sizes in both PD patients and healthy controls still remain elusive. Brain activities can be characterized in many different ways, ranging from conventional power spectral density of a single channel to the complex non-stationary dynamics of multiple channels simultaneously. High-dimensional feature spaces will likely need to be searched for to find the individually–specific EVS effect. State-of-the-art ma-

chine learning approaches are warranted to address this subject.

4. **Investigation of nonlinear effects:** The results from Chapters 4 and 5 indicate presence of nonlinear effects of EVS in that high-frequency stimulation (50–150 Hz) can significantly influence low-frequency (1–50 Hz) cortical oscillations, which has not been previously reported elsewhere. Moreover, it was shown in Chapter 5 that the non-linear effects are also dependent on the context (i.e., resting vs. movement), suggesting that the underlying vestibular information processing is influenced by several integrative processes in the brain. Future investigation with more finely tuned stimulation frequency parameters combined with EEG and/or fMRI is warranted to elucidate the non-linear effects of EVS.

Bibliography

[1] D. Aarsland, K. Bronnick, C. Williams-Gray, D. Weintraub, K. Marder, J. Kulisevsky, D. Burn, P. Barone, J. Pagonabarraga, L. Allcock, G. Santangelo, T. Foltynie, C. Janvin, J. P. Larsen, R. A. Barker, and M. Emre. Mild cognitive impairment in Parkinson disease: A multicenter pooled analysis. *Neurology*, 75(12):1062–1069, 9 2010.

[2] P. P. Acharjee, R. Phlypo, L. Wu, V. D. Calhoun, and T. Adali. Independent Vector Analysis for Gradient Artifact Removal in Concurrent EEG-fMRI Data. *IEEE transactions on bio-medical engineering*, 62(7):1750–8, 7 2015.

[3] M. Adib and E. Cretu. Wavelet-based artifact identification and separation technique for EEG signals during galvanic vestibular stimulation. *Computational and Mathematical Methods in Medicine*, 2013, 2013.

[4] S. Ahn, S. E. Zauber, R. M. Worth, T. Witt, and L. L. Rubchinsky. Interaction of synchronized dynamics in cortex and basal ganglia in Parkinson's disease. *European Journal of Neuroscience*, 42(5):2164–2171, 9 2015.

[5] A. D. Akkaya and M. L. Tiku. Robust estimation in multiple linear regression model with non-Gaussian noise. *Automatica*, 44(2):407–417, 2 2008.

[6] G. E. Alexander and M. D. Crutcher. Functional architecture of basal ganglia circuits: neural substrates of parallel processing. *Trends in neurosciences*, 13(7):266–71, 7 1990.

[7] G. E. Alexander, M. R. DeLong, and P. L. Strick. Parallel Organization of Functionally Segregated Circuits Linking Basal Ganglia and Cortex. *Annual Review of Neuroscience*, 9(1):357–381, 3 1986.

[8] P. J. Allen, O. Josephs, and R. Turner. A method for removing imaging artifact from continuous EEG recorded during functional MRI. *NeuroImage*, 12(2):230–9, 8 2000.

[9] F. Alonso-Frech. Slow oscillatory activity and levodopa-induced dyskinesias in Parkinson's disease. *Brain*, 129(7):1748–1757, 7 2006.

[10] J. L. Amengual, M. Vernet, C. Adam, and A. Valero-Cabré. Local entrainment of oscillatory activity induced by direct brain stimulation in humans. *Scientific Reports*, 7(1):41908, 12 2017.

[11] M. Anderson, X.-L. Li, and T. Adal. Nonorthogonal Independent Vector Analysis Using Multivariate Gaussian Model. pages 354–361. Springer, Berlin, Heidelberg, 2010.

[12] T. R. Anderson, B. Hu, K. Iremonger, and Z. H. T. Kiss. Selective Attenuation of Afferent Synaptic Transmission as a Mechanism of Thalamic Deep Brain Stimulation-Induced Tremor Arrest. *Journal of Neuroscience*, 26(3):841–850, 1 2006.

[13] F. G. Andres and C. Gerloff. Coherence of sequential movements and motor learning. *Journal of clinical neurophysiology : official publication of the American Electroencephalographic Society*, 16(6):520–7, 11 1999.

[14] A. G. Androulidakis, L. M. F. Doyle, T. P. Gilbertson, and P. Brown. Corrective movements in response to displacements in visual feedback are more effective during periods of 13-35 Hz oscillatory synchrony in the human corticospinal system. *European Journal of Neuroscience*, 24(11):3299–3304, 12 2006.

[15] A. G. Androulidakis, L. M. F. Doyle, K. Yarrow, V. Litvak, T. P. Gilbertson, and P. Brown. Anticipatory changes in beta synchrony in the human corticospinal system and associated improvements in task performance. *European Journal of Neuroscience*, 25(12):3758–3765, 6 2007.

[16] D. E. Angelaki and K. E. Cullen. Vestibular System: The Many Facets of a Multimodal Sense. *Annual Review of Neuroscience*, 31(1):125–150, 7 2008.

[17] A. Antal, K. Boros, C. Poreisz, L. Chaieb, D. Terney, and W. Paulus. Comparatively weak after-effects of transcranial alternating current

stimulation (tACS) on cortical excitability in humans. *Brain Stimulation*, 1(2):97–105, 4 2008.

[18] A. Antal and W. Paulus. Transcranial alternating current stimulation (tACS). *Frontiers in human neuroscience*, 7:317, 2013.

[19] M. S. Aymerich, P. Barroso-Chinea, M. Pérez-Manso, A. M. Muñoz-Patiño, M. Moreno-Igoa, T. González-Hernández, and J. L. Lanciego. Consequences of unilateral nigrostriatal denervation on the thalamostriatal pathway in rats. *European Journal of Neuroscience*, 23(8):2099–2108, 4 2006.

[20] B. Ballanger, S. Thobois, P. Baraduc, R. S. Turner, E. Broussolle, and M. Desmurget. Paradoxical Kinesis is not a Hallmark of Parkinson's disease but a general property of the motor system. *Movement Disorders*, 21(9):1490–1495, 9 2006.

[21] A. T. Barker. An introduction to the basic principles of magnetic nerve stimulation. *Journal of clinical neurophysiology : official publication of the American Electroencephalographic Society*, 8(1):26–37, 1 1991.

[22] M. J. Barrett, S. A. Wylie, M. B. Harrison, and G. F. Wooten. Handedness and motor symptom asymmetry in Parkinson's disease. *Journal of Neurology, Neurosurgery & Psychiatry*, 82(10):1122–1124, 10 2011.

[23] R. J. Barry, A. R. Clarke, S. J. Johnstone, C. A. Magee, and J. A. Rushby. EEG differences between eyes-closed and eyes-open resting conditions. *Clinical Neurophysiology*, 118(12):2765–2773, 12 2007.

[24] G. Batsikadze, V. Moliadze, W. Paulus, M.-F. Kuo, and M. A. Nitsche. Partially non-linear stimulation intensity-dependent effects of direct current stimulation on motor cortex excitability in humans. *The Journal of Physiology*, 591(7):1987–2000, 4 2013.

[25] B. S. Baxter, B. Edelman, X. Xiaotong Zhang, A. Roy, and B. Bin He. Simultaneous high-definition transcranial direct current stimulation of the motor cortex and motor imagery. In *2014 36th Annual International Conference of the IEEE Engineering in Medicine and Biology Society*, volume 2014, pages 454–456. IEEE, 8 2014.

[26] A. Belouchrani, K. Abed-Meraim, J.-F. Cardoso, and E. Moulines. A blind source separation technique using second-order statistics. *IEEE Transactions on Signal Processing*, 45(2):434–444, 1997.

[27] Y. Benjamini and Y. Hochberg. Controlling the false discovery rate: a practical and powerful approach to multiple testing. *Journal of the Royal Statistical Society*, 57(1):289–300, 1995.

[28] D. H. Benninger and M. Hallett. Non-invasive brain stimulation for Parkinsons disease: Current concepts and outlook 2015. *NeuroRehabilitation*, 37(1):11–24, 8 2015.

[29] D. H. Benninger, M. Lomarev, G. Lopez, E. M. Wassermann, X. Li, E. Considine, and M. Hallett. Transcranial direct current stimulation for the treatment of Parkinson's disease. *Journal of Neurology, Neurosurgery & Psychiatry*, 81(10):1105–1111, 10 2010.

[30] S. Bense, T. Stephan, T. A. Yousry, T. Brandt, and M. Dieterich. Multisensory Cortical Signal Increases and Decreases During Vestibular Galvanic Stimulation (fMRI). *J Neurophysiol*, 85(2):886–899, 2 2001.

[31] H. Bergman, A. Feingold, A. Nini, A. Raz, H. Slovin, M. Abeles, and E. Vaadia. Physiological aspects of information processing in the basal ganglia of normal and parkinsonian primates. *Trends in neurosciences*, 21(1):32–8, 1 1998.

[32] J. A. Bernard, S. J. Peltier, B. L. Benson, J. L. Wiggins, S. M. Jaeggi, M. Buschkuehl, J. Jonides, C. S. Monk, and R. D. Seidler. Dissociable Functional Networks of the Human Dentate Nucleus. *Cerebral Cortex*, 24(8):2151–2159, 8 2014.

[33] M. Bikson, A. Name, and A. Rahman. Origins of specificity during tDCS: anatomical, activity-selective, and input-bias mechanisms. *Frontiers in Human Neuroscience*, 7:688, 2013.

[34] W. Birkmayer and O. Hornykiewicz. The effect of l-3,4-dihydroxyphenylalanine (=DOPA) on akinesia in parkinsonism. *Parkinsonism & related disorders*, 4(2):59–60, 8 1998.

[35] A. Bisecco, M. A. Rocca, E. Pagani, L. Mancini, C. Enzinger, A. Gallo, H. Vrenken, M. L. Stromillo, M. Copetti, D. L. Thomas, F. Fazekas, G. Tedeschi, F. Barkhof, N. D. Stefano, M. Filippi, and MAGNIMS Network. Connectivity-based parcellation of the thalamus in multiple sclerosis and its implications for cognitive impairment: A multicenter study. *Human Brain Mapping*, 36(7):2809–2825, 7 2015.

[36] A. Björklund and S. B. Dunnett. Dopamine neuron systems in the brain: an update. *Trends in Neurosciences*, 30(5):194–202, 5 2007.

[37] F. Blandini, G. Nappi, C. Tassorelli, and E. Martignoni. Functional changes of the basal ganglia circuitry in Parkinson's disease. *Progress in neurobiology*, 62(1):63–88, 9 2000.

[38] P. S. Boggio, R. Ferrucci, S. P. Rigonatti, P. Covre, M. Nitsche, A. Pascual-Leone, and F. Fregni. Effects of transcranial direct current stimulation on working memory in patients with Parkinson's disease. *Journal of the Neurological Sciences*, 249(1):31–38, 11 2006.

[39] T. A. Boonstra, J. P. P. van Vugt, H. van der Kooij, and B. R. Bloem. Balance asymmetry in Parkinson's disease and its contribution to freezing of gait. *PloS one*, 9(7):e102493, 2014.

[40] J. L. W. Bosboom, D. Stoffers, C. J. Stam, B. W. van Dijk, J. Verbunt, H. W. Berendse, and E. C. Wolters. Resting state oscillatory brain dynamics in Parkinson's disease: an MEG study. *Clinical neurophysiology : official journal of the International Federation of Clinical Neurophysiology*, 117(11):2521–31, 12 2006.

[41] C. Bosch-Bouju, B. I. Hyland, and L. C. Parr-Brownlie. Motor thalamus integration of cortical, cerebellar and basal ganglia information: implications for normal and parkinsonian conditions. *Frontiers in Computational Neuroscience*, 7:163, 2013.

[42] G. Bottini, R. Sterzi, E. Paulesu, G. Vallar, S. F. Cappa, F. Erminio, R. E. Passingham, C. D. Frith, and R. S. Frackowiak. Identification of the central vestibular projections in man: a positron emission tomography activation study. *Experimental brain research*, 99(1):164–9, 1994.

[43] T. Brandt, M. Strupp, and M. Dieterich. Towards a concept of disorders of "higher vestibular function". *Frontiers in integrative neuroscience*, 8:47, 2014.

[44] J.-S. Brittain and P. Brown. Oscillations and the basal ganglia: motor control and beyond. *NeuroImage*, 85 Pt 2(Pt 2):637–47, 1 2014.

[45] J.-S. Brittain, H. Cagnan, A. R. Mehta, T. A. Saifee, M. J. Edwards, and P. Brown. Distinguishing the central drive to tremor in Parkinson's disease and essential tremor. *The Journal of neuroscience : the official journal of the Society for Neuroscience*, 35(2):795–806, 1 2015.

[46] D. Brooks and G. M. Halliday. Intralaminar nuclei of the thalamus in Lewy body diseases. *Brain Research Bulletin*, 78(2-3):97–104, 2 2009.

[47] P. Brown. Oscillatory nature of human basal ganglia activity: relationship to the pathophysiology of Parkinson's disease. *Movement disorders : official journal of the Movement Disorder Society*, 18(4):357–63, 4 2003.

[48] P. Brown. Abnormal oscillatory synchronisation in the motor system leads to impaired movement. *Current Opinion in Neurobiology*, 17(6):656–664, 12 2007.

[49] P. Brown, P. Mazzone, A. Oliviero, M. G. Altibrandi, F. Pilato, P. A. Tonali, and V. Di Lazzaro. Effects of stimulation of the subthalamic area on oscillatory pallidal activity in Parkinson's disease. *Experimental Neurology*, 188(2):480–490, 8 2004.

[50] P. Brown, A. Oliviero, P. Mazzone, A. Insola, P. Tonali, and V. Di Lazzaro. Dopamine dependency of oscillations between subthalamic nucleus and pallidum in Parkinson's disease. *The Journal of neuroscience : the official journal of the Society for Neuroscience*, 21(3):1033–8, 2 2001.

[51] P. Brown and D. Williams. Basal ganglia local field potential activity: character and functional significance in the human. *Clinical neurophysiology : official journal of the International Federation of Clinical Neurophysiology*, 116(11):2510–9, 11 2005.

[52] E. N. Bruce, M. C. Bruce, and S. Vennelaganti. Sample entropy tracks changes in electroencephalogram power spectrum with sleep state and aging. *Journal of clinical neurophysiology : official publication of the American Electroencephalographic Society*, 26(4):257–66, 8 2009.

[53] A. Bruck, T. Kurki, V. Kaasinen, T. Vahlberg, and J. O. Rinne. Hippocampal and prefrontal atrophy in patients with early non-demented Parkinson's disease is related to cognitive impairment. *Journal of Neurology, Neurosurgery & Psychiatry*, 75(10):1467–1469, 10 2004.

[54] R. Bruña, F. Maestú, and E. Pereda. Phase locking value revisited: teaching new tricks to an old dog. *Journal of neural engineering*, 15(5):056011, 10 2018.

[55] S. F. Bucher, M. Dieterich, M. Wiesmann, A. Weiss, R. Zink, T. a. Yousry, and T. Brandt. Cerebral functional magnetic resonance imaging of vestibular, auditory, and nociceptive areas during galvanic stimulation. *Annals of Neurology*, 44(1):120–125, 7 1998.

[56] G. Buzsaki and A. Draguhn. Neuronal Oscillations in Cortical Networks. *Science*, 304(5679):1926–1929, 6 2004.

[57] J. Cai, S. Lee, F. Ba, S. Garg, L. J. Kim, A. Liu, D. Kim, Z. J. Wang, and M. J. McKeown. Galvanic Vestibular Stimulation (GVS) Augments Deficient Pedunculopontine Nucleus (PPN) Connectivity in Mild Parkinson's Disease: fMRI Effects of Different Stimuli. *Frontiers in neuroscience*, 12:101, 2018.

[58] P. Calabresi, V. Ghiglieri, P. Mazzocchetti, I. Corbelli, and B. Picconi. Levodopa-induced plasticity: a double-edged sword in Parkinson's disease? *Philosophical Transactions of the Royal Society B: Biological Sciences*, 370(1672):20140184, 7 2015.

[59] E. F. Cardoso, F. M. Maia, F. Fregni, M. L. Myczkowski, L. M. Melo, J. R. Sato, M. A. Marcolin, S. P. Rigonatti, A. C. Cruz, E. R. Barbosa, and E. Amaro. Depression in Parkinson's disease: Convergence from voxel-based morphometry and functional magnetic resonance imaging in the limbic thalamus. *NeuroImage*, 47(2):467–472, 8 2009.

[60] M. Cassidy, P. Mazzone, A. Oliviero, A. Insola, P. Tonali, V. Di Lazzaro, and P. Brown. Movement-related changes in synchronization in the human basal ganglia. *Brain : a journal of neurology*, 125(Pt 6):1235–46, 6 2002.

[61] M. Castle, M. S. Aymerich, C. Sanchez-Escobar, N. Gonzalo, J. A. Obeso, and J. L. Lanciego. Thalamic innervation of the direct and indirect basal ganglia pathways in the rat: Ipsi- and contralateral projections. *The Journal of Comparative Neurology*, 483(2):143–153, 3 2005.

[62] A. S. Cauquil and B. L. Day. Galvanic vestibular stimulation modulates voluntary movement of the human upper body. *The Journal of physiology*, 513 (Pt 2:611–9, 12 1998.

[63] J. F. Cavanagh, L. Zambrano-Vazquez, and J. J. B. Allen. Theta lingua franca: A common mid-frontal substrate for action monitoring processes. *Psychophysiology*, 49(2):220–238, 2 2012.

[64] X. Chen, A. Liu, Q. Chen, Y. Liu, L. Zou, and M. J. McKeown. Simultaneous ocular and muscle artifact removal from EEG data by exploiting diverse statistics. *Computers in Biology and Medicine*, 88:1–10, 9 2017.

[65] X. Chen, A. Liu, J. Chiang, Z. J. Wang, M. J. McKeown, and R. K. Ward. Removing Muscle Artifacts From EEG Data: Multichannel or Single-Channel Techniques? *IEEE Sensors Journal*, 16(7):1986–1997, 4 2016.

[66] X. Chen, H. Peng, F. Yu, and K. Wang. Independent Vector Analysis Applied to Remove Muscle Artifacts in EEG Data. *IEEE Transactions on Instrumentation and Measurement*, 66(7):1770–1779, 7 2017.

[67] X. Chen, Z. J. Wang, and M. McKeown. Joint Blind Source Separation for Neurophysiological Data Analysis: Multiset and multimodal methods. *IEEE Signal Processing Magazine*, 33(3):86–107, 5 2016.

[68] S. J. Chung, J. J. Lee, J. H. Ham, B. S. Ye, P. H. Lee, and Y. H. Sohn. Striatal Dopamine Depletion Patterns and Early Non-Motor Burden in Parkinsons Disease. *PloS one*, 11(8):e0161316, 2016.

[69] D. O. Claassen, K. E. McDonell, M. Donahue, S. Rawal, S. A. Wylie, J. S. Neimat, H. Kang, P. Hedera, D. Zald, B. Landman, B. Dawant, and S. Rane. Cortical asymmetry in Parkinson's disease: early susceptibility of the left hemisphere. *Brain and behavior*, 6(12):e00573, 2016.

[70] L. Clemmensen, T. Hastie, D. Witten, and B. Ersbøll. Sparse Discriminant Analysis. *Technometrics*, 53(4):406–413, 11 2011.

[71] P. Cordo, J. T. Inglis, S. Verschueren, J. J. Collins, D. M. Merfeld, S. Rosenblum, S. Buckley, and F. Moss. Noise in human muscle spindles. *Nature*, 383(6603):769–770, 10 1996.

[72] N. Correa, T. Adali, Y.-O. Li, and V. Calhoun. Canonical Correlation Analysis for Data Fusion and Group Inferences. *IEEE Signal Processing Magazine*, 27(4):39–50, 2010.

[73] G. C. Cotzias, P. S. Papavasiliou, and R. Gellene. Modification of Parkinsonism Chronic Treatment with L-Dopa. *New England Journal of Medicine*, 280(7):337–345, 2 1969.

[74] R. C. Craddock, G. James, P. E. Holtzheimer, X. P. Hu, and H. S. Mayberg. A whole brain fMRI atlas generated via spatially constrained spectral clustering. *Human Brain Mapping*, 33(8):1914–1928, 8 2012.

[75] K. E. Cullen. The vestibular system: multimodal integration and encoding of self-motion for motor control. *Trends in neurosciences*, 35(3):185–96, 3 2012.

[76] R. G. Cury, V. Fraix, A. Castrioto, M. A. Pérez Fernández, P. Krack, S. Chabardes, E. Seigneuret, E. J. L. Alho, A.-L. Benabid, and E. Moro. Thalamic deep brain stimulation for tremor in Parkinson disease, essential tremor, and dystonia. *Neurology*, 89(13):1416–1423, 9 2017.

[77] D. Cyron. Mental Side Effects of Deep Brain Stimulation (DBS) for Movement Disorders: The Futility of Denial. *Frontiers in integrative neuroscience*, 10:17, 2016.

[78] N. Dahodwala, A. Siderowf, M. Xie, E. Noll, M. Stern, and D. S. Mandell. Racial differences in the diagnosis of Parkinson's disease. *Movement disorders : official journal of the Movement Disorder Society*, 24(8):1200–5, 6 2009.

[79] C. A. Davie. A review of Parkinson's disease. *British medical bulletin*, 86(1):109–27, 1 2008.

[80] B. L. Day, A. Séverac Cauquil, L. Bartolomei, M. A. Pastor, and I. N. Lyon. Human body-segment tilts induced by galvanic stimulation: a vestibularly driven balance protection mechanism. *The Journal of physiology*, 500 (Pt 3:661–72, 5 1997.

[81] B. L. Day, A. Séverac Cauquil, L. Bartolomei, M. A. Pastor, and I. N. Lyon. Human body-segment tilts induced by galvanic stimulation: a vestibularly driven balance protection mechanism. *The Journal of physiology*, 500 (Pt 3:661–72, 5 1997.

[82] L. Defebvre, J. L. Bourriez, K. Dujardin, P. Derambure, A. Destée, and J. D. Guieu. Spatiotemporal study of Bereitschaftspotential and event-related desynchronization during voluntary movement in Parkinson's disease. *Brain topography*, 6(3):237–44, 1994.

[83] M. DeLong and T. Wichmann. Changing views of basal ganglia circuits and circuit disorders. *Clinical EEG and neuroscience*, 41(2):61–7, 4 2010.

[84] A. Delorme and S. Makeig. EEGLAB: an open source toolbox for analysis of single-trial EEG dynamics including independent component analysis. *Journal of Neuroscience Methods*, 134(1):9–21, 3 2004.

[85] A. Delorme, J. Palmer, R. Oostenveld, J. Onton, and S. Makeig. Comparing Results of Algorithms Implementing Blind Source Separation of EEG Data. *unpublished*.

[86] A. Delorme, T. Sejnowski, and S. Makeig. Enhanced detection of artifacts in EEG data using higher-order statistics and independent component analysis. *NeuroImage*, 34(4):1443–9, 2 2007.

[87] Z.-D. Deng, S. H. Lisanby, and A. V. Peterchev. Electric field depthfocality tradeoff in transcranial magnetic stimulation: Simulation comparison of 50 coil designs. *Brain Stimulation*, 6(1):1–13, 1 2013.

[88] M. Desmurget and A. Sirigu. A parietal-premotor network for movement intention and motor awareness. *Trends in Cognitive Sciences*, 13(10):411–419, 10 2009.

[89] G. Deuschl, C. Schade-Brittinger, P. Krack, J. Volkmann, H. Schäfer, K. Bötzel, C. Daniels, A. Deutschländer, U. Dillmann, W. Eisner, D. Gruber, W. Hamel, J. Herzog, R. Hilker, S. Klebe, M. Kloß, J. Koy, M. Krause, A. Kupsch, D. Lorenz, S. Lorenzl, H. M. Mehdorn, J. R. Moringlane, W. Oertel, M. O. Pinsker, H. Reichmann, A. Reuß, G.-H. Schneider, A. Schnitzler, U. Steude, V. Sturm, L. Timmermann, V. Tronnier, T. Trottenberg, L. Wojtecki, E. Wolf, W. Poewe, J. Voges, and N. S. German Parkinson Study Group. A Randomized Trial of Deep-Brain Stimulation for Parkinson's Disease. *New England Journal of Medicine*, 355(9):896–908, 8 2006.

[90] D. Devos, E. Labyt, P. Derambure, J. L. Bourriez, F. Cassim, J. D. Guieu, A. Destée, and L. Defebvre. Effect of L-Dopa on the pattern of movement-related (de)synchronisation in advanced Parkinson's disease. *Neurophysiologie clinique = Clinical neurophysiology*, 33(5):203–12, 11 2003.

[91] J. P. Dmochowski, A. Datta, M. Bikson, Y. Su, and L. C. Parra. Optimized multi-electrode stimulation increases focality and intensity at target. *Journal of Neural Engineering*, 8(4):046011, 8 2011.

[92] D. Doruk, Z. Gray, G. L. Bravo, A. Pascual-Leone, and F. Fregni. Effects of tDCS on executive function in Parkinson's disease. *Neuroscience Letters*, 582:27–31, 10 2014.

[93] L. M. F. Doyle, A. A. Kühn, M. Hariz, A. Kupsch, G.-H. Schneider, and P. Brown. Levodopa-induced modulation of subthalamic beta oscillations during self-paced movements in patients with Parkinson's disease. *European Journal of Neuroscience*, 21(5):1403–1412, 3 2005.

[94] S. du Lac and S. G. Lisberger. Cellular processing of temporal information in medial vestibular nucleus neurons. *The Journal of neuroscience : the official journal of the Society for Neuroscience*, 15(12):8000–10, 12 1995.

[95] K. T. E. O. Dubbelink, M. M. Schoonheim., J. B. Deijen, J. W. R. Twisk, F. Barkhof, H. W. Berendse, K. T. E. Olde Dubbelink, M. M. Schoonheim, J. B. Deijen, J. W. R. Twisk, F. Barkhof, and H. W. Berendse. Functional connectivity and cognitive decline over 3 years in Parkinson disease. *Neurology*, 83(22):2046–2053, 11 2014.

[96] R. O. Duda, P. E. Hart, and D. G. Stork. Pattern Classification, 2001.

[97] A. K. Engel and P. Fries. Beta-band oscillations signalling the status quo? *Current Opinion in Neurobiology*, 20(2):156–165, 4 2010.

[98] D. Erskine, A. J. Thomas, J. Attems, J.-P. Taylor, I. G. McKeith, C. M. Morris, and A. A. Khundakar. Specific patterns of neuronal loss in the pulvinar nucleus in dementia with lewy bodies. *Movement Disorders*, 32(3):414–422, 3 2017.

[99] S. Espenhahn, A. O. de Berker, B. C. M. van Wijk, H. E. Rossiter, and N. S. Ward. Movement-related beta oscillations show high intra-individual reliability. *NeuroImage*, 147:175–185, 2017.

[100] A. Eusebio, A. Pogosyan, S. Wang, B. Averbeck, L. D. Gaynor, S. Cantiniaux, T. Witjas, P. Limousin, J.-P. Azulay, and P. Brown. Resonance in subthalamo-cortical circuits in Parkinson's disease. *Brain*, 132(8):2139–2150, 8 2009.

[101] E. Faught and W. Tatum. Trigeminal stimulation: A superhighway to the brain? *Neurology*, 80(9):780–781, 2 2013.

[102] J. M. Fearnley and A. J. Lees. Ageing and Parkinson's disease: substantia nigra regional selectivity. *Brain : a journal of neurology*, 114 (Pt 5:2283–301, 10 1991.

[103] J. Fell and N. Axmacher. The role of phase synchronization in memory processes. *Nature Reviews Neuroscience*, 12(2):105–118, 2 2011.

[104] S. J. Fellows and J. Noth. Grip force abnormalities in de novo Parkinson's disease. *Movement Disorders*, 19(5):560–565, 5 2004.

[105] R. Ferrucci, F. Cortese, M. Bianchi, D. Pittera, R. Turrone, T. Bocci, B. Borroni, M. Vergari, F. Cogiamanian, G. Ardolino, A. Di Fonzo, A. Padovani, and A. Priori. Cerebellar and Motor Cortical Transcranial Stimulation Decrease Levodopa-Induced Dyskinesias in Parkinsons Disease. *The Cerebellum*, 15(1):43–47, 2 2016.

[106] A. Fertonani and C. Miniussi. Transcranial Electrical Stimulation: What We Know and Do Not Know About Mechanisms. *The Neuroscientist*, 23(2):109–123, 4 2017.

[107] M. Feurra, G. Bianco, E. Santarnecchi, M. Del Testa, A. Rossi, and S. Rossi. Frequency-Dependent Tuning of the Human Motor System Induced by Transcranial Oscillatory Potentials. *Journal of Neuroscience*, 31(34):12165–12170, 8 2011.

[108] P. Filzmoser and V. Todorov. Review of robust multivariate statistical methods in high dimension. *Analytica Chimica Acta*, 705(1-2):2–14, 10 2011.

[109] S. D. Fisher and J. N. J. Reynolds. The intralaminar thalamus-an expressway linking visual stimuli to circuits determining agency and action selection. *Frontiers in Behavioral Neuroscience*, 8:115, 4 2014.

[110] R. Fitzpatrick, D. Burke, and S. C. Gandevia. Task-dependent reflex responses and movement illusions evoked by galvanic vestibular stimulation in standing humans. *The Journal of physiology*, 478 (Pt 2:363–72, 7 1994.

[111] R. C. Fitzpatrick and B. L. Day. Probing the human vestibular system with galvanic stimulation. *Journal of applied physiology*, 96(6):2301–16, 6 2004.

[112] G. Foffani, G. Ardolino, B. Meda, M. Egidi, P. Rampini, E. Caputo, G. Baselli, and A. Priori. Altered subthalamo-pallidal synchronisation in parkinsonian dyskinesias. *Journal of Neurology, Neurosurgery & Psychiatry*, 76(3):426–428, 3 2005.

[113] P. A. Forbes, C. J. Dakin, A. M. Geers, M. P. Vlaar, R. Happee, G. P. Siegmund, A. C. Schouten, and J.-S. Blouin. Electrical Vestibular Stimuli to Enhance Vestibulo-Motor Output and Improve Subject Comfort. *PLoS ONE*, 9(1):e84385, 2014.

[114] F. Fregni, P. S. Boggio, M. C. Santos, M. Lima, A. L. Vieira, S. P. Rigonatti, M. T. A. Silva, E. R. Barbosa, M. A. Nitsche, and A. Pascual-Leone. Noninvasive cortical stimulation with transcranial direct current stimulation in Parkinson's disease. *Movement Disorders*, 21(10):1693–1702, 10 2006.

[115] F. Fregni and A. Pascual-Leone. Technology Insight: noninvasive brain stimulation in neurologyperspectives on the therapeutic potential of rTMS and tDCS. *Nature Clinical Practice Neurology*, 3(7):383–393, 7 2007.

[116] P. Fries. Neuronal Gamma-Band Synchronization as a Fundamental Process in Cortical Computation. *Annual Review of Neuroscience*, 32(1):209–224, 6 2009.

[117] E. C. Fuchs, H. Doheny, H. Faulkner, A. Caputi, R. D. Traub, A. Bibbig, N. Kopell, M. A. Whittington, and H. Monyer. Genetically altered AMPA-type glutamate receptor kinetics in interneurons disrupt long-range synchrony of gamma oscillation. *Proceedings of the National Academy of Sciences*, 98(6):3571–3576, 3 2001.

[118] R. Fuentes, P. Petersson, W. B. Siesser, M. G. Caron, and M. A. L. Nicolelis. Spinal Cord Stimulation Restores Locomotion in Animal Models of Parkinson's Disease. *Science*, 323(5921):1578–1582, 3 2009.

[119] R. Galambos and S. Makeig. Physiological studies of central masking in man. I: The effects of noise on the 40-Hz steady-state response. *The Journal of the Acoustical Society of America*, 92(5):2683–90, 11 1992.

[120] M. N. Gallay, D. Jeanmonod, J. Liu, and A. Morel. Human pallidothalamic and cerebellothalamic tracts: anatomical basis for functional stereotactic neurosurgery. *Brain structure & function*, 212(6):443–63, 8 2008.

[121] A. Galvan and T. Wichmann. Pathophysiology of parkinsonism. *Clinical neurophysiology : official journal of the International Federation of Clinical Neurophysiology*, 119(7):1459–74, 7 2008.

[122] A. Garg, S. Appel-Cresswell, K. Popuri, M. J. McKeown, and M. F. Beg. Morphological alterations in the caudate, putamen, pallidum, and thalamus in Parkinson's disease. *Frontiers in neuroscience*, 9:101, 2015.

[123] D. D. Garrett, G. R. Samanez-Larkin, S. W. MacDonald, U. Lindenberger, A. R. McIntosh, and C. L. Grady. Moment-to-moment brain signal variability: A next frontier in human brain mapping? *Neuroscience & Biobehavioral Reviews*, 37(4):610–624, 5 2013.

[124] J. S. George, J. Strunk, R. Mak-McCully, M. Houser, H. Poizner, and A. R. Aron. Dopaminergic therapy in Parkinson's disease decreases cortical beta band coherence in the resting state and increases cortical beta band power during executive control. *NeuroImage: Clinical*, 3:261–270, 2013.

[125] J. Ghika, J.-G. Villemure, H. Fankhauser, J. Favre, G. Assal, and F. Ghika-Schmid. Efficiency and safety of bilateral contemporaneous pallidal stimulation (deep brain stimulation) in levodopa-responsive patients with Parkinson's disease with severe motor fluctuations: a 2-year follow-up review. *Journal of Neurosurgery*, 89(5):713–718, 11 1998.

[126] G. Giannicola, S. Marceglia, L. Rossi, S. Mrakic-Sposta, P. Rampini, F. Tamma, F. Cogiamanian, S. Barbieri, and A. Priori. The effects of levodopa and ongoing deep brain stimulation on subthalamic beta oscillations in Parkinson's disease. *Experimental Neurology*, 226(1):120–127, 11 2010.

[127] T. Gilbertson, E. Lalo, L. Doyle, V. Di Lazzaro, B. Cioni, and P. Brown. Existing Motor State Is Favored at the Expense of New Movement during 13-35 Hz Oscillatory Synchrony in the Human Corticospinal System. *Journal of Neuroscience*, 25(34):7771–7779, 8 2005.

[128] J. M. Goldberg, C. E. Smith, and C. Fernandez. Relation between discharge regularity and responses to externally applied galvanic currents in vestibular nerve afferents of the squirrel monkey. *Journal of Neurophysiology*, 51(6):1236–1256, 6 1984.

[129] A. M. Gordon, P. E. Ingvarsson, and H. Forssberg. Anticipatory Control of Manipulative Forces in Parkinson's Disease. *Experimental Neurology*, 145(2):477–488, 6 1997.

[130] L. T. Grinberg, U. Rueb, A. T. d. L. Alho, and H. Heinsen. Brainstem pathology and non-motor symptoms in PD. *Journal of the Neurological Sciences*, 289(1-2):81–88, 2 2010.

[131] S. J. Groiss, L. Wojtecki, M. Südmeyer, and A. Schnitzler. Deep brain stimulation in Parkinson's disease. *Therapeutic advances in neurological disorders*, 2(6):20–8, 11 2009.

[132] D. M. Groppe, S. Bickel, C. J. Keller, S. K. Jain, S. T. Hwang, C. Harden, and A. D. Mehta. Dominant frequencies of resting human brain activity as measured by the electrocorticogram. *NeuroImage*, 79:223–33, 10 2013.

[133] R. P. Guimarães, M. C. Arci Santos, A. Dagher, L. S. Campos, P. Azevedo, L. G. Piovesana, B. M. De Campos, K. Larcher, Y. Zeighami, A. C. Scarparo Amato-Filho, F. Cendes, and A. C. F. D'Abreu. Pattern of Reduced Functional Connectivity and Structural Abnormalities in Parkinson's Disease: An Exploratory Study. *Frontiers in neurology*, 7:243, 2016.

[134] C. Gurvich, J. J. Maller, B. Lithgow, S. Haghgooie, and J. Kulkarni. Vestibular insights into cognition and psychiatry. *Brain Research*, 1537:244–259, 11 2013.

[135] S. Haber and N. R. Mcfarland. The Place of the Thalamus in Frontal Cortical-Basal Ganglia Circuits. *The Neuroscientist*, 7(4):315–324, 8 2001.

[136] S. N. Haber and R. Calzavara. The cortico-basal ganglia integrative network: The role of the thalamus. *Brain Research Bulletin*, 78(2-3):69–74, 2 2009.

[137] M. Haghighat, M. Abdel-Mottaleb, and W. Alhalabi. Discriminant Correlation Analysis: Real-Time Feature Level Fusion for Multimodal Biometric Recognition. *IEEE Transactions on Information Forensics and Security*, 11(9):1984–1996, 9 2016.

[138] N. Hajos, J. Pálhalmi, E. O. Mann, B. Németh, O. Paulsen, and T. F. Freund. Spike Timing of Distinct Types of GABAergic Interneuron

during Hippocampal Gamma Oscillations In Vitro. *Journal of Neuroscience*, 24(41):9127–9137, 10 2004.

[139] G. M. Halliday. Thalamic changes in Parkinson's disease. *Parkinsonism & Related Disorders*, 15:S152–S155, 12 2009.

[140] G. M. Halliday, V. Macdonald, and J. M. Henderson. A comparison of degeneration in motor thalamus and cortex between progressive supranuclear palsy and Parkinson's disease. *Brain*, 128(10):2272–2280, 10 2005.

[141] S. Hanslmayr, W. Klimesch, P. Sauseng, W. Gruber, M. Doppelmayr, R. Freunberger, and T. Pecherstorfer. Visual discrimination performance is related to decreased alpha amplitude but increased phase locking. *Neuroscience letters*, 375(1):64–8, 2 2005.

[142] R. Hari, R. Salmelin, J. P. Mäkelä, S. Salenius, and M. Helle. Magnetoencephalographic cortical rhythms. *International journal of psychophysiology : official journal of the International Organization of Psychophysiology*, 26(1-3):51–62, 6 1997.

[143] S.-b. He, C.-y. Liu, L.-d. Chen, Z.-n. Ye, Y.-p. Zhang, W.-g. Tang, B.-d. Wang, and X. Gao. Meta-Analysis of Visual Evoked Potential and Parkinsons Disease. *Parkinson's Disease*, 2018:1–8, 7 2018.

[144] X. He, Y. Zhang, J. Chen, C. Xie, R. Gan, R. Yang, L. Wang, K. Nie, and L. Wang. The patterns of EEG changes in early-onset Parkinson's disease patients. *International Journal of Neuroscience*, 127(11):1028–1035, 11 2017.

[145] E. Heinrichs-Graham and T. W. Wilson. Is an absolute level of cortical beta suppression required for proper movement? Magnetoencephalographic evidence from healthy aging. *NeuroImage*, 134:514–521, 7 2016.

[146] E. Heinrichs-Graham, T. W. Wilson, P. M. Santamaria, S. K. Heithoff, D. Torres-Russotto, J. A. L. Hutter-Saunders, K. A. Estes, J. L. Meza, R. L. Mosley, and H. E. Gendelman. Neuromagnetic evidence of abnormal movement-related beta desynchronization in Parkinson's disease. *Cerebral cortex (New York, N.Y. : 1991)*, 24(10):2669–78, 10 2014.

[147] R. F. Helfrich, T. R. Schneider, S. Rach, S. A. Trautmann-Lengsfeld, A. K. Engel, and C. S. Herrmann. Entrainment of brain oscillations by transcranial alternating current stimulation. *Current biology : CB*, 24(3):333–9, 2 2014.

[148] R. C. Helmich, L. C. Derikx, M. Bakker, R. Scheeringa, B. R. Bloem, and I. Toni. Spatial Remapping of Cortico-striatal Connectivity in Parkinson's Disease. *Cerebral Cortex*, 20(5):1175–1186, 5 2010.

[149] J. M. Henderson, K. Carpenter, H. Cartwright, and G. M. Halliday. Loss of thalamic intralaminar nuclei in progressive supranuclear palsy and Parkinson's disease: clinical and therapeutic implications. *Brain : a journal of neurology*, 123 (Pt 7:1410–21, 7 2000.

[150] C. S. Herrmann. Human EEG responses to 1-100 Hz flicker: resonance phenomena in visual cortex and their potential correlation to cognitive phenomena. *Experimental Brain Research*, 137(3-4):346–353, 4 2001.

[151] C. S. Herrmann, S. Rach, T. Neuling, and D. Strüber. Transcranial alternating current stimulation: a review of the underlying mechanisms and modulation of cognitive processes. *Frontiers in Human Neuroscience*, 7:279, 2013.

[152] L. Hirsch, N. Jette, A. Frolkis, T. Steeves, and T. Pringsheim. The Incidence of Parkinson's Disease: A Systematic Review and Meta-Analysis. *Neuroepidemiology*, 46(4):292–300, 2016.

[153] S. W. Hughes and V. Crunelli. Thalamic mechanisms of EEG alpha rhythms and their pathological implications. *The Neuroscientist : a review journal bringing neurobiology, neurology and psychiatry*, 11(4):357–72, 8 2005.

[154] F. Hummel, P. Celnik, P. Giraux, A. Floel, W.-H. Wu, C. Gerloff, and L. G. Cohen. Effects of non-invasive cortical stimulation on skilled motor function in chronic stroke. *Brain*, 128(3):490–499, 1 2005.

[155] W. D. Hutchison, J. O. Dostrovsky, J. R. Walters, R. Courtemanche, T. Boraud, J. Goldberg, and P. Brown. Neuronal Oscillations in the Basal Ganglia and Movement Disorders: Evidence from Whole Animal and Human Recordings. *Journal of Neuroscience*, 24(42):9240–9243, 10 2004.

[156] K. Hwang, M. A. Bertolero, W. B. Liu, and M. D'Esposito. The Human Thalamus Is an Integrative Hub for Functional Brain Networks. *The Journal of neuroscience : the official journal of the Society for Neuroscience*, 37(23):5594–5607, 2017.

[157] I. A. Ilinsky, K. Kultas-Ilinsky, A. Rosina, and M. Haddy. Quantitative evaluation of crossed and uncrossed projections from basal ganglia and cerebellum to the cat thalamus. *Neuroscience*, 21(1):207–27, 4 1987.

[158] M. Inase, J. A. Buford, and M. E. Anderson. Changes in the control of arm position, movement, and thalamic discharge during local inactivation in the globus pallidus of the monkey. *Journal of Neurophysiology*, 75(3):1087–1104, 3 1996.

[159] C. James, A. Stathis, and V. G. Macefield. Vestibular and pulse-related modulation of skin sympathetic nerve activity during sinusoidal galvanic vestibular stimulation in human subjects. *Experimental brain research*, 202(2):291–8, 4 2010.

[160] J. Jankovic. Parkinson's disease: clinical features and diagnosis. *Journal of Neurology, Neurosurgery & Psychiatry*, 79(4):368–376, 4 2008.

[161] H. Jasper and W. Penfield. Electrocorticograms in man: Effect of voluntary movement upon the electrical activity of the precentral gyrus. *Archiv fur Psychiatrie und Nervenkrankheiten*, 183(1-2):163–174, 1949.

[162] N. Jenkinson and P. Brown. New insights into the relationship between dopamine, beta oscillations and motor function. *Trends in Neurosciences*, 34(12):611–618, 12 2011.

[163] J. Jeong. EEG dynamics in patients with Alzheimer's disease. *Clinical neurophysiology : official journal of the International Federation of Clinical Neurophysiology*, 115(7):1490–505, 7 2004.

[164] B. Ji, Z. Li, K. Li, L. Li, J. Langley, H. Shen, S. Nie, R. Zhang, and X. Hu. Dynamic thalamus parcellation from resting-state fMRI data. *Human Brain Mapping*, 37(3):954–967, 3 2016.

[165] W. Jian, M. Chen, and D. J. McFarland. EEG Based Zero-phase Phase-locking Value (PLV) and Effects of Spatial Filtering During Actual Movement. *Brain research bulletin*, 130:156, 2017.

[166] Jianbo Shi and J. Malik. Normalized cuts and image segmentation. *IEEE Transactions on Pattern Analysis and Machine Intelligence*, 22(8):888–905, 2000.

[167] S. M. Jones, T. A. Jones, K. N. Mills, and G. C. Gaines. Anatomical and Physiological Considerations in Vestibular Dysfunction and Compensation. *Seminars in hearing*, 30(4):231–241, 2009.

[168] N. Jordan, H. J. Sagar, and J. A. Cooper. Cognitive components of reaction time in Parkinson's disease. *Journal of neurology, neurosurgery, and psychiatry*, 55(8):658–64, 8 1992.

[169] R. A. Joundi, N. Jenkinson, J.-S. Brittain, T. Z. Aziz, and P. Brown. Driving oscillatory activity in the human cortex enhances motor performance. *Current Biology*, 22(5):403–407, 3 2012.

[170] T. Jubault, S. M. Brambati, C. Degroot, B. Kullmann, A. P. Strafella, A.-L. Lafontaine, S. Chouinard, and O. Monchi. Regional brain stem atrophy in idiopathic Parkinson's disease detected by anatomical MRI. *PloS one*, 4(12):e8247, 12 2009.

[171] H. Kataoka, Y. Okada, T. Kiriyama, Y. Kita, J. Nakamura, S. Morioka, K. Shomoto, and S. Ueno. Can Postural Instability Respond to Galvanic Vestibular Stimulation in Patients with Parkinsons Disease? *Journal of Movement Disorders*, 9(1):40–43, 12 2016.

[172] J. R. Kettenring. Canonical Analysis of Several Sets of Variables. *Biometrika*, 58(3):433, 12 1971.

[173] S. Khan and R. Chang. Anatomy of the vestibular system: a review. *NeuroRehabilitation*, 32(3):437–43, 2013.

[174] M. Khoshnam, D. M. C. Häner, E. Kuatsjah, X. Zhang, and C. Menon. Effects of Galvanic Vestibular Stimulation on Upper and Lower Extremities Motor Symptoms in Parkinsons Disease. *Frontiers in Neuroscience*, 12:633, 9 2018.

[175] B. E. Kilavik, M. Zaepffel, A. Brovelli, W. A. MacKay, and A. Riehle. The ups and downs of beta oscillations in sensorimotor cortex. *Experimental Neurology*, 245:15–26, 7 2013.

[176] D. Kim, B. Park, and H. Park. Functional connectivity-based identification of subdivisions of the basal ganglia and thalamus using mul-

tilevel independent component analysis of resting state fMRI. *Human Brain Mapping*, 34(6):1371–1385, 6 2013.

[177] D. J. Kim, V. Yogendrakumar, J. Chiang, E. Ty, Z. J. Wang, and M. J. McKeown. Noisy Galvanic Vestibular Stimulation Modulates the Amplitude of EEG Synchrony Patterns. *PLoS ONE*, 8(7):e69055, 7 2013.

[178] N. Kim, J. W. Barter, T. Sukharnikova, and H. H. Yin. Striatal firing rate reflects head movement velocity. *European Journal of Neuroscience*, 40(10):3481–3490, 11 2014.

[179] T. Kim, T. Eltoft, and T.-W. Lee. Independent Vector Analysis: An Extension of ICA to Multivariate Components. pages 165–172. Springer, Berlin, Heidelberg, 2006.

[180] K. Kitajo, S. M. Doesburg, K. Yamanaka, D. Nozaki, L. M. Ward, and Y. Yamamoto. Noise-induced large-scale phase synchronization of human-brain activity associated with behavioural stochastic resonance. *Europhysics Letters (EPL)*, 80(4):40009, 11 2007.

[181] G. Kleiner-Fisman, J. Herzog, D. N. Fisman, F. Tamma, K. E. Lyons, R. Pahwa, A. E. Lang, and G. Deuschl. Subthalamic nucleus deep brain stimulation: Summary and meta-analysis of outcomes. *Movement Disorders*, 21(S14):S290–S304, 6 2006.

[182] W. Klimesch. EEG alpha and theta oscillations reflect cognitive and memory performance: a review and analysis. *Brain research. Brain research reviews*, 29(2-3):169–95, 4 1999.

[183] W. Klimesch, M. Doppelmayr, A. Yonelinas, N. E. Kroll, M. Lazzara, D. Röhm, and W. Gruber. Theta synchronization during episodic retrieval: neural correlates of conscious awareness. *Brain research. Cognitive brain research*, 12(1):33–8, 8 2001.

[184] W. Klimesch, R. Freunberger, P. Sauseng, and W. Gruber. A short review of slow phase synchronization and memory: Evidence for control processes in different memory systems? *Brain Research*, 1235:31–44, 10 2008.

[185] W. Klimesch, P. Sauseng, and S. Hanslmayr. EEG alpha oscillations: The inhibitiontiming hypothesis. *Brain Research Reviews*, 53(1):63–88, 1 2007.

[186] W. Klomjai, R. Katz, and A. Lackmy-Vallée. Basic principles of transcranial magnetic stimulation (TMS) and repetitive TMS (rTMS). *Annals of Physical and Rehabilitation Medicine*, 58(4):208–213, 9 2015.

[187] S. Kohli and A. J. Casson. Removal of Transcranial a.c. Current Stimulation artifact from simultaneous EEG recordings by superposition of moving averages. *Conference proceedings : ... Annual International Conference of the IEEE Engineering in Medicine and Biology Society. IEEE Engineering in Medicine and Biology Society. Annual Conference*, 2015:3436–9, 1 2015.

[188] P. Krack, A. Batir, N. Van Blercom, S. Chabardes, V. Fraix, C. Ardouin, A. Koudsie, P. D. Limousin, A. Benazzouz, J. F. LeBas, A.-L. Benabid, and P. Pollak. Five-Year Follow-up of Bilateral Stimulation of the Subthalamic Nucleus in Advanced Parkinson's Disease. *New England Journal of Medicine*, 349(20):1925–1934, 11 2003.

[189] V. Krause, C. Wach, M. Südmeyer, S. Ferrea, A. Schnitzler, and B. Pollok. Cortico-muscular coupling and motor performance are modulated by 20 Hz transcranial alternating current stimulation (tACS) in Parkinson's disease. *Frontiers in human neuroscience*, 7:928, 2013.

[190] A. C. Kreitzer and R. C. Malenka. Endocannabinoid-mediated rescue of striatal LTD and motor deficits in Parkinson's disease models. *Nature*, 445(7128):643–647, 2 2007.

[191] A. A. Kühn, A. Tsui, T. Aziz, N. Ray, C. Brücke, A. Kupsch, G.-H. Schneider, and P. Brown. Pathological synchronisation in the subthalamic nucleus of patients with Parkinson's disease relates to both bradykinesia and rigidity. *Experimental Neurology*, 215(2):380–387, 2 2009.

[192] V. Kumar, S. Mang, and W. Grodd. Direct diffusion-based parcellation of the human thalamus. *Brain Structure and Function*, 220(3):1619–1635, 5 2015.

[193] Y. Kumar, M. L. Dewal, and R. S. Anand. Features extraction of EEG signals using approximate and sample entropy. In *2012 IEEE Students' Conference on Electrical, Electronics and Computer Science*, pages 1–5. IEEE, 3 2012.

[194] K. Kurata. Activity Properties and Location of Neurons in the Motor Thalamus That Project to the Cortical Motor Areas in Monkeys. *Journal of Neurophysiology*, 94(1):550–566, 7 2005.

[195] J. P. Lachaux, E. Rodriguez, J. Martinerie, and F. J. Varela. Measuring phase synchrony in brain signals. *Human brain mapping*, 8(4):194–208, 1999.

[196] H. Lai, T. Tsumori, T. Shiroyama, S. Yokota, K. Nakano, and Y. Yasui. Morphological evidence for a vestibulo-thalamo-striatal pathway via the parafascicular nucleus in the rat. *Brain research*, 872(1-2):208–14, 7 2000.

[197] P. Lakatos, M. N. O'Connell, and A. Barczak. Pondering the Pulvinar. *Neuron*, 89(1):5–7, 1 2016.

[198] D. E. Lake, J. S. Richman, M. P. Griffin, and J. R. Moorman. Sample entropy analysis of neonatal heart rate variability. *American Journal of Physiology-Regulatory, Integrative and Comparative Physiology*, 283(3):R789–R797, 9 2002.

[199] J. L. Lanciego, N. Luquin, and J. A. Obeso. Functional neuroanatomy of the basal ganglia. *Cold Spring Harbor perspectives in medicine*, 2(12):a009621, 12 2012.

[200] Lang Tong, Guanghan Xu, and T. Kailath. Blind identification and equalization based on second-order statistics: a time domain approach. *IEEE Transactions on Information Theory*, 40(2):340–349, 3 1994.

[201] T. Langheinrich, L. Tebartz van Elst, W. A. Lagrèze, M. Bach, C. H. Lücking, and M. W. Greenlee. Visual contrast response functions in Parkinson's disease: evidence from electroretinograms, visually evoked potentials and psychophysics. *Clinical neurophysiology : official journal of the International Federation of Clinical Neurophysiology*, 111(1):66–74, 1 2000.

[202] H. Laufs, A. Kleinschmidt, A. Beyerle, E. Eger, A. Salek-Haddadi, C. Preibisch, and K. Krakow. EEG-correlated fMRI of human alpha activity. *NeuroImage*, 19(4):1463–76, 8 2003.

[203] H. J. Lee, A. J. Weitz, D. Bernal-Casas, B. A. Duffy, M. Choy, A. V. Kravitz, A. C. Kreitzer, and J. H. Lee. Activation of Direct and Indirect Pathway Medium Spiny Neurons Drives Distinct Brain-wide Responses. *Neuron*, 91(2):412–424, 7 2016.

[204] S. Lee, D. Kim, and M. J. McKeown. Galvanic Vestibular Stimulation (GVS) effects on impaired interhemispheric connectivity in Parkinson's Disease. In *2017 39th Annual International Conference of the IEEE Engineering in Medicine and Biology Society (EMBC)*, volume 2017, pages 2109–2113. IEEE, 7 2017.

[205] S. Lee, D. J. Kim, D. Svenkeson, G. Parras, M. M. K. Oishi, and M. J. McKeown. Multifaceted effects of noisy galvanic vestibular stimulation on manual tracking behavior in Parkinson's disease. *Frontiers in Systems Neuroscience*, 9:5, 2015.

[206] S. Lee, A. Liu, Z. J. Wang, and M. J. McKeown. Abnormal Phase Coupling in Parkinsons Disease and Normalization Effects of Subthreshold Vestibular Stimulation. *Frontiers in Human Neuroscience*, 13:118, 4 2019.

[207] W. H. Lee and S. Frangou. Linking functional connectivity and dynamic properties of resting-state networks. *Scientific Reports*, 7(1):16610, 12 2017.

[208] W. Legon, T. F. Sato, A. Opitz, J. Mueller, A. Barbour, A. Williams, and W. J. Tyler. Transcranial focused ultrasound modulates the activity of primary somatosensory cortex in humans. *Nature Neuroscience*, 17(2):322–329, 2 2014.

[209] B. Lenggenhager, C. Lopez, and O. Blanke. Influence of galvanic vestibular stimulation on egocentric and object-based mental transformations. *Experimental Brain Research*, 184(2):211–221, 11 2007.

[210] D. K. Leventhal, G. J. Gage, R. Schmidt, J. R. Pettibone, A. C. Case, and J. D. Berke. Basal Ganglia Beta Oscillations Accompany Cue Utilization. *Neuron*, 73(3):523–536, 2 2012.

[211] R. Levy, P. Ashby, W. D. Hutchison, A. E. Lang, A. M. Lozano, and J. O. Dostrovsky. Dependence of subthalamic nucleus oscillations on movement and dopamine in Parkinson's disease. *Brain : a journal of neurology*, 125(Pt 6):1196–209, 6 2002.

[212] R. Levy, L. N. Hazrati, M. T. Herrero, M. Vila, O. K. Hassani, M. Mouroux, M. Ruberg, H. Asensi, Y. Agid, J. Féger, J. A. Obeso, A. Parent, and E. C. Hirsch. Re-evaluation of the functional anatomy of the basal ganglia in normal and Parkinsonian states. *Neuroscience*, 76(2):335–43, 1 1997.

[213] R. Levy, W. D. Hutchison, A. M. Lozano, and J. O. Dostrovsky. High-frequency Synchronization of Neuronal Activity in the Subthalamic Nucleus of Parkinsonian Patients with Limb Tremor. *Journal of Neuroscience*, 20(20), 2000.

[214] R. Levy, W. D. Hutchison, A. M. Lozano, and J. O. Dostrovsky. Synchronized neuronal discharge in the basal ganglia of parkinsonian patients is limited to oscillatory activity. *The Journal of neuroscience : the official journal of the Society for Neuroscience*, 22(7):2855–61, 4 2002.

[215] W. Li, J. Liu, F. Skidmore, Y. Liu, J. Tian, and K. Li. White Matter Microstructure Changes in the Thalamus in Parkinson Disease with Depression: A Diffusion Tensor MR Imaging Study. *American Journal of Neuroradiology*, 31(10):1861–1866, 11 2010.

[216] K. Lieb, S. Brucker, M. Bach, T. Els, C. H. Lücking, and M. W. Greenlee. Impairment in preattentive visual processing in patients with Parkinson's disease. *Brain*, 122(2):303–313, 2 1999.

[217] D. Liebetanz, M. A. Nitsche, F. Tergau, and W. Paulus. Pharmacological approach to the mechanisms of transcranial DC-stimulation-induced after-effects of human motor cortex excitability. *Brain : a journal of neurology*, 125(Pt 10):2238–47, 10 2002.

[218] S. Lippe, N. Kovacevic, and A. R. McIntosh. Differential maturation of brain signal complexity in the human auditory and visual system. *Frontiers in Human Neuroscience*, 3:48, 2009.

[219] V. Litvak, A. Eusebio, A. Jha, R. Oostenveld, G. Barnes, T. Foltynie, P. Limousin, L. Zrinzo, M. I. Hariz, K. Friston, and P. Brown. Movement-related changes in local and long-range synchronization in Parkinson's disease revealed by simultaneous magnetoencephalography and intracranial recordings. *The Journal of neuroscience : the official journal of the Society for Neuroscience*, 32(31):10541–53, 8 2012.

[220] E. Lobel, J. F. Kleine, D. L. Bihan, A. Leroy-Willig, and A. Berthoz. Functional MRI of galvanic vestibular stimulation. *Journal of neurophysiology*, 80(5):2699–709, 11 1998.

[221] C. Lopez and O. Blanke. The thalamocortical vestibular system in animals and humans. *Brain Research Reviews*, 67(1-2):119–146, 6 2011.

[222] C. Lopez, O. Blanke, and F. Mast. The human vestibular cortex revealed by coordinate-based activation likelihood estimation meta-analysis. *Neuroscience*, 212:159–179, 6 2012.

[223] S. Luan, I. Williams, K. Nikolic, and T. G. Constandinou. Neuromodulation: present and emerging methods. *Frontiers in Neuroengineering*, 7:27, 7 2014.

[224] C. D. B. Luft, E. Pereda, M. J. Banissy, and J. Bhattacharya. Best of both worlds: promise of combining brain stimulation and brain connectome. *Frontiers in Systems Neuroscience*, 8:132, 7 2014.

[225] K. E. Lyons, S. B. Wilkinson, J. Overman, and R. Pahwa. Surgical and hardware complications of subthalamic stimulation: a series of 160 procedures. *Neurology*, 63(4):612–6, 8 2004.

[226] A. D. Macleod, K. S. Taylor, and C. E. Counsell. Mortality in Parkinson's disease: A systematic review and meta-analysis. *Movement Disorders*, 29(13):1615–1622, 11 2014.

[227] G. Magnani, M. Cursi, L. Leocani, M. A. Volonté, and G. Comi. Acute effects of L-dopa on event-related desynchronization in Parkinson's disease. *Neurological Sciences*, 23(3):91–97, 9 2002.

[228] Q. Mai. A review of discriminant analysis in high dimensions. *Wiley Interdisciplinary Reviews: Computational Statistics*, 5(3):190–197, 5 2013.

[229] E. Mak, L. Su, G. B. Williams, M. J. Firbank, R. A. Lawson, A. J. Yarnall, G. W. Duncan, A. M. Owen, T. K. Khoo, D. J. Brooks, J. B. Rowe, R. A. Barker, D. J. Burn, and J. T. OBrien. Baseline and longitudinal grey matter changes in newly diagnosed Parkinsons disease: ICICLE-PD study. *Brain*, 138(10):2974–2986, 10 2015.

[230] R. Manenti, M. Brambilla, S. Rosini, I. Orizio, C. Ferrari, B. Borroni, and M. Cotelli. Time up and go task performance improves after transcranial direct current stimulation in patient affected by Parkinson's disease. *Neuroscience Letters*, 580:74–77, 9 2014.

[231] E. Manjarrez, G. Rojas-Piloni, I. Méndez, and A. Flores. Stochastic resonance within the somatosensory system: effects of noise on evoked field potentials elicited by tactile stimuli. *The Journal of neuroscience : the official journal of the Society for Neuroscience*, 23(6):1997–2001, 3 2003.

[232] F. Mars, K. Popov, and J. L. Vercher. Supramodal effects of galvanic vestibular stimulation on the subjective vertical. *Neuroreport*, 12(13):2991–4, 9 2001.

[233] J. F. Marsden, P. Limousin-Dowsey, P. Ashby, P. Pollak, and P. Brown. Subthalamic nucleus, sensorimotor cortex and muscle interrelationships in Parkinson's disease. *Brain : a journal of neurology*, 124(Pt 2):378–88, 2 2001.

[234] K. Matsunami and B. Cohen. Afferent modulation of unit activity in globus pallidus and caudate nucleus: changes induced by vestibular nucleus and pyramidal tract stimulation. *Brain Research*, 91(1):140–146, 6 1975.

[235] V. S. Mattay, J. H. Callicott, A. Bertolino, A. K. Santha, J. D. Van Horn, K. A. Tallent, J. A. Frank, and D. R. Weinberger. Hemispheric control of motor function: a whole brain echo planar fMRI study. *Psychiatry research*, 83(1):7–22, 7 1998.

[236] P. Mazzoni, B. Shabbott, and J. C. Cortés. Motor control abnormalities in Parkinson's disease. *Cold Spring Harbor perspectives in medicine*, 2(6):a009282, 6 2012.

[237] M. D. McDonnell and D. Abbott. What is stochastic resonance? Definitions, misconceptions, debates, and its relevance to biology. *PLoS computational biology*, 5(5):e1000348, 5 2009.

[238] M. D. McDonnell and L. M. Ward. The benefits of noise in neural systems: bridging theory and experiment. *Nature Reviews Neuroscience*, 12(7):415–426, 6 2011.

[239] E. G. McGeer, W. A. Staines, and P. L. McGeer. Neurotransmitters in the basal ganglia. *The Canadian journal of neurological sciences. Le journal canadien des sciences neurologiques*, 11(1 Suppl):89–99, 2 1984.

[240] P. D. McGeoch and V. S. Ramachandran. Vestibular stimulation can relieve central pain of spinal origin. *Spinal Cord*, 46(11):756–757, 11 2008.

[241] P. D. McGeoch, L. E. Williams, R. R. Lee, and V. S. Ramachandran. Behavioural evidence for vestibular stimulation as a treatment for central post-stroke pain. *Journal of Neurology, Neurosurgery & Psychiatry*, 79(11):1298–1301, 6 2008.

[242] J. G. McHaffie, T. R. Stanford, B. E. Stein, V. Coizet, and P. Redgrave. Subcortical loops through the basal ganglia. *Trends in Neurosciences*, 28(8):401–407, 8 2005.

[243] A. R. McIntosh, N. Kovacevic, and R. J. Itier. Increased brain signal variability accompanies lower behavioral variability in development. *PLoS computational biology*, 4(7):e1000106, 7 2008.

[244] C. C. McIntyre, M. Savasta, L. Kerkerian-Le Goff, and J. L. Vitek. Uncovering the mechanism(s) of action of deep brain stimulation: activation, inhibition, or both. *Clinical Neurophysiology*, 115(6):1239–1248, 6 2004.

[245] M. J. McKeown, A. Uthama, R. Abugharbieh, S. Palmer, M. Lewis, and X. Huang. Shape (but not volume) changes in the thalami in Parkinson disease. *BMC Neurology*, 8(1):8, 12 2008.

[246] I. Mendez-Balbuena, E. Manjarrez, J. Schulte-Monting, F. Huethe, J. A. Tapia, M.-C. Hepp-Reymond, and R. Kristeva. Improved Sensorimotor Performance via Stochastic Resonance. *Journal of Neuroscience*, 32(36):12612–12618, 9 2012.

[247] H. Meng, P. J. May, J. D. Dickman, and D. E. Angelaki. Vestibular Signals in Primate Thalamus: Properties and Origins. *Journal of Neuroscience*, 27(50):13590–13602, 12 2007.

[248] R. A. Menke, J. Scholz, K. L. Miller, S. Deoni, S. Jbabdi, P. M. Matthews, and M. Zarei. MRI characteristics of the substantia nigra in Parkinson's disease: A combined quantitative T1 and DTI study. *NeuroImage*, 47(2):435–441, 8 2009.

[249] C. Miniussi, D. Brignani, and M. C. Pellicciari. Combining Transcranial Electrical Stimulation With Electroencephalography. *Clinical EEG and Neuroscience*, 43(3):184–191, 7 2012.

[250] C. Miniussi, J. A. Harris, and M. Ruzzoli. Modelling non-invasive brain stimulation in cognitive neuroscience. *Neuroscience & Biobehavioral Reviews*, 37(8):1702–1712, 9 2013.

[251] A. S. Mitchell and S. Chakraborty. What does the mediodorsal thalamus do? *Frontiers in systems neuroscience*, 7:37, 2013.

[252] D. J. Mitchell, N. McNaughton, D. Flanagan, and I. J. Kirk. Frontal-midline theta from the perspective of hippocampal theta. *Progress in Neurobiology*, 86(3):156–185, 11 2008.

[253] Y. Miyagi. Thalamic Stimulation for Parkinsons Disease: Clinical Studies on DBS. In *Deep Brain Stimulation for Neurological Disorders*, pages 103–120. Springer International Publishing, Cham, 2015.

[254] M. Moazami-Goudarzi, J. Sarnthein, L. Michels, R. Moukhtieva, and D. Jeanmonod. Enhanced frontal low and high frequency power and synchronization in the resting EEG of parkinsonian patients. *NeuroImage*, 41(3):985–97, 7 2008.

[255] K. Monte-Silva, M.-F. Kuo, S. Hessenthaler, S. Fresnoza, D. Liebetanz, W. Paulus, and M. A. Nitsche. Induction of Late LTP-Like Plasticity in the Human Motor Cortex by Repeated Non-Invasive Brain Stimulation. *Brain Stimulation*, 6(3):424–432, 5 2013.

[256] F. Mormann, K. Lehnertz, P. David, and C. E. Elger. Mean phase coherence as a measure for phase synchronization and its application to the EEG of epilepsy patients. *Physica D: Nonlinear Phenomena*, 144(3-4):358–369, 10 2000.

[257] F. Moss, L. M. Ward, and W. G. Sannita. Stochastic resonance and sensory information processing: a tutorial and review of application. *Clinical neurophysiology : official journal of the International Federation of Clinical Neurophysiology*, 115(2):267–81, 2 2004.

[258] D. Muslimovic, B. Schmand, J. D. Speelman, and R. J. De Haan. Course of cognitive decline in Parkinson's disease: A meta-analysis. *Journal of the International Neuropsychological Society*, 13(06):920–32, 11 2007.

[259] A. B. Nelson, C. Moisello, J. Lin, P. Panday, S. Ricci, A. Canessa, A. Di Rocco, A. Quartarone, G. Frazzitta, I. U. Isaias, G. Tononi, C. Cirelli, and M. F. Ghilardi. Beta Oscillatory Changes and Retention of Motor Skills during Practice in Healthy Subjects and in Patients with Parkinson's Disease. *Frontiers in Human Neuroscience*, 11:104, 3 2017.

[260] M. Y. Neufeld, R. Inzelberg, and A. D. Korczyn. EEG in demented and non-demented parkinsonian patients. *Acta neurologica Scandinavica*, 78(1):1–5, 7 1988.

[261] T. Neuling, S. Rach, and C. S. Herrmann. Orchestrating neuronal networks: sustained after-effects of transcranial alternating current stimulation depend upon brain states. *Frontiers in Human Neuroscience*, 7:161, 2013.

[262] S. M. Nicola, D. J. Surmeier, and R. C. Malenka. Dopaminergic Modulation of Neuronal Excitability in the Striatum and Nucleus Accumbens. *Annual Review of Neuroscience*, 23(1):185–215, 3 2000.

[263] F. Nieuwhof, B. R. Bloem, M. F. Reelick, E. Aarts, I. Maidan, A. Mirelman, J. M. Hausdorff, I. Toni, and R. C. Helmich. Impaired dual tasking in Parkinsons disease is associated with reduced focusing of cortico-striatal activity. *Brain*, 140(5):1384–1398, 5 2017.

[264] M. A. Nitsche and W. Paulus. Excitability changes induced in the human motor cortex by weak transcranial direct current stimulation. *The Journal of physiology*, 527 Pt 3:633–9, 9 2000.

[265] Y. Niv, N. D. Daw, D. Joel, and P. Dayan. Tonic dopamine: opportunity costs and the control of response vigor. *Psychopharmacology*, 191(3):507–520, 3 2007.

[266] G. Nolte, O. Bai, L. Wheaton, Z. Mari, S. Vorbach, and M. Hallett. Identifying true brain interaction from EEG data using the imaginary part of coherency. *Clinical neurophysiology : official journal of the International Federation of Clinical Neurophysiology*, 115(10):2292–307, 10 2004.

[267] A. Notbohm, J. Kurths, and C. S. Herrmann. Modification of Brain Oscillations via Rhythmic Light Stimulation Provides Evidence for Entrainment but Not for Superposition of Event-Related Responses. *Frontiers in human neuroscience*, 10:10, 2016.

[268] N. Noury, J. F. Hipp, and M. Siegel. Physiological processes nonlinearly affect electrophysiological recordings during transcranial electric stimulation. *NeuroImage*, 140:99–109, 10 2016.

[269] N. Noury and M. Siegel. Phase properties of transcranial electrical stimulation artifacts in electrophysiological recordings. *NeuroImage*, 158:406–416, 9 2017.

[270] M. Nowak, C. Zich, and C. J. Stagg. Motor Cortical Gamma Oscillations: What Have We Learnt and Where Are We Headed? *Current behavioral neuroscience reports*, 5(2):136–142, 2018.

[271] M. Oh, J. S. Kim, J. Y. Kim, K.-H. Shin, S. H. Park, H. O. Kim, D. H. Moon, S. J. Oh, S. J. Chung, and C. S. Lee. Subregional Patterns of Preferential Striatal Dopamine Transporter Loss Differ in Parkinson Disease, Progressive Supranuclear Palsy, and Multiple-System Atrophy. *Journal of Nuclear Medicine*, 53(3):399–406, 3 2012.

[272] Y. Okada, Y. Kita, J. Nakamura, H. Kataoka, T. Kiriyama, S. Ueno, M. Hiyamizu, S. Morioka, and K. Shomoto. Galvanic vestibular stimulation may improve anterior bending posture in Parkinson's disease. *Neuroreport*, 26(7):405–10, 5 2015.

[273] M. S. Okun. Deep-Brain Stimulation for Parkinson's Disease. *New England Journal of Medicine*, 367(16):1529–1538, 10 2012.

[274] M. S. Okun, B. V. Gallo, G. Mandybur, J. Jagid, K. D. Foote, F. J. Revilla, R. Alterman, J. Jankovic, R. Simpson, F. Junn, L. Verhagen, J. E. Arle, B. Ford, R. R. Goodman, R. M. Stewart, S. Horn, G. H. Baltuch, B. H. Kopell, F. Marshall, D. Peichel, R. Pahwa, K. E. Lyons, A. I. Tröster, J. L. Vitek, M. Tagliati, and SJM DBS Study Group. Subthalamic deep brain stimulation with a constant-current device in Parkinson's disease: an open-label randomised controlled trial. *The Lancet Neurology*, 11(2):140–149, 2 2012.

[275] A. Oswal, P. Brown, and V. Litvak. Synchronized neural oscillations and the pathophysiology of Parkinson's disease. *Current opinion in neurology*, 26(6):662–70, 12 2013.

[276] M. L. Otten, C. B. Mikell, B. E. Youngerman, C. Liston, M. B. Sisti, J. N. Bruce, S. A. Small, and G. M. McKhann. Motor deficits correlate with resting state motor network connectivity in patients with brain tumours. *Brain*, 135(4):1017–1026, 4 2012.

[277] S. Pal, S. M. Rosengren, and J. G. Colebatch. Stochastic galvanic vestibular stimulation produces a small reduction in sway in Parkinson's disease. *Journal of vestibular research : equilibrium & orientation*, 19(3-4):137–42, 2009.

[278] W. Pan, R. Soma, S. Kwak, and Y. Yamamoto. Improvement of motor functions by noisy vestibular stimulation in central neurodegenerative disorders. *Journal of neurology*, 255(11):1657–61, 11 2008.

[279] J. Parkinson. An Essay on the Shaking Palsy. *The Journal of Neuropsychiatry and Clinical Neurosciences*, 14(2):223–236, 5 2002.

[280] S. Parnaudeau, S. S. Bolkan, and C. Kellendonk. The Mediodorsal Thalamus: An Essential Partner of the Prefrontal Cortex for Cognition. *Biological Psychiatry*, 83(8):648–656, 4 2018.

[281] S. Parnaudeau, P.-K. O'Neill, S. S. Bolkan, R. D. Ward, A. I. Abbas, B. L. Roth, P. D. Balsam, J. A. Gordon, and C. Kellendonk. Inhibition of mediodorsal thalamus disrupts thalamofrontal connectivity and cognition. *Neuron*, 77(6):1151–62, 3 2013.

[282] T. D. Parsons, S. A. Rogers, A. J. Braaten, S. P. Woods, and A. I. Tröster. Cognitive sequelae of subthalamic nucleus deep brain stimulation in Parkinson's disease: a meta-analysis. *The Lancet Neurology*, 5(7):578–588, 7 2006.

[283] M. A. Pastor, B. L. Day, and C. D. Marsden. Vestibular induced postural responses in Parkinson's disease. *Brain : a journal of neurology*, 116 (Pt 5:1177–90, 10 1993.

[284] S. J. Pelletier and F. Cicchetti. Cellular and molecular mechanisms of action of transcranial direct current stimulation: evidence from in vitro and in vivo models. *The international journal of neuropsychopharmacology*, 18(2), 10 2014.

[285] M. Penttilä, J. V. Partanen, H. Soininen, and P. J. Riekkinen. Quantitative analysis of occipital EEG in different stages of Alzheimer's disease. *Electroencephalography and clinical neurophysiology*, 60(1):1–6, 1 1985.

[286] G. Percheron, C. François, B. Talbi, J. Yelnik, and G. Fénelon. The primate motor thalamus. *Brain research. Brain research reviews*, 22(2):93–181, 8 1996.

[287] J. B. Pereira, C. Junqué, D. Bartrés-Faz, M. J. Martí, R. Sala-Llonch, Y. Compta, C. Falcón, P. Vendrell, . Pascual-Leone, J. Valls-Solé, and E. Tolosa. Modulation of verbal fluency networks by transcranial direct current stimulation (tDCS) in Parkinsons disease. *Brain Stimulation*, 6(1):16–24, 1 2013.

[288] S. Perez-Lloret and F. J. Barrantes. Deficits in cholinergic neurotransmission and their clinical correlates in Parkinson's disease. *NPJ Parkinson's disease*, 2:16001, 2016.

[289] G. Pfurtscheller, C. Brunner, A. Schlögl, and F. Lopes da Silva. Mu rhythm (de)synchronization and EEG single-trial classification of different motor imagery tasks. *NeuroImage*, 31(1):153–159, 5 2006.

[290] G. Pfurtscheller, B. Graimann, J. E. Huggins, S. P. Levine, and L. A. Schuh. Spatiotemporal patterns of beta desynchronization and gamma synchronization in corticographic data during self-paced movement. *Clinical neurophysiology : official journal of the International Federation of Clinical Neurophysiology*, 114(7):1226–36, 7 2003.

[291] G. Pfurtscheller and F. H. Lopes da Silva. Event-related EEG/MEG synchronization and desynchronization: basic principles. *Clinical neurophysiology : official journal of the International Federation of Clinical Neurophysiology*, 110(11):1842–57, 11 1999.

[292] G. Pfurtscheller, C. Neuper, and J. Kalcher. 40-Hz oscillations during motor behavior in man. *Neuroscience letters*, 164(1-2):179–82, 12 1993.

[293] A. Pikovsky, M. Rosenblum, and J. Kurths. *Synchronization: a universal concept in nonlinear sciences*. Cambridge University Press, 2003.

[294] R. Pintelon and J. Schoukens. *System identification: a frequency domain approach*. John Wiley & Sons, Inc., Hoboken, NJ, USA, 3 2012.

[295] B. Pinter, A. Diem-Zangerl, G. K. Wenning, C. Scherfler, W. Oberaigner, K. Seppi, and W. Poewe. Mortality in Parkinson's disease: A 38-year follow-up study. *Movement Disorders*, 30(2):266–269, 2 2015.

[296] C. Pirulli, A. Fertonani, and C. Miniussi. The Role of Timing in the Induction of Neuromodulation in Perceptual Learning by Transcranial Electric Stimulation. *Brain Stimulation*, 6(4):683–689, 7 2013.

[297] W. Poewe, K. Seppi, C. M. Tanner, G. M. Halliday, P. Brundin, J. Volkmann, A.-E. Schrag, and A. E. Lang. Parkinson disease. *Nature Reviews Disease Primers*, 3:17013, 3 2017.

[298] A. Pogosyan, L. D. Gaynor, A. Eusebio, and P. Brown. Boosting Cortical Activity at Beta-Band Frequencies Slows Movement in Humans. *Current Biology*, 19(19):1637–1641, 10 2009.

[299] R. Polanía, M. A. Nitsche, and W. Paulus. Modulating functional connectivity patterns and topological functional organization of the human brain with transcranial direct current stimulation. *Human Brain Mapping*, 32(8):1236–1249, 8 2011.

[300] R. Polanía, M. A. Nitsche, and C. C. Ruff. Studying and modifying brain function with non-invasive brain stimulation. *Nature Neuroscience*, 21(2):174–187, 2 2018.

[301] B. Pollok, D. Kamp, M. Butz, L. Wojtecki, L. Timmermann, M. Südmeyer, V. Krause, and A. Schnitzler. Increased SMA-M1 coherence in Parkinson's disease - Pathophysiology or compensation? *Experimental neurology*, 247:178–81, 9 2013.

[302] G. Pontone, J. R. Williams, S. S. Bassett, and L. Marsh. Clinical features associated with impulse control disorders in Parkinson disease. *Neurology*, 67(7):1258–1261, 10 2006.

[303] B. D. Prakash, Y.-Y. Sitoh, L. C. Tan, and W. L. Au. Asymmetrical diffusion tensor imaging indices of the rostral substantia nigra in Parkinson's disease. *Parkinsonism & Related Disorders*, 18(9):1029–1033, 11 2012.

[304] M. J. Price, R. G. Feldman, D. Adelberg, and H. Kayne. Abnormalities in color vision and contrast sensitivity in Parkinson's disease. *Neurology*, 42(4):887–90, 4 1992.

[305] T. Pringsheim, N. Jette, A. Frolkis, and T. D. Steeves. The prevalence of Parkinson's disease: A systematic review and meta-analysis. *Movement Disorders*, 29(13):1583–1590, 11 2014.

[306] A. Priori, A. Berardelli, S. Rona, N. Accornero, and M. Manfredi. Polarization of the human motor cortex through the scalp. *Neuroreport*, 9(10):2257–60, 7 1998.

[307] A. Priori, G. Foffani, A. Pesenti, F. Tamma, A. Bianchi, M. Pellegrini, M. Locatelli, K. Moxon, and R. Villani. Rhythm-specific pharmacological modulation of subthalamic activity in Parkinson's disease. *Experimental Neurology*, 189(2):369–379, 10 2004.

[308] A. Priori, G. Foffani, L. Rossi, and S. Marceglia. Adaptive deep brain stimulation (aDBS) controlled by local field potential oscillations. *Experimental Neurology*, 245:77–86, 7 2013.

[309] M. V. Puig, A. Watakabe, M. Ushimaru, T. Yamamori, and Y. Kawaguchi. Serotonin Modulates Fast-Spiking Interneuron and Synchronous Activity in the Rat Prefrontal Cortex through 5-HT1A and 5-HT2A Receptors. *Journal of Neuroscience*, 30(6):2211–2222, 2 2010.

[310] J. D. Putzke, R. E. Wharen, Z. K. Wszolek, M. F. Turk, A. J. Strongosky, and R. J. Uitti. Thalamic deep brain stimulation for tremor-predominant Parkinson's disease. *Parkinsonism & related disorders*, 10(2):81–8, 12 2003.

[311] N. Pyatigorskaya, C. Gallea, D. Garcia-Lorenzo, M. Vidailhet, and S. Lehericy. A review of the use of magnetic resonance imaging in Parkinson's disease. *Therapeutic advances in neurological disorders*, 7(4):206–20, 7 2014.

[312] A. Rajagopalan, K. V. Jinu, K. S. Sailesh, S. Mishra, U. K. Reddy, and J. K. Mukkadan. Understanding the links between vestibular and limbic systems regulating emotions. *Journal of natural science, biology, and medicine*, 8(1):11–15, 2017.

[313] A. H. Rajput, H. H. Sitte, A. Rajput, M. E. Fenton, C. Pifl, and O. Hornykiewicz. Globus pallidus dopamine and Parkinson motor subtypes: Clinical and brain biochemical correlation. *Neurology*, 70(Issue 16, Part 2):1403–1410, 4 2008.

[314] E. A. Rancz, J. Moya, F. Drawitsch, A. M. Brichta, S. Canals, and T. W. Margrie. Widespread vestibular activation of the rodent cortex. *The Journal of neuroscience : the official journal of the Society for Neuroscience*, 35(15):5926–34, 4 2015.

[315] J. S. Richman and J. R. Moorman. Physiological time-series analysis using approximate entropy and sample entropy. *American Journal of Physiology-Heart and Circulatory Physiology*, 278(6):H2039–H2049, 6 2000.

[316] L. Ris, M. Hachemaoui, N. Vibert, E. Godaux, P. P. Vidal, and L. E. Moore. Resonance of Spike Discharge Modulation in Neurons of the Guinea Pig Medial Vestibular Nucleus. *Journal of Neurophysiology*, 86(2):703–716, 8 2001.

[317] M. C. Rodriguez-Oroz, M. Jahanshahi, P. Krack, I. Litvan, R. Macias, E. Bezard, and J. A. Obeso. Initial clinical manifestations of

Parkinson's disease: features and pathophysiological mechanisms. *The Lancet Neurology*, 8(12):1128–1139, 12 2009.

[318] M. C. Rodriguez-Oroz, J. A. Obeso, A. E. Lang, J.-L. Houeto, P. Pollak, S. Rehncrona, J. Kulisevsky, A. Albanese, J. Volkmann, M. I. Hariz, N. P. Quinn, J. D. Speelman, J. Guridi, I. Zamarbide, A. Gironell, J. Molet, B. Pascual-Sedano, B. Pidoux, A. M. Bonnet, Y. Agid, J. Xie, A.-L. Benabid, A. M. Lozano, J. Saint-Cyr, L. Romito, M. F. Contarino, M. Scerrati, V. Fraix, and N. Van Blercom. Bilateral deep brain stimulation in Parkinson's disease: a multicentre study with 4 years follow-up. *Brain*, 128(10):2240–2249, 10 2005.

[319] S. Rossi, M. Hallett, P. M. Rossini, A. Pascual-Leone, and Safety of TMS Consensus Group. Safety, ethical considerations, and application guidelines for the use of transcranial magnetic stimulation in clinical practice and research. *Clinical Neurophysiology*, 120(12):2008–2039, 12 2009.

[320] P. Rossini, L. Rosinni, and F. Ferreri. Brain-Behavior Relations: Transcranial Magnetic Stimulation: A Review. *IEEE Engineering in Medicine and Biology Magazine*, 29(1):84–96, 1 2010.

[321] A. Roy, B. Baxter, and B. He. High-definition transcranial direct current stimulation induces both acute and persistent changes in broadband cortical synchronization: a simultaneous tDCS-EEG study. *IEEE transactions on bio-medical engineering*, 61(7):1967–78, 7 2014.

[322] K. S. Rufener, P. Ruhnau, H.-J. Heinze, and T. Zaehle. Transcranial Random Noise Stimulation (tRNS) Shapes the Processing of Rapidly Changing Auditory Information. *Frontiers in cellular neuroscience*, 11:162, 2017.

[323] G. Ruffini, M. D. Fox, O. Ripolles, P. C. Miranda, and A. Pascual-Leone. Optimization of multifocal transcranial current stimulation for weighted cortical pattern targeting from realistic modeling of electric fields. *NeuroImage*, 89:216–225, 4 2014.

[324] Y. U. Ryu and J. J. Buchanan. Accuracy, Stability, and Corrective Behavior in a Visuomotor Tracking Task: A Preliminary Study. *PLoS ONE*, 7(6):e38537, 6 2012.

[325] R. J. Sadleir, T. D. Vannorsdall, D. J. Schretlen, and B. Gordon. Transcranial direct current stimulation (tDCS) in a realistic head model. *NeuroImage*, 51(4):1310–1318, 7 2010.

[326] S. E. Safo and Q. Long. Sparse linear discriminant analysis in structured covariates space. *Statistical Analysis and Data Mining: The ASA Data Science Journal*, 4 2018.

[327] J. D. Salamone, M. Correa, A. M. Farrar, E. J. Nunes, and M. Pardo. Dopamine, Behavioral Economics, and Effort. *Frontiers in Behavioral Neuroscience*, 3:13, 2009.

[328] S. Salenius, R. Salmelin, C. Neuper, G. Pfurtscheller, and R. Hari. Human cortical 40 Hz rhythm is closely related to EMG rhythmicity. *Neuroscience letters*, 213(2):75–8, 8 1996.

[329] Y. Salimpour, Z. K. Mari, and R. Shadmehr. Altering Effort Costs in Parkinson's Disease with Noninvasive Cortical Stimulation. *The Journal of neuroscience : the official journal of the Society for Neuroscience*, 35(35):12287–302, 9 2015.

[330] G. Samoudi, M. Jivegård, A. P. Mulavara, and F. Bergquist. Effects of Stochastic Vestibular Galvanic Stimulation and LDOPA on Balance and Motor Symptoms in Patients With Parkinson's Disease. *Brain Stimulation*, 8(3):474–480, 5 2015.

[331] G. Samoudi, H. Nissbrandt, M. B. Dutia, and F. Bergquist. Noisy Galvanic Vestibular Stimulation Promotes GABA Release in the Substantia Nigra and Improves Locomotion in Hemiparkinsonian Rats. *PLoS ONE*, 7(1):e29308, 1 2012.

[332] J. Sarnthein and D. Jeanmonod. High thalamocortical theta coherence in patients with Parkinson's disease. *The Journal of neuroscience : the official journal of the Society for Neuroscience*, 27(1):124–31, 1 2007.

[333] P. Sauseng and W. Klimesch. What does phase information of oscillatory brain activity tell us about cognitive processes? *Neuroscience & Biobehavioral Reviews*, 32(5):1001–1013, 7 2008.

[334] R. Savica, B. R. Grossardt, J. H. Bower, J. E. Ahlskog, and W. A. Rocca. Incidence and Pathology of Synucleinopathies and Tauopathies Related to Parkinsonism. *JAMA Neurology*, 70(7):859, 7 2013.

[335] T. A. Scandalis, A. Bosak, J. C. Berliner, L. L. Helman, and M. R. Wells. Resistance training and gait function in patients with Parkinson's disease. *American journal of physical medicine & rehabilitation*, 80(1):38–43, 1 2001.

[336] C. Scherfler, K. Seppi, K. J. Mair, E. Donnemiller, I. Virgolini, G. K. Wenning, and W. Poewe. Left hemispheric predominance of nigrostriatal dysfunction in Parkinsons disease. *Brain*, 135(11):3348–3354, 11 2012.

[337] W. Schlee, M. Schecklmann, A. Lehner, P. M. Kreuzer, V. Vielsmeier, T. B. Poeppl, and B. Langguth. Reduced variability of auditory alpha activity in chronic tinnitus. *Neural plasticity*, 2014:436146, 2014.

[338] J. E. Schlerf, J. M. Galea, D. Spampinato, and P. A. Celnik. Laterality Differences in CerebellarMotor Cortex Connectivity. *Cerebral Cortex*, 25(7):1827–1834, 7 2015.

[339] L. Schmidt, K. S. Utz, L. Depper, M. Adams, A.-K. Schaadt, S. Reinhart, and G. Kerkhoff. Now You Feel both: Galvanic Vestibular Stimulation Induces Lasting Improvements in the Rehabilitation of Chronic Tactile Extinction. *Frontiers in Human Neuroscience*, 7:90, 2013.

[340] E. Schneider, S. Glasauer, and M. Dieterich. Comparison of Human Ocular Torsion Patterns During Natural and Galvanic Vestibular Stimulation. *Journal of Neurophysiology*, 87(4):2064–2073, 4 2002.

[341] J. Schoukens, P. Guillaume, and R. Pintelon. *Perturbation signals for system identification*. Prentice Hall, 1993.

[342] A. Schouten, E. de Vlugt, and F. van der Helm. Design of Perturbation Signals for the Estimation of Proprioceptive Reflexes. *IEEE Transactions on Biomedical Engineering*, 55(5):1612–1619, 5 2008.

[343] M. Schreckenberger, C. Lange-Asschenfeldt, C. Lange-Asschenfeld, M. Lochmann, K. Mann, T. Siessmeier, H.-G. Buchholz, P. Bartenstein, G. Gründer, and G. Gründer. The thalamus as the generator and modulator of EEG alpha rhythm: a combined PET/EEG study with lorazepam challenge in humans. *NeuroImage*, 22(2):637–44, 6 2004.

[344] T. M. Seibert, E. A. Murphy, E. J. Kaestner, and J. B. Brewer. Interregional Correlations in Parkinson Disease and Parkinson-related De-

mentia with Resting Functional MR Imaging. *Radiology*, 263(1):226–234, 4 2012.

[345] K. Sethi. Levodopa unresponsive symptoms in Parkinson disease. *Movement Disorders*, 23(S3):S521–S533, 1 2008.

[346] A. Séverac Cauquil, M. Faldon, K. Popov, B. L. Day, and A. M. Bronstein. Short-latency eye movements evoked by near-threshold galvanic vestibular stimulation. *Experimental brain research*, 148(3):414–8, 2 2003.

[347] M. Sharman, R. Valabregue, V. Perlbarg, L. Marrakchi-Kacem, M. Vidailhet, H. Benali, A. Brice, and S. Lehéricy. Parkinson's disease patients show reduced cortical-subcortical sensorimotor connectivity. *Movement Disorders*, 28(4):447–454, 4 2013.

[348] H. A. Shill, S. Obradov, Y. Katsnelson, and R. Pizinger. A randomized, double-blind trial of transcranial electrostimulation in early Parkinson's disease. *Movement Disorders*, 26(8):1477–1480, 7 2011.

[349] S. Shin, J. E. Lee, J. Y. Hong, M.-K. Sunwoo, Y. H. Sohn, and P. H. Lee. Neuroanatomical substrates of visual hallucinations in patients with non-demented Parkinson's disease. *Journal of neurology, neurosurgery, and psychiatry*, 83(12):1155–61, 12 2012.

[350] P. Silberstein, A. A. Kühn, A. Kupsch, T. Trottenberg, J. K. Krauss, J. C. Wöhrle, P. Mazzone, A. Insola, V. Di Lazzaro, A. Oliviero, T. Aziz, and P. Brown. Patterning of globus pallidus local field potentials differs between Parkinson's disease and dystonia. *Brain*, 126(12):2597–2608, 9 2003.

[351] P. Silberstein, A. Pogosyan, A. A. Kühn, G. Hotton, S. Tisch, A. Kupsch, P. Dowsey-Limousin, M. I. Hariz, and P. Brown. Cortico-cortical coupling in Parkinson's disease and its modulation by therapy. *Brain*, 128(Pt 6):1277–91, 6 2005.

[352] R. F. Silva, S. M. Plis, J. Sui, M. S. Pattichis, T. Adali, and V. D. Calhoun. Blind Source Separation for Unimodal and Multimodal Brain Networks: A Unifying Framework for Subspace Modeling. *IEEE Journal of Selected Topics in Signal Processing*, 10(7):1134–1149, 10 2016.

[353] G. Simon and J. Schoukens. Robust broadband periodic excitation design. *IEEE Transactions on Instrumentation and Measurement*, 49(2):270–274, 4 2000.

[354] H. A. Slagter, A. Mazaheri, L. C. Reteig, R. Smolders, M. Figee, M. Mantione, P. R. Schuurman, and D. Denys. Contributions of the Ventral Striatum to Conscious Perception: An Intracranial EEG Study of the Attentional Blink. *The Journal of Neuroscience*, 37(5):1081–1089, 2 2017.

[355] R. Smolders, A. Mazaheri, G. van Wingen, M. Figee, P. P. de Koning, and D. Denys. Deep Brain Stimulation Targeted at the Nucleus Accumbens Decreases the Potential for Pathologic Network Communication. *Biological Psychiatry*, 74(10):e27–e28, 11 2013.

[356] V. S. Sohal. Insights into Cortical Oscillations Arising from Optogenetic Studies. *Biological Psychiatry*, 71(12):1039–1045, 6 2012.

[357] R. Soma, S. Kwak, and Y. Yamamoto. Functional stochastic resonance in human baroreflex induced by 1/f-type noisy galvanic vestibular stimulation. In S. M. Bezrukov, H. Frauenfelder, and F. Moss, editors, *Proc. SPIE 5110, Fluctuations and Noise in Biological, Biophysical, and Biomedical Systems*, volume 5110, page 69. International Society for Optics and Photonics, 5 2003.

[358] Y. Song, J. Crowcroft, and J. Zhang. Automatic epileptic seizure detection in EEGs based on optimized sample entropy and extreme learning machine. *Journal of Neuroscience Methods*, 210(2):132–146, 9 2012.

[359] K. M. Spencer, P. G. Nestor, R. Perlmutter, M. A. Niznikiewicz, M. C. Klump, M. Frumin, M. E. Shenton, and R. W. McCarley. Neural synchrony indexes disordered perception and cognition in schizophrenia. *Proceedings of the National Academy of Sciences*, 101(49):17288–17293, 12 2004.

[360] M. B. Spraker, H. Yu, D. M. Corcos, and D. E. Vaillancourt. Role of Individual Basal Ganglia Nuclei in Force Amplitude Generation. *Journal of Neurophysiology*, 98(2):821–834, 8 2007.

[361] R. Srebro and P. Malladi. Stochastic resonance of the visually evoked potential. *Physical Review E*, 59(3):2566–2570, 3 1999.

[362] R. J. St George and R. C. Fitzpatrick. The sense of self-motion, orientation and balance explored by vestibular stimulation. *The Journal of physiology*, 589(Pt 4):807–13, 2 2011.

[363] C. J. Stagg and M. A. Nitsche. Physiological Basis of Transcranial Direct Current Stimulation. *The Neuroscientist*, 17(1):37–53, 2 2011.

[364] C. J. Stam, G. Nolte, and A. Daffertshofer. Phase lag index: Assessment of functional connectivity from multi channel EEG and MEG with diminished bias from common sources. *Human Brain Mapping*, 28(11):1178–1193, 11 2007.

[365] A. Stancák and G. Pfurtscheller. Desynchronization and recovery of beta rhythms during brisk and slow self-paced finger movements in man. *Neuroscience letters*, 196(1-2):21–4, 8 1995.

[366] T. Stephan, A. Deutschländer, A. Nolte, E. Schneider, M. Wiesmann, T. Brandt, and M. Dieterich. Functional MRI of galvanic vestibular stimulation with alternating currents at different frequencies. *NeuroImage*, 26(3):721–732, 7 2005.

[367] M. B. Sterman, D. A. Kaiser, and B. Veigel. Spectral analysis of event-related EEG responses during short-term memory performance. *Brain Topography*, 9(1):21–30, 1996.

[368] L. Stiles and P. F. Smith. The vestibularbasal ganglia connection: Balancing motor control. *Brain Research*, 1597:180–188, 2 2015.

[369] L. Stiles, Y. Zheng, and P. F. Smith. The effects of electrical stimulation of the peripheral vestibular system on neurochemical release in the rat striatum. *PloS one*, 13(10):e0205869, 2018.

[370] D. Stoffers, J. L. W. Bosboom, J. B. Deijen, E. C. Wolters, H. W. Berendse, and C. J. Stam. Slowing of oscillatory brain activity is a stable characteristic of Parkinson's disease without dementia. *Brain*, 130(7):1847–1860, 5 2007.

[371] F. M. Stoll, C. R. Wilson, M. C. Faraut, J. Vezoli, K. Knoblauch, and E. Procyk. The Effects of Cognitive Control and Time on Frontal Beta Oscillations. *Cerebral Cortex*, 26(4):1715–1732, 4 2016.

[372] D. Strüber, S. Rach, T. Neuling, and C. S. Herrmann. On the possible role of stimulation duration for after-effects of transcranial alternating current stimulation. *Frontiers in Cellular Neuroscience*, 9:311, 8 2015.

[373] M. K. Sunwoo, K. H. Cho, J. Y. Hong, J. E. Lee, Y. H. Sohn, and P. H. Lee. Thalamic volume and related visual recognition are associated

with freezing of gait in non-demented patients with Parkinson's disease. *Parkinsonism & Related Disorders*, 19(12):1106–1109, 12 2013.

[374] M. Tahmasian, L. M. Bettray, T. van Eimeren, A. Drzezga, L. Timmermann, C. R. Eickhoff, S. B. Eickhoff, and C. Eggers. A systematic review on the applications of resting-state fMRI in Parkinson's disease: Does dopamine replacement therapy play a role? *Cortex*, 73:80–105, 12 2015.

[375] K. Tanaka, M. Kawakatsu, and I. Nemoto. Stochastic resonance in auditory steady-state responses in a magnetoencephalogram. *Clinical Neurophysiology*, 119(9):2104–2110, 9 2008.

[376] L. M. Teles-Grilo Ruivo and J. R. Mellor. Cholinergic modulation of hippocampal network function. *Frontiers in Synaptic Neuroscience*, 5:2, 2013.

[377] C. E. Tenke and J. Kayser. Surface Laplacians (SL) and phase properties of EEG rhythms: Simulated generators in a volume-conduction model. *International Journal of Psychophysiology*, 97(3):285–298, 9 2015.

[378] M. A. Thenganatt and J. Jankovic. Parkinson Disease Subtypes. *JAMA Neurology*, 71(4):499, 4 2014.

[379] W. Thevathasan, P. Mazzone, A. Jha, A. Djamshidian, M. Dileone, V. Di Lazzaro, and P. Brown. Spinal cord stimulation failed to relieve akinesia or restore locomotion in Parkinson disease. *Neurology*, 74(16):1325–7, 4 2010.

[380] S. Thobois, B. Ballanger, P. Baraduc, D. Le Bars, F. Lavenne, E. Broussolle, and M. Desmurget. Functional anatomy of motor urgency. *NeuroImage*, 37(1):243–252, 8 2007.

[381] G. Thut, T. O. Bergmann, F. Fröhlich, S. R. Soekadar, J.-S. Brittain, A. Valero-Cabré, A. T. Sack, C. Miniussi, A. Antal, H. R. Siebner, U. Ziemann, and C. S. Herrmann. Guiding transcranial brain stimulation by EEG/MEG to interact with ongoing brain activity and associated functions: A position paper. *Clinical Neurophysiology*, 128(5):843–857, 5 2017.

[382] G. Thut, P. G. Schyns, and J. Gross. Entrainment of perceptually relevant brain oscillations by non-invasive rhythmic stimulation of the human brain. *Frontiers in psychology*, 2:170, 2011.

[383] C. L. Tomlinson, R. Stowe, S. Patel, C. Rick, R. Gray, and C. E. Clarke. Systematic review of levodopa dose equivalency reporting in Parkinson's disease. *Movement disorders : official journal of the Movement Disorder Society*, 25(15):2649–53, 11 2010.

[384] S. Tran, M. Shafiee, C. B. Jones, S. Garg, S. Lee, E. P. Pasman, M. G. Carpenter, and M. J. McKeown. Subthreshold stochastic vestibular stimulation induces complex multi-planar effects during standing in Parkinson's disease. *Brain Stimulation*, 11(5):1180–1182, 9 2018.

[385] R. Tremblay, S. Lee, and B. Rudy. GABAergic Interneurons in the Neocortex: From Cellular Properties to Circuits. *Neuron*, 91(2):260–292, 7 2016.

[386] Y. Tufail, A. Matyushov, N. Baldwin, M. L. Tauchmann, J. Georges, A. Yoshihiro, S. I. H. Tillery, and W. J. Tyler. Transcranial Pulsed Ultrasound Stimulates Intact Brain Circuits. *Neuron*, 66(5):681–694, 6 2010.

[387] D. Twelves, K. S. Perkins, and C. Counsell. Systematic review of incidence studies of Parkinson's disease. *Movement Disorders*, 18(1):19–31, 1 2003.

[388] W. J. Tyler. Noninvasive Neuromodulation with Ultrasound? A Continuum Mechanics Hypothesis. *The Neuroscientist*, 17(1):25–36, 2 2011.

[389] S. Tyll, E. Budinger, and T. Noesselt. Thalamic influences on multisensory integration. *Communicative & integrative biology*, 4(4):378–81, 7 2011.

[390] P. J. Uhlhaas, C. Haenschel, D. Nikolić, and W. Singer. The role of oscillations and synchrony in cortical networks and their putative relevance for the pathophysiology of schizophrenia. *Schizophrenia bulletin*, 34(5):927–43, 9 2008.

[391] R. J. Uitti, Y. Baba, N. R. Whaley, Z. K. Wszolek, and J. D. Putzke. Parkinson disease: Handedness predicts asymmetry. *Neurology*, 64(11):1925–1930, 6 2005.

[392] K. S. Utz, V. Dimova, K. Oppenländer, and G. Kerkhoff. Electrified minds: Transcranial direct current stimulation (tDCS) and Galvanic Vestibular Stimulation (GVS) as methods of non-invasive brain

stimulation in neuropsychologyA review of current data and future implications. *Neuropsychologia*, 48(10):2789–2810, 2010.

[393] K. S. Utz, K. Korluss, L. Schmidt, A. Rosenthal, K. Oppenländer, I. Keller, and G. Kerkhoff. Minor adverse effects of galvanic vestibular stimulation in persons with stroke and healthy individuals. *Brain Injury*, 25(11):1058–1069, 10 2011.

[394] V. A. Vakorin, S. M. Doesburg, L. d. Costa, R. Jetly, E. W. Pang, and M. J. Taylor. Detecting Mild Traumatic Brain Injury Using Resting State Magnetoencephalographic Connectivity. *PLoS Computational Biology*, 12(12), 2016.

[395] F. Valentino, G. Cosentino, F. Brighina, N. G. Pozzi, G. Sandrini, B. Fierro, G. Savettieri, M. D'Amelio, and C. Pacchetti. Transcranial direct current stimulation for treatment of freezing of gait: A cross-over study. *Movement Disorders*, 29(8):1064–1069, 7 2014.

[396] S. K. Van Den Eeden, C. M. Tanner, A. L. Bernstein, R. D. Fross, A. Leimpeter, D. A. Bloch, and L. M. Nelson. Incidence of Parkinson's disease: variation by age, gender, and race/ethnicity. *American journal of epidemiology*, 157(11):1015–22, 6 2003.

[397] M. P. van den Heuvel and H. E. Hulshoff Pol. Exploring the brain network: A review on resting-state fMRI functional connectivity. *European Neuropsychopharmacology*, 20(8):519–534, 8 2010.

[398] O. van der Groen and N. Wenderoth. Transcranial Random Noise Stimulation of Visual Cortex: Stochastic Resonance Enhances Central Mechanisms of Perception. *The Journal of Neuroscience*, 36(19):5289–5298, 5 2016.

[399] A. van der Hoorn, H. Burger, K. L. Leenders, and B. M. de Jong. Handedness correlates with the dominant Parkinson side: A systematic review and meta-analysis. *Movement Disorders*, 27(2):206–210, 2 2012.

[400] E. Van der Ouderaa, J. Schoukens, and J. Renneboog. Peak factor minimization of input and output signals of linear systems. *IEEE Transactions on Instrumentation and Measurement*, 37(2):207–212, 6 1988.

[401] E. Van der Ouderaa, J. Schoukens, and J. Renneboog. Peak factor minimization using a time-frequency domain swapping algorithm. *IEEE Transactions on Instrumentation and Measurement*, 37(1):145–147, 3 1988.

[402] J. Van Doren, B. Langguth, and M. Schecklmann. Electroencephalographic Effects of Transcranial Random Noise Stimulation in the Auditory Cortex. *Brain Stimulation*, 7(6):807–812, 11 2014.

[403] B. C. M. van Wijk, P. J. Beek, and A. Daffertshofer. Neural synchrony within the motor system: what have we learned so far? *Frontiers in Human Neuroscience*, 6:252, 2012.

[404] J. H. Villafañe, K. Valdes, R. Buraschi, M. Martinelli, L. Bissolotti, and S. Negrini. Reliability of the Handgrip Strength Test in Elderly Subjects With Parkinson Disease. *Hand (New York, N.Y.)*, 11(1):54–8, 3 2016.

[405] J. L. Vitek, J. Ashe, M. R. DeLong, and G. E. Alexander. Physiologic properties and somatotopic organization of the primate motor thalamus. *Journal of Neurophysiology*, 71(4):1498–1513, 4 1994.

[406] J. Voges, R. Hilker, K. Bötzel, K. L. Kiening, M. Kloss, A. Kupsch, A. Schnitzler, G.-H. Schneider, U. Steude, G. Deuschl, and M. O. Pinsker. Thirty days complication rate following surgery performed for deep-brain-stimulation. *Movement Disorders*, 22(10):1486–1489, 7 2007.

[407] U. Voss, R. Holzmann, A. Hobson, W. Paulus, J. Koppehele-Gossel, A. Klimke, and M. A. Nitsche. Induction of self awareness in dreams through frontal low current stimulation of gamma activity. *Nature Neuroscience*, 17(6):810–812, 5 2014.

[408] A. Vossen, J. Gross, and G. Thut. Alpha Power Increase After Transcranial Alternating Current Stimulation at Alpha Frequency (α-tACS) Reflects Plastic Changes Rather Than Entrainment. *Brain stimulation*, 8(3):499–508, 2015.

[409] J. Vosskuhl, D. Strüber, and C. S. Herrmann. Non-invasive Brain Stimulation: A Paradigm Shift in Understanding Brain Oscillations. *Frontiers in Human Neuroscience*, 12:211, 5 2018.

[410] M. Vreugdenhil, J. G. R. Jefferys, M. R. Celio, and B. Schwaller. Parvalbumin-Deficiency Facilitates Repetitive IPSCs and Gamma Oscillations in the Hippocampus. *Journal of Neurophysiology*, 89(3):1414–1422, 3 2003.

[411] K. Wakabayashi, K. Tanji, F. Mori, and H. Takahashi. The Lewy body in Parkinson's disease: molecules implicated in the formation and degradation of alpha-synuclein aggregates. *Neuropathology : official journal of the Japanese Society of Neuropathology*, 27(5):494–506, 10 2007.

[412] J. Wang, C.-T. Zuo, Y.-P. Jiang, Y.-H. Guan, Z.-P. Chen, J.-D. Xiang, L.-Q. Yang, Z.-T. Ding, J.-j. Wu, and H.-L. Su. 18F-FP-CIT PET imaging and SPM analysis of dopamine transporters in Parkinsons disease in various Hoehn & Yahr stages. *Journal of Neurology*, 254(2):185–190, 2 2007.

[413] L. M. Ward, S. E. MacLean, and A. Kirschner. Stochastic Resonance Modulates Neural Synchronization within and between Cortical Sources. *PLoS ONE*, 5(12):e14371, 12 2010.

[414] D. L. Wardman, B. L. Day, and R. C. Fitzpatrick. Position and velocity responses to galvanic vestibular stimulation in human subjects during standing. *The Journal of physiology*, 547(Pt 1):293–9, 2 2003.

[415] G. S. Watson and J. B. Leverenz. Profile of Cognitive Impairment in Parkinson's Disease. *Brain Pathology*, 20(3):640–645, 5 2010.

[416] R. S. Weil, A. E. Schrag, J. D. Warren, S. J. Crutch, A. J. Lees, and H. R. Morris. Visual dysfunction in Parkinsons disease. *Brain*, 139(11):2827–2843, 11 2016.

[417] M. Weinberger, W. D. Hutchison, and J. O. Dostrovsky. Pathological subthalamic nucleus oscillations in PD: Can they be the cause of bradykinesia and akinesia? *Experimental Neurology*, 219(1):58–61, 9 2009.

[418] M. Weinberger, N. Mahant, W. D. Hutchison, A. M. Lozano, E. Moro, M. Hodaie, A. E. Lang, and J. O. Dostrovsky. Beta oscillatory activity in the subthalamic nucleus and its relation to dopaminergic response in Parkinson's disease. *Journal of neurophysiology*, 96(6):3248–56, 12 2006.

[419] L. A. Wheaton, H. Shibasaki, and M. Hallett. Temporal activation pattern of parietal and premotor areas related to praxis movements. *Clinical Neurophysiology*, 116(5):1201–1212, 5 2005.

[420] T. Wichmann, M. R. DeLong, J. Guridi, and J. A. Obeso. Milestones in research on the pathophysiology of Parkinson's disease. *Movement disorders*, 26(6):1032–41, 5 2011.

[421] R. Wijesinghe, D. A. Protti, and A. J. Camp. Vestibular Interactions in the Thalamus. *Frontiers in Neural Circuits*, 9:79, 12 2015.

[422] D. Wilkinson, H. J. Ferguson, and A. Worley. Galvanic vestibular stimulation modulates the electrophysiological response during face processing. *Visual neuroscience*, 29(4-5):255–62, 9 2012.

[423] D. Wilkinson, P. Ko, P. Kilduff, R. McGlinchey, and W. Milberg. Improvement of a face perception deficit via subsensory galvanic vestibular stimulation. *Journal of the International Neuropsychological Society : JINS*, 11(7):925–9, 11 2005.

[424] D. Wilkinson, S. Nicholls, C. Pattenden, P. Kilduff, and W. Milberg. Galvanic vestibular stimulation speeds visual memory recall. *Experimental Brain Research*, 189(2):243–248, 8 2008.

[425] D. Wilkinson, O. Zubko, M. Sakel, S. Coulton, T. Higgins, and P. Pullicino. Galvanic vestibular stimulation in hemi-spatial neglect. *Frontiers in Integrative Neuroscience*, 8:4, 1 2014.

[426] D. Williams, A. Kühn, A. Kupsch, M. Tijssen, G. van Bruggen, H. Speelman, G. Hotton, C. Loukas, and P. Brown. The relationship between oscillatory activity and motor reaction time in the parkinsonian subthalamic nucleus. *European Journal of Neuroscience*, 21(1):249–258, 1 2005.

[427] D. Williams, M. Tijssen, G. Van Bruggen, A. Bosch, A. Insola, V. Di Lazzaro, P. Mazzone, A. Oliviero, A. Quartarone, H. Speelman, and P. Brown. Dopamine-dependent changes in the functional connectivity between basal ganglia and cerebral cortex in humans. *Brain : a journal of neurology*, 125(Pt 7):1558–69, 7 2002.

[428] J. Wills, J. Jones, T. Haggerty, V. Duka, J. N. Joyce, and A. Sidhu. Elevated tauopathy and alpha-synuclein pathology in postmortem Parkinson's disease brains with and without dementia. *Experimental Neurology*, 225(1):210–218, 9 2010.

[429] B. Wingeier, T. Tcheng, M. M. Koop, B. C. Hill, G. Heit, and H. M. Bronte-Stewart. Intra-operative STN DBS attenuates the prominent beta rhythm in the STN in Parkinson's disease. *Experimental Neurology*, 197(1):244–251, 1 2006.

[430] T. Wu, X. Long, L. Wang, M. Hallett, Y. Zang, K. Li, and P. Chan. Functional connectivity of cortical motor areas in the resting state in Parkinson's disease. *Human Brain Mapping*, 32(9):1443–1457, 9 2011.

[431] T. Wu, L. Wang, Y. Chen, C. Zhao, K. Li, and P. Chan. Changes of functional connectivity of the motor network in the resting state in Parkinson's disease. *Neuroscience Letters*, 460(1):6–10, 8 2009.

[432] Y. Yamamoto, Z. R. Struzik, R. Soma, K. Ohashi, and S. Kwak. Noisy vestibular stimulation improves autonomic and motor responsiveness in central neurodegenerative disorders. *Annals of Neurology*, 58(2):175–181, 7 2005.

[433] C.-G. Yan, X.-D. Wang, X.-N. Zuo, and Y.-F. Zang. DPABI: Data Processing & Analysis for (Resting-State) Brain Imaging. *Neuroinformatics*, 14(3):339–351, 7 2016.

[434] Yi-Ou Li, T. Adali, Wei Wang, and V. Calhoun. Joint Blind Source Separation by Multiset Canonical Correlation Analysis. *IEEE Transactions on Signal Processing*, 57(10):3918–3929, 10 2009.

[435] H. H. Yin and B. J. Knowlton. The role of the basal ganglia in habit formation. *Nature Reviews Neuroscience*, 7(6):464–476, 6 2006.

[436] T. Zaehle, S. Rach, and C. S. Herrmann. Transcranial Alternating Current Stimulation Enhances Individual Alpha Activity in Human EEG. *PLoS ONE*, 5(11):e13766, 11 2010.

[437] R. Zink, S. F. Bucher, A. Weiss, T. Brandt, and M. Dieterich. Effects of galvanic vestibular stimulation on otolithic and semicircular canal eye movements and perceived vertical. *Electroencephalography and clinical neurophysiology*, 107(3):200–5, 9 1998.

[438] R. Zink, S. Steddin, A. Weiss, T. Brandt, and M. Dieterich. Galvanic vestibular stimulation in humans: effects on otolith function in roll. *Neuroscience letters*, 232(3):171–4, 9 1997.